FLORIDA INTERNATIONAL UNIVERSITY

Miami, Florida

HIERARCHICALLY STRUCTURED BORON NITRIDE NANOTUBE REINFORCED CYANATE ESTER COMPOSITES

A dissertation submitted in partial fulfillment of

the requirements for the degree of

DOCTOR OF PHILOSOPHY

in

MATERIAL SCIENCE AND ENGINEERING

by

Tyler Dolmetsch

2023

To: Dean John L. Volakis
College of Engineering and Computing

This dissertation, written by Tyler Dolmetsch, and entitled Hierarchically Structured Boron Nitride Nanotube Reinforced Cyanate Ester Composites, having been approved in respect to style and intellectual content, is referred to you for judgment.

We have read this dissertation and recommend that it be approved.

Daniela Radu

Seung Jae Lee

Arvind Agarwal,Co-Major Professor

Benjamin Boesl,Co-Major Professor

Date of Defense: March 28, 2023

The dissertation of Tyler Dolmetsch is approved.

Dean John L. Volakis
College of Engineering and Computing

Andrés G. Gil
Vice President for Research and Economic Development
and Dean of the University Graduate School

Florida International University, 2023

DEDICATION

I humbly dedicate this work to my beloved mother Kristina Tompkins, stepmother Tracey Dolmetsch, and Grandfather (Grandad) Jack Barnhardt. They were my unwavering pillars of support throughout my life, and especially during my pursuit of this doctoral degree. Though they left this world before witnessing the completion of this thesis, their unwavering presence in my life endures, and I carry their memories and inspiration with me every day. I know that they would be proud of my resilience and determination to achieve this milestone, even in the face of personal and global challenges. Their love, guidance, and encouragement will always be engraved in my heart and immortalized in this document, which I offer as a tribute to their enduring legacy. They will be forever remembered and loved.

Kristina M. Tompkins (May 12, 1968 – October 19th, 2022)

Tracey Dolmetsch (October 20th, 1963 – December 9th, 2021)

John "Jack" Barnhardt (Grandad) (May 18, 1945 – October 12th, 2022)

With heartfelt gratitude, I further dedicate this work to the rest of my family, my loving fiancé, and dear friends. Your unwavering support and encouragement have been invaluable in helping me navigate the challenges of pursuing this academic journey. Your constant love, guidance, and care have been a constant source of inspiration and motivation, propelling me forward through the highs and lows of this endeavor. Your love, acceptance, and embrace have created a sanctuary of warmth and comfort that I carry with me always. Thank you for your unwavering faith in me and for standing by my side through thick and thin. I am forever grateful for your presence in my life.

ACKNOWLEDGMENTS

I am deeply grateful to Dr. Benjamin Boesl and Dr. Arvind Agarwal for their unwavering guidance, support, and mentorship during my academic journey as a master's and doctoral student over the last five years. Their dedication to every student is truly commendable, and I cannot express enough how grateful I am for everything they have done for me. Their expertise, patience, and support have been critical to my academic and professional development and have shaped my future research interests profoundly. Their extensive knowledge and experience in the field have been invaluable in enhancing my understanding of complex research concepts. I am also grateful for the numerous opportunities that they have provided me as a student, including the privilege to travel and present my research work at several national and international conferences. These experiences have not only enriched my academic and professional growth but have also broadened my perspective and enriched my personal development. Furthermore, I want to express my appreciation for the privilege of using all of their state-of-the-art research facilities and equipment to complete my work. The access to advanced equipment and technology has been critical in advancing my research and achieving my academic goals.

I would also like to thank Dr. Daniela Radu and Dr. Seung Jae Lee for being a part of my dissertation committee. Their yearly feedback on my research progress was very helpful in assuring that I meet my dissertation objectives on time. Their time and effort given has been greatly appreciated.

I would like to express my heartfelt gratitude to all the current and former members of the Plasma Forming Group for their continued support, guidance, and collaboration

throughout my research journey. Not only have we worked together on several successful projects and publications, but we have also formed lifelong friendships. Their expertise, companionship, and support have played an instrumental role in my success, and I am grateful for their contributions.

Most of my research was conducted in the Advanced Materials Engineering Research Institute (AMERI) at FIU, so I would also like to extend my sincere thanks to Dr. Alex Franco and the other faculty members for their dedication, hard work, and expertise in training, conducting experiments, and fixing equipment. They have been invaluable in helping me achieve my research goals. Without their assistance, completing my work would have been impossible.

I want to acknowledge the financial support received from the FIU Graduate School through the Presidential Fellowship award. I would also like to acknowledge the National Science Foundation Research Programs PRE-CCAP, PREM, and Cell-Met for supporting the different projects that I have worked on over the years.

Most importantly, I want to express my deepest appreciation and gratitude to my fiancé, family, and friends who have been unwavering in their support and encouragement throughout my academic and professional journey. Their endless love, support, and patience have been a source of motivation and inspiration for me. Without them, I would not have been able to overcome the various challenges and obstacles that come with pursuing this degree. They have provided me with the strength and resilience to pursue my dreams, and I am truly fortunate to have them in my life.

ABSTRACT OF THE DISSERTATION

HIERARCHICALLY STRUCTURED BORON NITRIDE NANOTUBE REINFORCED CYANATE ESTER COMPOSITES

by

Tyler Dolmetsch

Florida International University, 2023

Miami, Florida

Professor Benjamin Boesl, Co-Major Professor

Professor Arvind Agarwal, Co-Major Professor

The objective of this study was to develop a novel strategy for fabricating thermally stable, hierarchical boron nitride-based reinforced cyanate ester composites by leveraging the known degradation mechanisms of cyanate esters and utilizing the exceptional properties of 1D and 2D boron nitride nanoparticles.

Specifically, we covalently bonded hydroxyl functionalized boron nitride nanotubes (BNNTs) with cyanate ester monomers, forming imino-carbonate linkages. By exploiting this bonding pathway, a new class of composites that exhibit superior mechanical and thermal properties were created. The addition of just one volume percent of functionalized BNNTs to cyanate ester reduced the curing activation energy to a value lower than any previously reported literature value, increased the hardness and elastic modulus by 18.48% and 12.42%, respectively, and improved the thermal conductivity by 5.69%. These results were attributed to the covalent bond allowing for superior interfacial

interactions between the two materials, improving the dispersion within the matrix and leading to more efficient thermal and mechanical energy transfer.

A significant outcome of this research was the fabrication of novel hierarchically structured foam composites consisting of boron nitride nanoplatelets (BNNPs) and BNNTs. Through reinforcing cyanate ester with these highly aligned and high-volume percent architectures, the thermal conductivity was increased by an incredible 104.5%. The enhanced thermal conductivity of the foam structure was primarily attributed to the tailored orientation of its constituent materials, the BNNPs and BNNTs. The alignment of the BNNPs along the walls of the foam and the networked formed by BNNTs interconnecting individual nanoplatelets and micro-pores created a synergistic effect which facilitated a highly conductive pathway for heat transfer, making it a promising candidate for a wide range of thermal management applications.

This research provides a pathway for reinforcement of other polymer systems and can lead to the development of incredibly strong and thermally stable polymers for high temperature applications. The multifunctionality of the boron nitride system in these composites can be exploited for advanced applications such as sensors and radiation shielding structures. Overall, these findings provide valuable insights into the design and manufacturing of high-performance materials and have significant implications for a range of industrial and scientific applications.

TABLE OF CONTENTS

CHAPTER PAGE

LIST OF TABLES

TABLE PAGE

LIST OF FIGURES

FIGURE PAGE

ABBREVIATIONS AND ACRONYMS

BNNP	Boron Nitride Nanoplatelet
BNNT	Boron Nitride Nanotube
CE	Cyanate Ester
DIC	Digital Image Correlation
DSC	Differential Scanning Calorimetry
DMA	Dynamic Mechanical Analysis
F-BNNT	Functionalized Boron Nitride Nanotube
FIB	Focused Ion Beam Machining
FTIR	Fourier Transform Infrared Spectroscope/ Spectroscopy
IPA	Isopropyl Alcohol
IR	Infrared Radiation
SEM	Scanning Electron Microscope/ Microscopy
TGA	Thermal Gravimetric Analysis
Vol %	Volume Percent

Chapter 1 Introduction

The progress of space travel and commercialization is contingent on the development of innovative materials and composites that possess exceptional properties. These new materials must be able to withstand the harsh conditions of space, including extreme temperatures, thermal cycling, radiation, and mechanical stresses. Without these advanced materials, space exploration and communication would be impossible[1]. High temperature polymers, which can maintain their physical and mechanical properties at high temperatures, are ideal for use in these conditions. Among these high temperature polymers, cyanate esters (CEs) are particularly noteworthy for their exceptional performance at high temperatures. With high glass transition temperatures (>220°C), excellent thermal stability (up to 450°C), and low flammability, cyanate esters are ideal for use in aerospace vehicle wing components, satellite antennas, heat sinks, and adhesives for electronic packaging[2], [3].

Due to the increased demand for high-temperature polymers such as these cyanate esters, extensive studies have been done to characterize and improve their degradation mechanisms[4]. The degradation mechanisms of cyanate esters can be categorized into three regimes, which are closely associated with the bonding mechanisms within the polymer chain. Various studies have demonstrated that bonding a thermally stable hydroxyl-functionalized additive to a specific location can mitigate certain regimes and enhance the thermal stability or flame retardance[5]–[9]. However, it is crucial to improve not only the degradation mechanisms but also the mechanical, thermal, and multifunctional properties to meet the growing demand for space adaptation. To address this challenge,

boron nitride nanotubes (BNNTs) have been identified as a promising solution, as they can equally be hydroxyl functionalized[10], possess exceptional strength (~1TPa)[11]–[13] and thermal conductivity (~600W/m*K)[14], [15], and demonstrate multifunctionality such as radiation shielding and piezoelectricity[16], [17].

Therefore, the primary goal of this study was to develop a novel strategy for fabricating thermally stable, hierarchical boron nitride-based reinforced cyanate ester composites by leveraging the known degradation mechanisms of cyanate esters and utilizing the exceptional properties of 1D and 2D boron nitride nanoparticles. Specifically, this was accomplished using two methods:

(1) through covalently bonding hydroxyl functionalized boron nitride nanotubes (BNNTs) with cyanate ester monomers, forming imino-carbonate linkages and improving the interfacial interactions between the nanotube and the polymer matrix, and

(2) fabricating novel highly aligned and high-volume percent boron nitride reinforced architectures consisting of boron nitride nanoplatelets (BNNPs) and BNNTs that creates a synergistic effect for facilitating a highly conductive pathway for thermal and mechanical transport.

By exploiting this bonding pathway and the unique properties of BNNPs and BNNTs, a new class of high temperature polymer composites that exhibit superior mechanical and thermal properties were successfully created.

This document will first provide a comprehensive overview of high-temperature polymer composites by conducting a thorough literature review. Specifically, it will examine the application and need for such composites, evaluate the state-of-the-art products currently available in the market, and identify the gaps in the current research that need to be addressed. The next section will focus on manufacturing processing maps, which will provide a detailed roadmap for dispersing BNNTs into cyanate ester resins and fabricating and infiltrating hierarchical BNNP and BNNT foams. Finally, this document will investigate the mechanical and thermal properties of these new composites and determine the optimal environments in which they can be utilized. By presenting these findings in a clear and concise manner, this document aims to provide a valuable resource for researchers, engineers, and others working in the field of high-temperature polymer composites.

Significant outcomes of this research for the field of materials science and engineering include:

(1) providing a manufacturing processing map for reinforcing high temperature polymers with novel hierarchical boron nitride structures

(2) understanding how the functionalization of micro-scale reinforcement influences the resulting chemical structure, curing kinetics, and mechanical and thermal properties of cyanate ester resins,

(3) fabrication of novel hierarchically structured foam composites consisting of boron nitride nanoplatelets (BNNPs) and boron nitride nanotubes (BNNTs) that exhibit exceptional thermal properties, and

(4) establishing the mechanisms governing the interfacial interactions and efficiency of energy transfer between high-volume fraction boron nitride structures and the surrounding matrix.

The addition of functionalized BNNTs to cyanate ester reduced the curing activation energy to a value lower than any previously reported literature value and increased the hardness and elastic modulus by 18.48% and 12.42%, respectively. Furthermore, through reinforcing cyanate ester with highly aligned and high-volume percent boron nitride architectures, the thermal conductivity was increased by an incredible 104.5%. This research provides a manufacturing pathway for reinforcement of other polymer systems and can lead to the development of incredibly strong and thermally stable polymers for high temperature applications and demanding environments. Overall, these findings provide valuable insights into the design and manufacture of high-performance materials and have significant implications for a range of industrial and scientific applications.

Chapter 2 Background Information

2.1 Polymers

Polymers are a class of materials composed of long chains of repeating units. They possess a wide range of properties, including high strength-to-weight ratios, flexibility, and resistance to temperature, chemicals, and radiation[18]. These properties make them ideal for a variety of space applications, such as spacecraft construction, thermal insulation, and radiation shielding[19]. For instance, polymers such as polyimides and cyanate esters have been used to make lightweight, durable components for spacecraft[20], [21], while polyethylene and polyurethane foams are commonly used for thermal insulation[22]. Additionally, polymers like polyethylene terephthalate and polypropylene are utilized for space suits due to their ability to withstand extreme temperatures and mechanical stresses[23].

2.2 Thermosets

Thermoset polymers, which are cross-linked through chemical reactions and cannot be melted or reshaped once formed, are particularly well-suited for space applications due to their high strength, stiffness, and dimensional stability[24]. Examples of thermoset polymers used in space include cyanate esters, epoxy resins, and phenolics[18]. These materials have excellent thermal stability, low outgassing, and resistance to atomic oxygen and ultraviolet radiation, making them ideal for use in spacecraft components and structures[25]. Cyanate esters, in particular, are known for their high-temperature performance and resistance to radiation, and are used in applications such as thermal control coatings and electronic packaging[26]. Epoxy resins are commonly used in

composite materials for space structures due to their excellent bonding and mechanical properties[27]. Phenolics, on the other hand, are often used in ablative materials for heat shields and re-entry vehicles due to their ability to withstand high temperatures and heat fluxes[28].

2.3 Cyanate Esters

Cyanate esters are a class of thermoset polymers with exceptional thermal and mechanical properties, making them highly desirable for space applications[2], [26]. They have high glass transition temperatures (>220°C), low dielectric constants, and low water absorption, and excellent thermal stability (up to 450°C), making them an ideal choice for electronic components and high-temperature adhesives[29]. However, cyanate esters also have certain limitations, such as their brittleness, low fracture toughness, and sensitivity to moisture during processing[25]. The processing of cyanate esters requires specialized equipment and techniques to maintain low moisture levels, as even small amounts of moisture can result in the formation of bubbles and voids in the final product.

Cyanate ester monomers are identified by the characteristic -OCN absorbance peaks within the 2200-2300cm^{-1} range. These bands usually display 2-3 partially resolved peaks and their exact location and number of peaks depend on the exact chemistry of the monomer. As the cyanate ester undergoes polymerization, also known as curing, the -OCN absorbance peak begins to dissipate and is replaced by the emergence of the triazine ring peaks around 1360 and 1570cm^{-1}. This transformation, which involves the cyclotrimerization reaction to form the triazine ring, occurs between 100°C and 200°C. As

the temperature increases and approaches the glass transition temperature (T_g) of the polymer, the full curing is achieved[4], [30], [31].

While cyanate esters are stable at higher temperatures than most polymers, they still fall short of the thermal stability that most metals and ceramics exhibit. Therefore, to understand how to improve the thermal stability of cyanate esters, it is important to understand how they degrade. In a seminal study, the thermal degradation chemistry of nine different CE resins was studied using simultaneous thermogravimetric analysis (TGA) and infrared analysis[4]. The released gases during degradation were further investigated using infrared spectroscopy and gas chromatography-mass spectrometry. They found that the degradation of CEs progresses in three steps as seen in Figure 1.1. Regime 1: between 400-450°C there is random cutting and cross-linking of the hydrocarbon backbone, but this does not significantly contribute to mass loss. Regime 2: between 450-500°C the triazine ring breaks down which creates volatile compounds, produces an initial solid residue, and leads to rapid mass loss. Regime 3: over 500°C there is the final elimination of alkenes and hydrogen leaving a secondary carbonaceous char containing leftover oxygen and nitrogen. By 1000°C all the CE will be converted to char or completely disintegrated. They discovered that the char yield in cyanate esters is dependent on the chemical structure of the monomer, and it was found that the yield of char increases as the glass transition temperature (T_g) for the polymer increases. The reasoning behind this correlation is linked to the unsaturated carbon-carbon bonds present in the structure of the material. Therefore, the amount of char yield can be proportionally related to the number of unsaturated carbon-carbon bonds in the polymer[4].

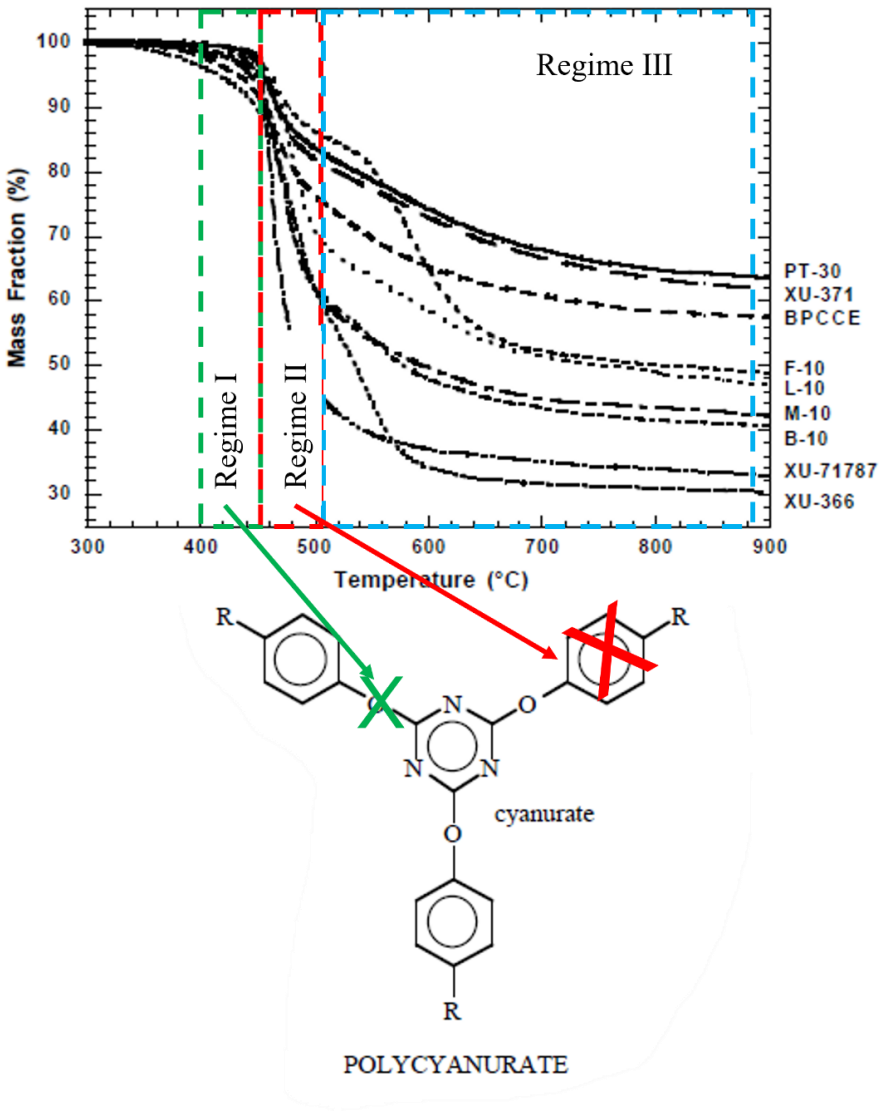

Figure 1.1. TGA curves for cyanate ester resins and their degradation regimes[4].

The present study employed PT-30s resin, obtained from Arxada through commercial procurement. According to the manufacturer, the characteristics and performance of the resin are described in Table 1.1. The selection of PT-30 for this investigation was based on its exceptional features, notably its elevated glass transition temperature. This attribute is highly relevant to this study, given the direct correlation between the glass transition temperature and thermal stability. Therefore, if the thermal stability of this polymer could

be improved, it would follow that the stability of other cyanate ester resins would also be enhanced. The use of PT-30 in this study will enable a better understanding of the factors that influence the thermal stability of cyanate ester resins and will provide valuable insights into the development of more advanced materials for industrial applications.

Table 1.1. Features and performance highlights for PT-30 resin from the manufacturer[32].

Features and Performance Highlights of PT-30	
Tg (°C) tan delta by DMA	> 405
CTE (in/in, -40 to 315°C)	28 x 10-6
Tensile Strength (MPa)	41
Tensile Modulus (GPa)	4.07
Elongation (%)	1.2-1.5
Flexural Strength (MPa)	110
Flexural Modulus (GPa)	4.69
Compressive Strength (MPa)	317
Decomposition onset temperature (°C) by TGA	420
Char yield of cure resin by TGA, in nitrogen (%)	62-65

2.4 Reinforcement of Cyanate Esters

As polymers undergo heating, they are prone to degradation, a process known as pyrolysis, which results in the formation of carbonaceous char and volatile flammable

products. This situation creates a detrimental cycle for the polymer, whereby the volatile products ignite in the vapor phase, generate more heat, and further the pyrolysis process. To address this issue, Lu and Hamerton conducted an extensive review of the various strategies that can be employed to improve the thermal stability and flammability resistance of polymers. These approaches encompassed the use of inorganic compounds, such as boron, phosphorous, silicon, and nitrogen, which can be incorporated into the polymer matrix to enhance its thermal and oxidative stability. Additionally, the use of intumescent systems, which form a protective barrier upon heating, was also explored. The incorporation of flame retardants, either inorganic or organic, has been identified as a crucial method for suppressing the ignition and slowing down the propagation of flames. Moreover, the design and synthesis of polymers with inherent fire-resistant properties can offer a promising solution to improve the overall flammability resistance of polymers[33].

The incorporation of particles, such as silica, into cyanate ester polymers is a common strategy to enhance their mechanical and thermal properties. However, the addition of particles can also have a complex effect on the material's properties. Generally, particle addition leads to an increase in the Young’s modulus and thermal conductivity, while a decrease in flexural strength is observed. In a study conducted by Wooster et al., the addition of silica particles to cyanate ester was investigated. The results showed that an increase in the weight percent of silica led to an increase in the Young's modulus, owing to the inherent strength of the particles and their interfacial interaction with the matrix. This interaction allowed for efficient stress transfer between the matrix and the silica. Additionally, an increase in thermal conductivity was observed, mainly due to the higher thermal conductivity of the silica. However, the flexural strength decreased, which was

attributed to the concentration of stress at the particle-matrix interface. The thermal stability of the material was assessed using TGA, and the results showed that as the concentration of silica was increased, the mass remaining after pyrolysis was also increased. However, the increase in mass was equivalent to the amount of filler added, indicating that no actual improvement to the matrix occurred[34]. Thus, while the addition of particles can improve certain properties, careful consideration must be given to the overall impact on the material's properties, particularly in relation to its thermal stability.

To achieve optimal thermal stability in polymer chains, covalent bonding with a more thermally stable material is necessary. In a study conducted by Liang et al., polyhedral oligomeric silsesquioxanes (POSS) functionalized with hydroxyl groups were covalently bonded to the cyanate ester matrix, resulting in an improvement in the composite's properties. The incorporation of hydroxyl groups onto POSS was confirmed by the appearance of new peaks in the FTIR spectra. Specifically, a new N-H on-plane bending peak was observed at 1570 cm^{-1} and a new C=N peak appeared at 1595 cm^{-1}, which are indicative of the imino-carbonate linkage $(RO)_2C=NH$. The presence of functionalized additives also increased the rate of curing, as demonstrated by an increase in the ratio of the absorbance peak intensity of the cyanate ester at 2240 and 2270 cm^{-1} to the phenyl ring symmetric peak at 1500 cm^{-1}. The phenyl ring was used as a reference peak because it is not involved in the curing reaction. Further, the functionalization of POSS led to an increase in the glass transition temperature, char yield, flexural strength, and storage modulus of the composite. The increase in the glass transition temperature was attributed to the rigid POSS molecules, which restricted the movements of the polymer chains. As

the concentration of the additive increased, the mechanical properties of the composite decreased due to agglomeration[35].

Cyanate ester resins have also been modified with hydroxyl functionalized additives such as graphene oxide (GO) nanoplatelets and boron-based carboranes. In a study by Wang et al., the effects of GO on the curing kinetics and network formation of PT-30 cyanate ester resin were investigated. The presence of hydroxyl groups on the surface of the GO platelets was confirmed using FTIR spectroscopy. During the curing process, the absorbance of the -OH band at 3500 cm^{-1} decreased, while a new band at 3374 cm^{-1} corresponding to the imino-carbonate -O-(C=NH)-O- group was formed, indicating a chemical reaction between the GO platelet and the cyanate ester matrix. Differential scanning calorimetry (DSC) results showed that the addition of GO reduced the required initial curing activation energy and temperature, with 1 wt% of GO being the most effective. Although GO catalyzed the initial reaction, the 2D platelet hindered further cross-linking of the polymer chains as the curing process continued, and this effect was proportional to the weight percent reinforcement[36].

In a recent study by Goyal et al., boron-based hydroxyl-functionalized carboranes were added to PT-30 cyanate ester resin at concentrations of 0-40 wt%. The carboranes were solvently blended into the resin and were cured using standard manufacturer recommended parameters. FTIR spectroscopy was used to confirm the presence of the imino-carbonate linkage, indicated by a new imine peak at 1649 cm^{-1} and the disappearance of the -OH peak on the carborane at 3249 cm^{-1} during the curing process. The Kissinger method was used to calculate the curing activation energy required, and it was found to decrease by 54%

with the addition of 10 wt% carboranes. It was found that the carboranes initially catalyzed the cross-linking reaction, but eventually, the reaction became diffusion-controlled, and the curing activation energy plateaus. TGA showed that the addition of 30 wt% carboranes increased the final char yield to 76% in air at 1000°C, thereby improving thermal stability. Additionally, the addition of 10 wt% carboranes mitigated the final regime of degradation. This increase in thermal stability was attributed to the free hydroxyl groups on the carboranes covalently bonding with the cyanate ester matrix, leading to chain extensions, cross-linking, and trapping of organic components formed during pyrolysis[2]. However, no other improvements in thermal or mechanical properties were reported. This study suggests that functionalized boron-based materials can dramatically increase the thermal stability of cyanate ester composites.

Fang et al. compared the effect of functionalized multiwalled carbon nanotubes (MWCNTs) to non-functionalized MWCNTs when added to a cyanate ester matrix. They observed that functionalized MWCNTs were better dispersed within the matrix, and the interfacial interactions between the matrix and nanotubes were improved compared to non-functionalized MWCNTs. This improved interface led to increased flexural and impact strength, which was attributed to better dispersion of the nanotubes within the matrix. The glass transition temperature decreased with the addition of MWCNTs, as the nanotubes hindered further cross-linking. In terms of thermal stability, functionalized MWCNTs increased the initial degradation temperature by blocking the diffusion and extravasation of small molecules in the matrix and improving adhesion between the nanotubes and matrix. This suggests that functionalization of nanotubes can improve both mechanical and thermal properties of the composite material[37].

In a study conducted by Wu et al., boron nitride nanoplatelets (BNNPs) were utilized to enhance the properties of a cyanate ester matrix. The researchers discovered that the free amine ($-NH_2$) molecules located on the nanoparticle's end can covalently bond with the cyanate ester, thereby leading to improved mechanical and thermal characteristics. Dynamic mechanical analysis demonstrated that adding up to 15wt% of BNNPs had no effect on the cyanate ester's glass transition temperature (T_g). However, it more than doubled both the storage modulus and thermal conductivity. The thermal conductivity improved from 0.27 to 0.55 W/(m*K), and the thermal stability also increased with the weight percent of BNNP loading. When loaded with 15wt% of BNNPs, the final char yield at 800°C increased to 28%, indicating that it helped prevent thermal degradation of the cyanate ester[38].

Molecular dynamic modeling was employed to investigate the potential of boron nitride-based additives for reinforcing high-temperature polymers. Sachdeva et al. examined the impact of a large-diameter double-walled BNNT on four different high-temperature polymers, including cyanate esters, using LAMMPS. The researchers discovered that the interaction energy between the BNNT and the cyanate ester was -6038 Kcal/mol, which is more negative than that for BNNT/epoxy systems (-5823 Kcal/mol). This indicates that BNNTs can establish a stronger interface with cyanate esters than epoxies. As a result, the stronger interface leads to increased load transfer between the polymer and the BNNT, resulting in enhanced mechanical properties. This molecular modeling study demonstrates that the use of boron nitride-based additives can significantly improve the performance of high-temperature polymers[39].

2.5 Boron Nitride Nanotubes

Previous studies have indicated that for effective thermal and mechanical reinforcement of cyanate esters, it is crucial to disperse a thermally stable, high-strength, and hydroxyl-functionalized additive appropriately within the cyanate ester matrix. Boron nitride nanotubes (BNNTs) fulfill all of these requirements and have already been demonstrated to be compatible with cyanate ester polymers using molecular dynamics.

Boron nitride nanotubes (BNNTs) share a similar chemical and physical structure to carbon nanotubes. However, they exhibit superior thermal stability of up to ~900°C and higher resistance to oxidation at elevated temperatures, making them more chemically stable than their carbon counterparts. Also, while CNTs are electrically conductive, BNNTs are electrically insulating which is of great interest for smart BNNT applications [40], [41]. Moreover, BNNTs have additional multifunctional capabilities, including piezoelectricity and neutron radiation shielding[42]–[45]. These unique properties make BNNTs an optimal choice for reinforcing new composites designed for space applications.

Boron nitride nanotubes (BNNTs) possess exceptional mechanical and thermal properties, making them an ideal choice for reinforcement in polymers. With a high elastic modulus ranging from 750-1200 GPa, BNNTs also exhibit high tensile strength (~30 GPa)[46] and remain thermally stable up to 900°C in air. By comparison, carbon nanotubes (CNTs) are stable only up to ~400°C[47], [48]. BNNTs offer several advantages over CNTs as a reinforcement for polymers: they exhibit a stronger bonding with polymers than CNTs[49]; they possess higher interfacial strength with epoxy than CNTs[50]; they exhibit higher interwall friction leading to increased interwall load transfer, thus making them

more efficient reinforcers[51]; and superior wetting and infiltration were observed between BNNT buckypaper and epoxy than CNT buckypaper[52]. Therefore, BNNTs represent a highly promising material for improving the mechanical and thermal properties of polymers for a wide range of applications.

2.5.1 Mechanical Properties of Boron Nitride Nanotubes-Polymer Matrix Composites

Boron nitride nanotubes (BNNTs) are characterized by their remarkable tensile strength. In-situ tensile tests conducted inside high-resolution transmission electron microscopes (HRTEMs) have demonstrated that the measured tensile strength is sensitive to the failure location[40]. The intrinsic fracture strength of BNNTs varies from 26.9 to 33.2 GPa, but it is worth noting that prominent structural defects such as irregular cross-sections, vacancies, impurities, or dislocations can lower the strength of BNNTs. Therefore, to ensure that BNNTs exhibit their maximum strength potential, efforts must be made to minimize the presence of such defects during their synthesis or growth. The morphology of the BNNTs are also important, some BNNTs exhibit a bamboo-like structure and it was found that these nodes act as stress concentrators that negatively affect the resulting mechanical properties[53]. Multiwalled boron nitride nanotubes (MWBNNTs) offer a compelling option for even greater reinforcement in materials due to their unique breaking mechanism. MWBNNTs break between their shell layers, requiring significantly more energy to induce failure. This stick-and-slide mechanism is fundamentally different from the telescopic sliding exhibited by multiwalled carbon nanotubes (MWCNTs). Consequently, MWBNNTs are more efficient reinforcers than MWCNTs[54], [55]. The breaking mechanism of MWBNNTs provides additional

mechanical support, making them an attractive option for improving the mechanical properties of composite materials.

Numerous studies have investigated the integration of BNNTs (1-5wt%) into casted polymers such as epoxy[56], poly(dimethylsiloxane) (PDMS)[57], and polyvinyl alcohol (PVA)[10], resulting in significant improvements in the elastic modulus of 10%-50%. For instance, Lu et al. observed a remarkable 46% increase in tensile fracture strength, a 55% increase in Young's modulus, and a 45% increase in elongation at failure when 1wt% of BNNT was added to PVA[10]. Kang et al. reported an increase in hardness from 238 MPa to 488 MPa (a 104.9% increase) when 5wt% of BNNT was added to a polyimide[16]. These notable improvements in mechanical properties can be attributed to the intrinsic characteristics of BNNTs and their strong interfacial interactions with the polymer matrix[10], [41], [52].

Moreover, during failure, BNNTs act as bridges between cracks, thereby dissipating the energy required for crack advancement, slowing crack propagation, and increasing the toughness and fatigue of the material[11], [12]. Furthermore, multilayered composites of BNNT, CNT, and polyurethane layers have exhibited even greater improvements, with an increase of 1143.8% in the elastic modulus compared to the base polymer[47].

2.5.2 Thermal Properties of Boron Nitride Nanotubes-Polymer Composites

BNNTs possess exceptional thermal stability, maintaining their structural integrity even at temperatures as high as 900°C. Additionally, their remarkable thermal conductivity in the axial direction reaches up to approximately 600W/(m*K), which is significantly

higher compared to their radial direction, which exhibits a thermal conductivity of only around 20 W/(m*K). This pronounced thermal stability is more than double that of CNTs, making BNNTs a superior choice for composites employed in high-temperature applications such as cyanate ester polymers[58], [59].

The morphology of BNNTs can also affect the resulting thermal properties. Chen et al. found that finer nanotubes (<20nm) did not oxidize and degrade as much as larger nanotubes (20-200nm) when exposed to temperatures reaching 900°C. They revealed that the oxidation begins at the end of the nanotubes and along the broken walls and defect sites[60]. Therefore, longer, and purer BNNTs will be more efficient at thermal transport.

In the study conducted by Lu et al., it was observed that incorporating as little as 1wt% of BNNTs to polyvinyl alcohol (PVA) resulted in a 25% increase in its thermal conductivity [10]. Despite this noteworthy enhancement, the effectiveness of adding only a few weight percentages of BNNTs is limited due to the absence of significant continuity in BNNT-BNNT interactions for effective thermal stress transfer [41]. However, research has demonstrated that the most significant improvements in thermal conductivity (10-20x the base polymer) are achievable through high-BNNT concentration composites (20-30wt% BNNTs) [15], [41], [48]. Such high-BNNT concentration composites were fabricated by infiltrating the polymer into the BNNT buckypaper. Therefore, the greater the addition of BNNTs, the higher the thermal conductivity that can be achieved, as higher BNNT concentration leads to more effective heat transfer within the composite material.

2.5.3 Multifunctionality of Boron Nitride Nanotubes-Polymer Composites

The exceptional mechanical and thermal properties of BNNTs are not their only unique features. BNNTs have also been found to possess intrinsic piezoelectric properties and radiation shielding capabilities[16], [17], [41], [47], [48], [57].These piezoelectric properties make them suitable for use in a range of applications, including sensors, actuators, and energy conversion systems. Piezoelectric polymers are a great alternative to other materials like ceramics, such as lead zirconate titanate (PZT), due to their lightweight, flexible, and non-toxic properties. This makes them an excellent choice for use in aerospace and biomedical applications [16], [41], [57].Incorporating BNNTs into an already piezoelectric polyimide led to a 460% increase in both the piezoelectric coefficient (d33) and electrostrictive coefficient (M33) in a previous study. When BNNT buckypaper was sandwiched between two single-wall CNT electrodes, both coefficients were at least two orders of magnitude larger [16]. Snapp et al. created a stretchable composite by adding 9wt% of BNNT into PDMS, which had a competitive piezoelectric coefficient of approximately 18 pm V^{-1} compared to other piezoelectric polymers like PVDF, which has a coefficient of 33 pm V^{-1}. They also found that the piezoelectric coefficient increased with alignment and was linearly proportional to the amount of BNNTs added [57]. Therefore, maximizing the piezoelectric properties of the resulting composite requires increasing the concentration of BNNTs and aligning the nanotubes. Furthermore, even small additions of BNNTs into a polymer can induce piezoelectric capabilities. For example, Zhang et al. developed a polymer composite with 0.2wt% BNNT reinforcement using a stereolithography additive manufacturing approach. They found that the piezoelectric

sensitivity was 10 times higher (120 mV/(kPa·wt%)) than the base polymer, resulting in a working sensor for a robotic sensing system[61].

Space radiation, which includes cosmic radiation and solar flares, is a major concern for the health of astronauts and aerospace structures during extended space missions[17], [47], [62].However, protective shielding adds extra weight to the structures and increases fuel costs. BNNTs could be a promising solution to reinforce space structures because they have a large neutron absorption cross-section, which makes them effective in radiation shielding and eliminates the need for additional shielding [16], [17], [62]. Further research and testing are necessary to achieve this goal. In the meantime, BNNTs can be used to enhance current shielding layers and mitigate radiation effects due to their exceptional radiation absorption abilities.

2.5.4 Processing Considerations of BNNT-Polymer Composites

One of the most important factors for manufacturing nanocomposites is the quality of dispersion. Nanoparticles and specifically BNNTs have an extremely surface energy that leads to agglomeration. BNNTs can also tangle and intertwine, further leading to agglomeration and requiring more energy to disperse. Agglomerations can be detrimental to nanocomposites because they act as stress concentrations and lead to failure locations. Therefore, to improve mechanical and thermal properties, the dispersion must be optimized[63], [64].

One common technique for dispersing nanotubes is the wet-mixing approach. This approach involves dispersing the nanotubes in a liquid medium, such as deionized (DI) water, acetone, ethanol, or isopropyl alcohol (IPA), and subjecting them to ultrasonication

to achieve deagglomeration and dispersion of the BNNTs. Studies on the wet-mixing method suggest varying sonication times ranging from 1 to 3 hours. Longer sonication times are preferred to break apart BNNT clusters, but excessive sonication can lead to nanotube damage and shorten their length, which can compromise their mechanical reinforcement capabilities. Therefore, identifying the optimal balance between sonication time and nanotube integrity is critical. It can be achieved by imaging the composite mixtures at different sonication levels before composite manufacturing, enabling the precise control of the nanotube dispersion and the avoidance of nanotube damage, resulting in a uniform and mechanically robust composite[65]–[67].

2.6 Boron Nitride Nanoplatelets

Boron nitride nanoplates (BNNPs) or hexagonal boron nitride (hBN) or boron nitride nanosheets (BNNS) are 2D flat sheets consisting of the alternating boron-nitrogen chemical structure and are atomically thin. Similar to BNNTs, they possess exceptional thermal conductivity along the aligned basal-plane (diameter), with a value of ~600 W/(m*K), and through-plane (thickness) conductivity of 30 W/(m*K)[68]. These 2D materials also exhibit remarkably high basal-plane stiffness and strength, which can exceed 950 GPa[69]. However, their through-plane strength is significantly lower, with values as low as 30 GPa[70]. Therefore, due to their tunability, BNNPs offer great potential as additives for electrically insulating packaging and thermal management systems in polymer nanocomposites[71]. By incorporating aligned BNNPs along the basal-plane direction, these composites can achieve enhanced thermal conductivity and mechanical strength.

2.7 Freeze-Dried Foam Structures and Composites

Freeze-drying, is a powerful technique that can overcome agglomeration challenges in 2D material-polymer composites[72]. This technique can be used to assemble 2D nanomaterials into rigid free-standing three-dimensional (3D) architectures or foams[73]–[75]. In this process, the liquid component of a mixture is frozen and then removed by sublimation, leaving behind a porous solid material. Free-standing foams can then be infiltrated with polymers to form foam reinforced polymer composites with tailorable thermal conductivity and structural stability[76]. The freeze-drying process allows the design of the foams with tailored properties and morphology, such as pore size, shape, and orientation by engineering the processing parameters[77]. This technique can be used to create highly porous, lightweight, and mechanically strong materials, making it a promising method for the fabrication of high-performance composites.

A few freeze-dried boron nitride structures have been fabricated and reported in literature. Zhao et al. created a 80wt% BNNP – polyurethane composite using a bidirectional freezing processing coupled with hot-pressing. They discuss the importance of how the freezing parameters can affect the orientation of the BNNPs within the architecture and how this can vary the resulting thermal properties. The more aligned the BNNPs, the greater the thermal conductivity[78]. Lei et al. used a one-step exfoliation and functionalization technique to create BN aerogels that had a reticulated morphology. This resulted in limited property tailoring, as there was only short-range order creating isotropic properties[79]. Owuor et al. also made an isotropic BNNP foam, but reinforced it with polyvinyl alcohol (PVA) resulting in a composite structure which was more mechanically stable than the foam alone[80]. Han et al. was able to make an anisotropic foam reinforced

epoxy composite in a similar fashion to the bidirectional freezing method used by Zhao et al. This allowed for the tailoring of thermal and electrical properties and can lead to similar composite systems being made with different polymers[81].

2.8 Missing Gaps in the Current Understanding

At present, the literature reveals a critical gap in the thermal and mechanical reinforcement of cyanate ester resins. While various studies have succeeded in enhancing the thermal stability of composites, mechanical improvement and multifunctionality have been lacking. Boron-based hydroxyl-functionalized carboranes, for instance, significantly improve the thermal stability of composites, but do not offer mechanical enhancement or multifunctionality. To address this gap, the incorporation of boron nitride nanotubes (BNNTs) into cyanate esters presents an opportunity to improve both the mechanical and thermal properties of the composite, as well as to add multifunctionality. However, research on the interaction between BNNTs and the cyanate ester matrix is still lacking. Moreover, fundamental questions regarding the catalyzation of the cyclotrimerization process by hydroxyl-functionalized additives remain unanswered.

Another crucial gap is the lack of manufacturing process maps for infiltrating boron nitride nanoplatelet (BNNP) foams with high-temperature polymers, specifically cyanate esters. Such maps are essential for scalability and future use of BNNP foams in aerospace applications. The development of these maps will allow for greater predictability, reproducibility, and optimization of the manufacturing process, ultimately enabling the use of BNNP foams in high-temperature applications.

Chapter 3 Materials and Methodology

3.1 Materials.

Isopropyl alcohol (IPA) (>99%) was used as received from Sigma-Aldrich. Cyanate ester (CE) resin (PT-30s) was provided by Arxada. PT-30s contains 80% polymer (PT-30) and 20% solvent (methyl ethyl ketone (MEK)) by volume. PT-30s has a viscosity of 80-150 mPa x s at 20°C which makes it much more suitable to process than the original PT-30 which has a viscosity of 400 mPa x s even at 80°C. PT-30s is characterized as a multifunctional cyanate ester with a light, yellow appearance and exhibits an impressive glass transition temperature of above 405°C. Commercially available boron nitride nanotubes (BNNTs) were used as received from BNNT, LLC (Virginia, USA). They are classified as the SP10 refined puffball and are already purified when received. The

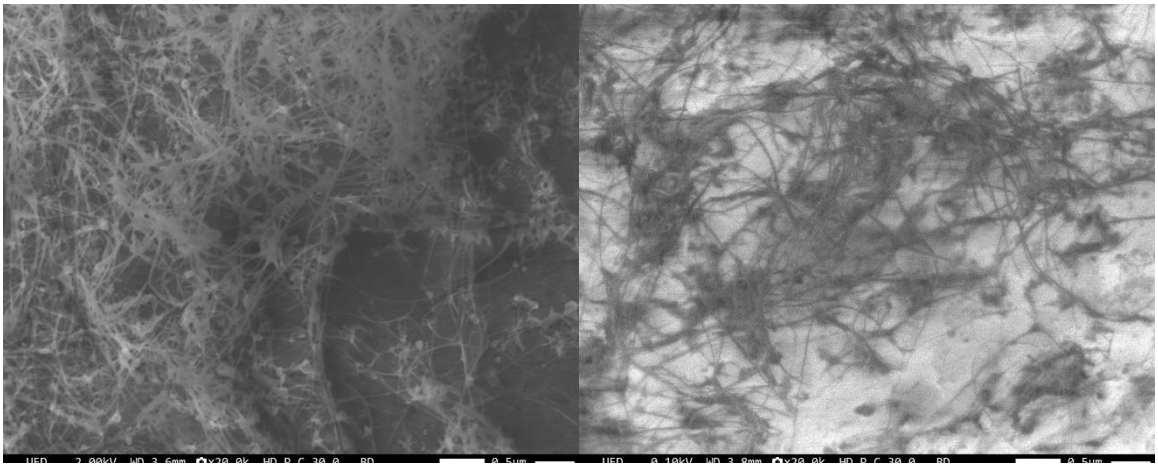

Figure 3.1. SEM images of as received BNNTs.

purification process removes excess boron agglomerations from the nanotubes, thus leaving them a pure white color. As a bulk material, they have a shape and appearance similar to a white cotton ball. Although the purification process removes most of the boron agglomerations, scanning electron microscopy (SEM) images of the as-received BNNTs

still show some of the boron agglomerations, indicated by the dark spheres in the SEM images of Figure 3.1.

Boron nitride nanoplatelets (BNNPs) were commercially bought from pH Matter Inc. (Columbus, OH). BNNPs are a 2D material with a white color and have a flake-like morphology. Their sizes can range from 100 nm to 3 μm in the basal direction (roughly the diameter of the flake) and have a thickness ranging from 40 to 65 nm. Carboxymethyl cellulose (CMC, Mw~700,000, Millipore Sigma, Burlington, MA) was commercially obtained and used as a dispersant for the BNNPs and BNNTs during the freeze-drying process. Deionized (DI) water was used as the freezing agent during the freeze-drying process. Styrene-butadiene rubber (SBR, MTI Corporation, Richmond, CA) was used as a binder agent to hold the freeze-dried foam structure together after sublimation.

3.2 Functionalization and Synthesis of CE – BNNT Nanocomposites

Figure 3.2. BNNTs in an aluminum weighing dish

The as-received BNNTs come in a cotton ball-like shape, as seen in Figure 3.2. As BNNTs have very high surface energy, it takes a high amount of energy to break them apart for proper dispersion. Therefore, before the dispersion of the BNNTs, they must be partially pulled apart. BNNTs were weighed using a high-precision balance (Explorer Precision Balance Model EX223N, OHAUS, NJ). The weight of the BNNTs was determined based on the desired final volumetric percentage of reinforcement for the

Figure 3.3. Pulled apart BNNTs in a glass beaker before tip sonication.

overall sample (0-1vol%). The calculation for the weight of BNNTs needed can be seen in Equation 3.1 with the results shown in Table 3.1. The bulk density of BNNTs is taken as 0.34 g/cm^3. Once weighed, they were further pulled apart using tweezers and carefully inserted into a 50mL glass beaker. The pulled-apart BNNTs in the beaker can be seen in Figure 3.3.

Equation 3.1. Calculation of the needed weight of BNNTs

$$Weight\ BNNTs\ (mg)$$

$$= (mL\ of\ Polymer)(vol\%\ BNNT\ desired)(bulk\ density\ of\ BNNTs)(\frac{1000mg}{g})$$

Table 3.1. Calculation of the BNNTs required for each volumetric loading.

Volume % Reinforcement	Weight of BNNTs needed (mg)
0.125	5.95
0.25	11.9
0.5	23.8
0.75	35.7
1	47.6

BNNTs were first functionalized with hydroxyl groups using a method highlighted by Lu et al [10]. BNNTs were tip ultrasonicated (VCX750, SONICS & MATERIALS, INC.,) with a tip diameter of 19mm in 10mL of DI water for 30 minutes with an amplitude of 40% and pulse settings 30s on – 30s off. The beaker was placed in a container containing ice water at a level equal to the water line in the beaker. This ice bath prevents the solution from getting too hot, as the tip ultrasonication process is an extremely high-energy process. After the first few pulses, it can be seen that the chunks of BNNTs begin to come apart and

start dispersing in the DI water. As the sonication process continues, the chunks are fully removed and the BNNTs become homogenously dispersed in the solution. After 30 minutes of tip sonication, the aqueous solution was then left to dry in a furnace at 80°C, thus leaving only functionalized BNNTs (F-BNNTs). After the BNNTs are completely dry, they form a thin film layer on the bottom of the beaker. They can be scraped into flakes using a small spatula and become softer if IPA has already been added to the beaker. This will allow them to disperse better once added to the IPA. Next, the BNNTs were tip sonicated again, but this time in IPA using the same method and parameters. The ice bath is especially important for this step because if the solution is too hot the IPA can begin to evaporate much faster. Once the BNNTs were dispersed in the IPA, the proper volumetric loading of PT-30s was introduced into the aqueous solution and further tip sonicated for 30 minutes using the same pulse settings. Again, if the solution is too hot during this step, there becomes a separation of the PT-30s from the IPA and thus the dispersion is not as good or reliable. The solution was then left in a bath sonicator for approximately 120 minutes at 65°C to remove the solvent (IPA). The resin was then transferred into an aluminum weighing dish with a capacity of 80mL purchased from McMaster-Carr. This meant the diameter was about 73mm. The mixtures were cured in a muffle furnace following the manufacturer's recommended curing parameters: 1 hour at 150°C, 3 hours at 200°C, and 1 hour at 260°C. The full manufacturing process can be seen in Figure 3.4.

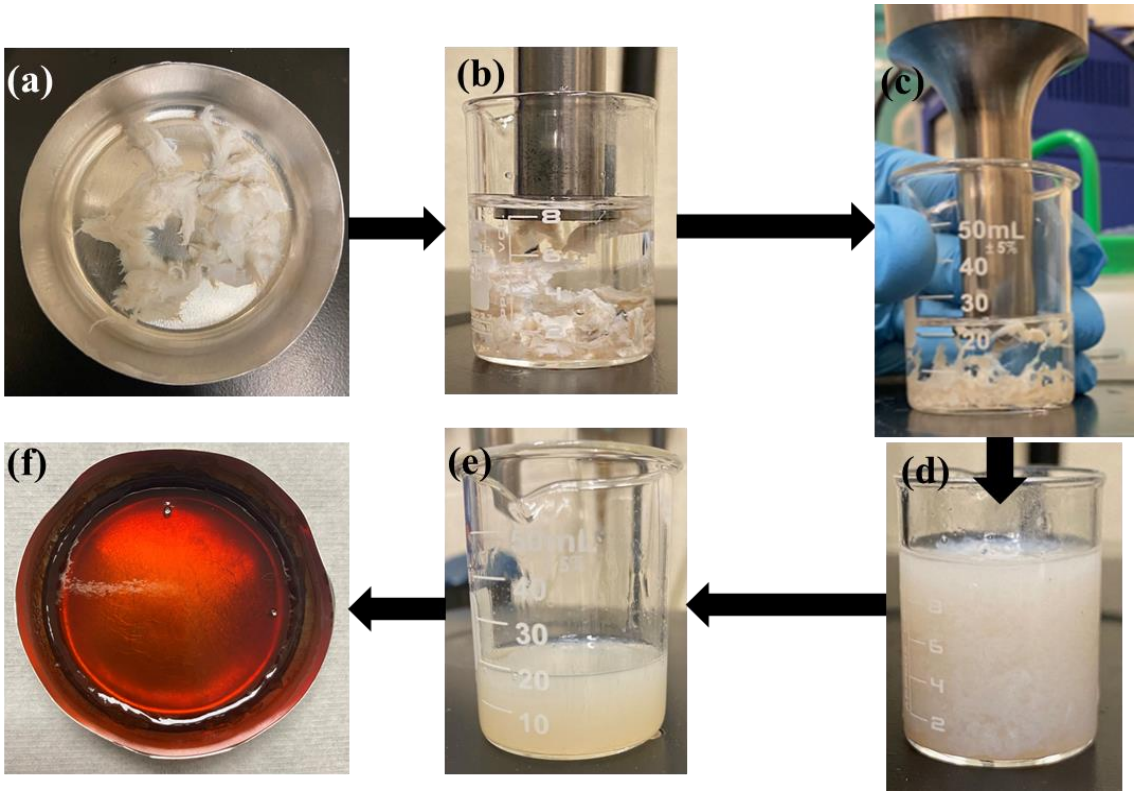

Figure 3.4. (a) BNNTs in an aluminum weighing dish. (b) Chunks of BNNTs in DI water before sonication. (c) BNNTs being dispersed using the tip ultrasonication method. (d) The BNNT and DI water solution after dispersion. (e) Homogeneously dispersed PT-30 and BNNT resin. (f) Cured PT-30 sample

3.3 Synthesis of BNNP and BNNP/BNNT Foams

The Freeze-Drying slurry for BNNP foam-reinforced cyanate ester composites has a composition of 93 wt.% deionized water, 4 wt.% BNNPs, 2 wt.% SBR, and 1 wt.% CMC. For the combination of BNNP and BNNT foam-reinforced cyanate ester composites, the composition is as follows: 4 wt.% BNNPs, 0.125wt% BNNTs, 2 wt.% SBR, and 1 wt.% CMC. Due to the small weight fraction of BNNTs, the other weight fraction of materials was not changed. The small weight fraction of BNNTs still results in a large number of BNNTs being added. The containers obtained from BNNT LLC generally contain about 600mg of BNNTs. Multiple dishes of foam are usually made in one batch, with each

aluminum dish needing 20g total of material for each foam. Therefore, for each dish, the amount of BNNTs needed is 25 mg. The amount of BNNTs can quickly add up and can become difficult to properly disperse in one batch.

For the BNNP foam-reinforced composites, the first step is to vortex mix SBR in deionized (DI) water using a magnetic stirrer at 500rpm for 30 minutes at room temperature. This forms a homogeneous white solution. Then the CMC is slowly added into the solution as the vortex mixing is still occurring. If the CMC is added too quickly it will agglomerate and will not be able to disperse. The solution is left to vortex mix for 30 min at room temperature to prepare the solvent solution. Then, the BNNPs were added to the solution and vortex mixed at 600-700 rpm for 60 minutes at room temperature. The entire solution was then bath-sonicated for 60 minutes at room temperature to create a

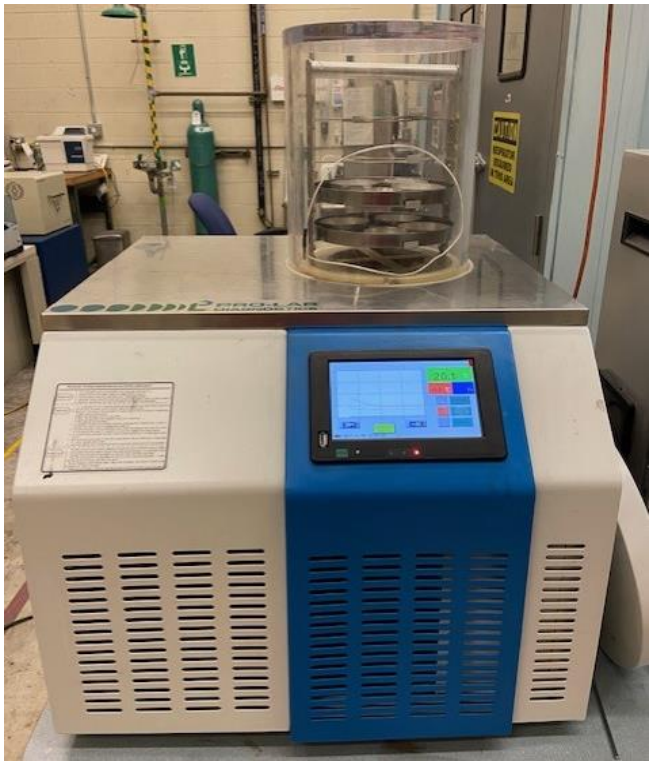

Figure 3.5. Freeze-Dryer showing the sublimation process of BNNP Foams.

homogenously dispersed BNNP slurry. The slurry was poured into an aluminum weighing dish of equal size (~73 mm diameter) as the rest of the cured cyanate ester samples. An aluminum pan was chosen for the freeze-drying process because the heat transfer needs to happen from the base of the freeze-dryer. Therefore, the aluminum dish acts as a high thermal transport pathway to create nucleation for the water to freeze. Once the slurry was prepared and properly dispersed, it was subjected to the freezing process for 4 hours at -56 °C with ambient pressure. Upon completion of the freezing process, the frozen slurry began the sublimation process that lasts for 24 h at -56° C and pressure of 1 Pa in the freeze drier (Pro-Freeze Dryer PLT300, ProLab Inc., Fort Worth, TX), see Figure 3.5 and Figure 3.6. The result of this process is a rigid, free-standing, porous structure consisting of mostly BNNP with residual CMC and SBR.

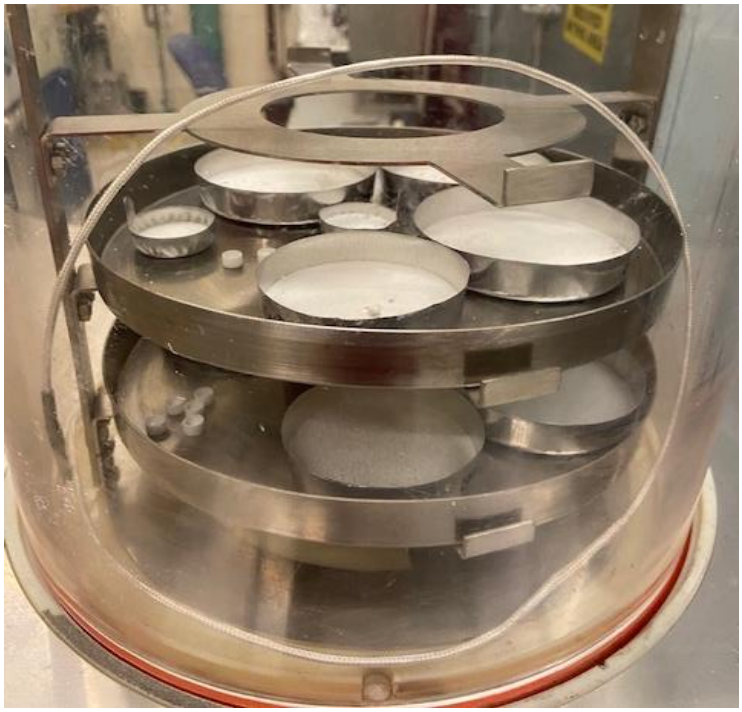

Figure 3.6. BNNP (top rack) and BNNP/BNNT (bottom rack) foams during the sublimation process.

The combination of BNNP and BNNT in a free-standing foam structure has not been accomplished in previous literature. Therefore, the manufacturing processing methods had to be determined. The manufacturing processing steps of the free-standing foams with a combination of BNNPs and BNNTs were similar to the manufacturing processing steps of the BNNP foams, but with a few extra steps at the beginning. The weight percentage of BNNTs was 0.125% of the entire mass of the solution. For instance, if 80g of the solution is going to be made, then 100mg of BNNTs needed to be added and dispersed. The BNNTs were first weighed, pulled apart into small chunks, and placed in a 200mL glass beaker. The appropriate mass of DI water was then added to the beaker (93wt%). The entire beaker was placed in an ice bath with an ice water level similar to the water level within the beaker. The solution was then tip ultrasonicated for 30 minutes at a 40% amplitude and pulse settings of 30 seconds on followed by 30 seconds off. After sonication, and the BNNTs were visually homogeneously dispersed, the manufacturing process followed the same methodology for the BNNP foams. SBR was added into the solution and vortex mixed with a magnetic stirrer at room temperature for 30 minutes. Then the CMC was slowly added to the solution and the mixing continued for another 30 minutes at room temperature. Next, the BNNPs were added to the solution and then everything was bath sonicated for 60 minutes. Once the slurry was ready, it was poured into an 80mL aluminum pan and subjected to the freezing process of 4 hours at -56 °C followed by sublimation for 24 h at -56° C and pressure of 1 Pa in the freeze drier. After 24 hours, the porous, free-standing BNNP/BNNT foams were ready.

3.4 Synthesis of BNNP and BNNP/BNNT Foam Reinforced CE Composites

These hierarchically structured composites consisting of BNNP, BNNT, and cyanate ester have not been reported in the literature. Therefore, the methodology and manufacturing processing maps needed to be created for infiltrating these free-standing foams with the cyanate ester and also the curing parameters. Our group has previously infiltrated BNNP foams with other polymer systems using the vacuum system connected to the freeze drier. This was the logical first trial for manufacturing.

Trial 1: Using a 5mL pipette, PT-30s was poured over the top of the BNNP foam, still sitting in the 80mL aluminum pan, and allowed to soak into the foam slowly. The low viscosity of the PT-30s, due to the 20vol% of solvent, allowed the polymer to rapidly soak into the foam, thus showing that there was good wettability between the polymer and the foam. Roughly 30mL of the polymer was used to sufficiently cover the foam and allow ample room for shrinkage during the known curing process of the pure polymer. The uncured polymer/foam sample was then placed in the vacuum chamber of the freeze dryer.

Figure 3.7. BNNP reinforced cyanate ester during the vacuuming process. Both the air trapped in the foam and solvent in the polymer is evaporating

A vacuum was pulled slowly, and it was noticed that both the air trapped within the foam and the solvent within the polymer were evaporating and essentially boiling, as seen in Figure 3.7.

The vacuum for the freeze dryer is quite intense and causes this highly volatile process. The integrity of the foams was in question, so the vacuum pump was allowed to run until the boiling became too intense, and then the air was allowed back into the chamber. This process was repeated for about an hour. The indication of complete infiltration is when no more bubbles are being created during the process. The samples were taken from the vacuum chamber straight to the furnace where they were cured using the regular manufacturer-recommended curing parameters for the neat polymer resin: 150°C for one hour, 200°C for three hours, and 260°C for one hour. Upon removing the samples it was quickly noticed that they did not have the same appearance as the neat PT-30 samples or as the PT-30 samples with the addition of BNNTs, these samples were almost black in

Figure 3.8. Reacted BNNP-CE composite samples after curing.

appearance and looked and smelled burnt. There were many bubbles on the surface of the sample and through the cross-section, as seen in Figure 3.8. This indicated that a reaction was occurring during the curing process.

After these unfortunate reactions, it was hypothesized that there were four possibilities for this reaction:

- Trapped water in the BNNP foams, from the freeze-drying process, reacted with the cyanate ester during curing.
- Trapped solvent from the polymer which cannot escape during the curing process due to the foam structure and change in viscosity as the curing occurs.
- The small amount of CMC inside the foam is reacting with the cyanate ester at some point during the curing process.
- The binding agent SBR is reacting with the cyanate ester during the curing process.

Therefore, a series of trials were performed to identify or eliminate each possibility for this reaction.

Trial 2: This second trial for making a BNNP – cyanate ester composite was to test if the trapped water inside the foam was causing a reaction with the cyanate ester during the curing process. This is a known problem with cyanate esters and thus was the first idea that came to mind. A BNNP foam sample was allowed to dry out in a furnace at 120°C for 4 hours to eliminate any trapped moisture. The foam was then infiltrated with received PT-30s resin inside the vacuum chamber of the freeze-dryer. After infiltration, the sample was placed directly inside the furnace and cured following the step-curing cycle mentioned

above. After curing, the reaction was still visible on the surface of the sample and throughout the cross-section. This indicated that any trapped moisture was not the major cause of this reaction.

Trial 3: This third trial for manufacturing a BNNP – cyanate ester composite tested if it was the trapped solvent in PT-30s that was causing this reaction and bubbling. The solvent (MEK) evaporates around 90°C and the first curing stage for the resin is at 150°C. This signals that the solvent is getting removed during the early stages of the curing process. The desired total resin was measured out into a glass beaker, accounting for the 20vol% of solvent that will be removed. The beaker of resin was placed in an oven at 120°C for an hour. The resin was removed and it was noticed that most of the solvent was still in the polymer, evident from the lack of total volume change. The resin was then placed inside a vacuum desiccator and the vacuum was pulled until -0.9 MPa. The solvent could be seen boiling out of the resin, but eventually slowed down and stopped when the viscosity of the resin began to increase. The resin was transferred back into the oven and allowed to heat up again before it was placed back into the vacuum desiccator. This process worked well, but the 20vol% removal of solvent was not completed. A new idea for removing the solvent was identified and a magnetic stirrer was placed inside the beaker, which is inside the desiccator, and the whole setup was placed on top of a hot plate with stirrer capabilities. The combination of the hot resin, the vacuum being pulled, and the magnetic stirrer allowed for all of the solvent to be removed from the resin. This was further demonstrated by the resin having a very high viscosity. Now that the solvent was removed, a BNNP foam sample was placed in an oven at 120°C for 4 hours as highlighted in Trial 2 to remove any possible moisture. The resin was then poured over the foam sample and allowed to settle

and soak into the foam. Due to the change in viscosity of the resin, it took much longer to soak into the foam. The sample was placed in the oven again to allow the resin to further settle into the foam. The sample was then placed into a desiccator and a vacuum was pulled to remove the trapped air inside the foam. As the resin began to cool, the air bubbles began to get trapped in the resin due to the high viscosity. Therefore, this process of furnace to vacuum had to be repeated many times until no more air bubbles were visually seen. Once all the air was removed, the sample was placed in the furnace and allowed to cure following the same curing cycle. Upon completion of curing, the sample was removed from the furnace, and once again the reaction was visually seen immediately. Although, there seemed to be a lesser amount of air bubbles in the cross-section of the foam. This meant that the trapped solvent was still part of the problem.

Trial 4: Now that the possibility of trapped water and solvent were eliminated from the list, this meant that there was some reaction occurring between the cyanate ester and one of the additives in the BNNP foams, CMC or SBR. BNNPs were eliminated as a possibility because this reaction was not seen with the BNNTs and they are of the same chemical composition. To understand the degradation of these additives throughout the curing process required for the cyanate ester, their mass loss over the temperature range of 25°C – 1000°C was measured using thermal gravimetric analysis (TGA). A heating rate of 10°C/minute was used during the experiments. The TGA curves for both SBR and CMC can be seen in Figure 3.9 below. The results reveal that SBR is the likely cause of the reaction process, as it is shown to degrade about 50% during the first stage of the curing process. CMC is also shown to degrade slightly and has a more significant mass loss at around 280°C. While this means that it should be fine during the curing process, it would

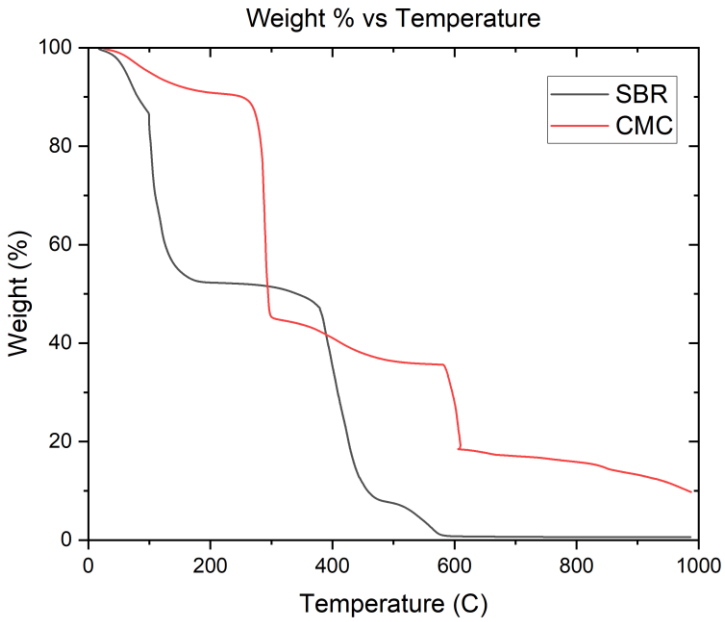

Figure 3.9. TGA curves for the degradation of SBR and CMC.

cause a decrease in the overall thermal stability of the composite. From the TGA curve, it is shown that by 600°C the SBR is completely degraded, and the CMC is 80% degraded. Therefore, to remove these additives from the BNNP foams, the foams were placed in a furnace at 600°C for 4 hours. The foams went into the furnace white and came out looking white, indicating that the additives were sufficiently removed. While these additives were removed, they left the BNNP foams without their binding agent. The foams became very fragile and could easily break if touched or mishandled. Following the methodology described in Trial 3, the MEK solvent was removed from the PT-30s resin and then the resin was poured over the top of the foam and allowed to infiltrate. Since the foam was now more porous, the resin was able to infiltrate at a faster rate than previously seen. The sample was placed in an oven at 120°C to decrease the viscosity of the resin and then placed in a desiccator to pull a vacuum and remove the trapped air. This was a delicate process,

as pulling the vacuum too fast could cause volatile boiling to occur and damage the foam, but pulling too slowly allowed the resin to cool and trap the air. Thus, a similar method was used to repeatedly place the sample in an oven and then pull a vacuum. Over time it was visually seen that the foam structure is degrading, as there are only weak Van der Waals forces holding the structure together. The foam can also break as the air bubbles find a pathway of least resistance to escape. Once the air was removed, the sample was cured in a furnace following the step cure cycle previously mentioned. This methodology

Figure 3.10. Optical image of infiltrated BNNP-cyanate ester composite.

finally proved successful in creating a highly infiltrated BNNP–cyanate ester foam, as seen in the optical image in Figure 3.10.

After multiple trials, the recommended methodology for infiltrating BNNP or BNNP/BNNT foams with cyanate ester resins is as follows:

1. Remove all the additives and binder inside the foams by placing them in a furnace at 600°C for 4 hours.

2. Remove any solvent in the resin through a combination of heating the resin at 120°C and then placing it inside a vacuum chamber that can pull at least -0.8 MPa while magnetically stirring the resin.

3. Pour the resin onto the foam and allow it to soak into the foam. Placing the entire sample in the oven at 120°C helps this process.

4. Repeatedly place the sample from the oven into the vacuum chamber to slowly pull out the trapped air inside the foam.

5. Cure the sample in a furnace following the step curing procedure: 1 hour at 150°C, 3 hours at 200°C, and 1 hour at 260°C.

It is also recommended that the sample is left to slowly cool after curing to prevent thermal shock from cracking the sample.

3.5 Machining and Preparation of Samples for Thermal and Mechanical Testing

The cured BNNT-reinforced cyanate ester composites had a thickness between 2-2.5mm which was a good thickness for most of the testing methods (tensile, flash diffusivity, DMA, etc.). The BNNP and BNNP/BNNT foam-reinforced cyanate ester composites had a thickness greater than 10mm due to the excess polymer being used to ensure proper infiltration. Therefore, these samples need to be ground down using 120 grit sandpaper to a thickness of less than 6mm which was ideal for cutting using a waterjet (WAZER, Yonkers, NY). All of the samples were manufactured using the same aluminum weighing pans, so, therefore, a template of specimen designs was created for machining. These templates can be seen in Figure 3.12 and Figure 3.11 with the individual dimensions

shown in Figure 3.13 - Figure 3.16 with all the dimensions being in millimeters. The samples were held in place on the bed of the water jet using screws. The waterjet has a nozzle of 0.8mm and was set to a cutting speed of 38 mm/min with a pierce time of 19 seconds. The lead in and out was set to 0.82mm. The path followed was set to cut on the outside of the desired dimensions. This ensures that the nozzle diameter is accounted for by the movement of the waterjet. While the use of the waterjet allowed for samples to be machined quickly and in a cost-effective manner, there were a few adverse effects. This included abrasive embedding in the polymer and rough edges due to the brittle nature of the polymer. The embedded abrasive was partially removed by bath-sonicating the samples

in DI water for 30 minutes after machining. The rough edges were mitigated through light sanding using 400-grit sandpaper.

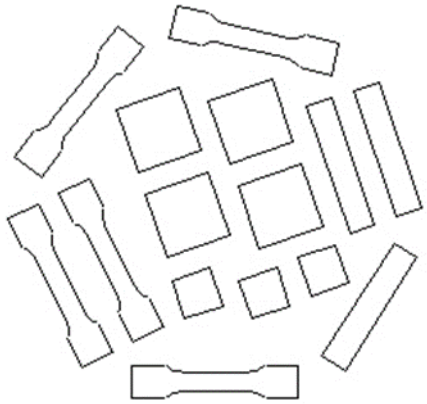

Figure 3.12. Waterjet template used for BNNT reinforced CE composites.

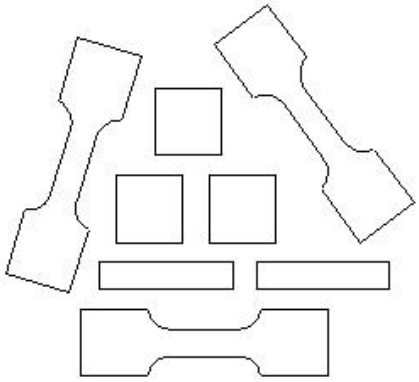

Figure 3.11. Waterjet template used for BNNP and BNNT foam reinforced CE composites.

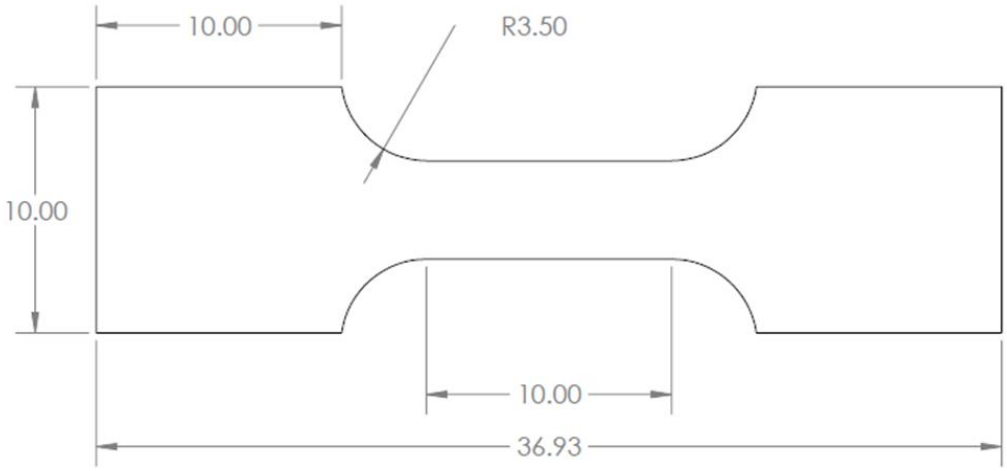

Figure 3.13. Dogbone dimensions for BNNP and BNNT foam-reinforced CE composites.

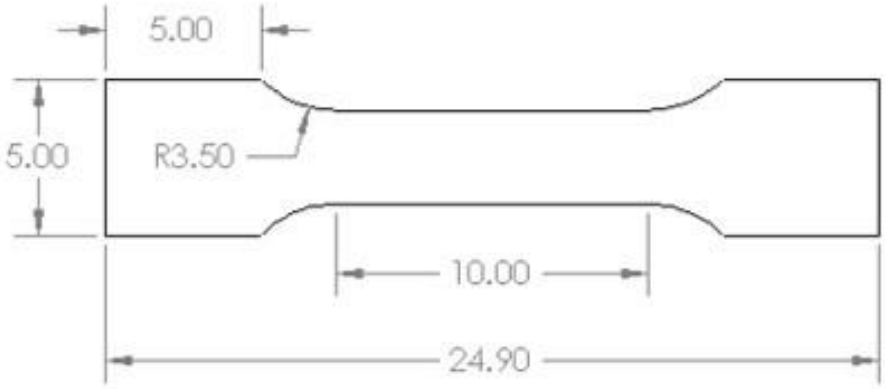

Figure 3.14. Dogbone dimensions for BNNT reinforced CE composites.

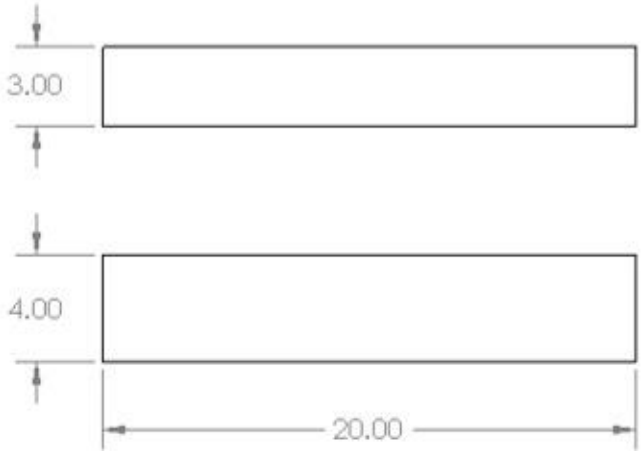

Figure 3.15. DMA specimen dimensions.

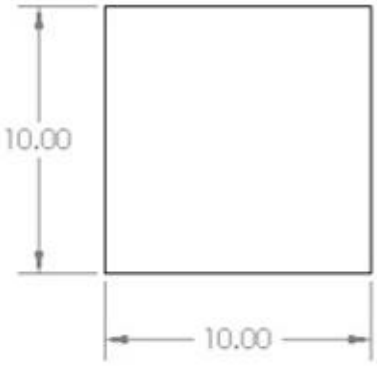

Figure 3.16. Flash diffusivity specimen dimensions

3.6 Characterization

Thermal. The thermal stability of these nanocomposites was evaluated through thermal gravimetric analysis (TGA) (SDT Q600, TA Instruments) with a heating rate of 10°C/min from room temperature to 1000°C in air in alumina crucibles. The dynamic heating cure kinetics (curing activation energies) were determined using differential scanning calorimetry (DSC) (SDT Q600, TA Instruments) with heating rates ranging from 2°C/min to 15°C/min in air to 350°C. Curing is characterized by a broad exothermic peak in the heat flow vs temperature plot. The temperature corresponding to this maximum peak

is denoted by T_p. The T_p shifts with increasing heating rates (β), therefore the Kissinger method was used to calculate the curing activation energy (E_a). The Kissinger equation can be defined as:

Equation 3.2. Kissinger equation

$$\ln\left(\frac{\beta}{{T_p}^2}\right) = -\frac{E_a}{RT_p} + ln\frac{AR}{E_a}$$

where R is the universal gas constant. The curing activation energy can be estimated by plotting $\ln(\beta/T_p^2)$ vs $1/T_p$ and taking the linear fit slope. The pre-exponential factor A is estimated by finding the y-intercept of this line. Thermal conductivity was obtained through a laser flash technique (NETZSH LFA 467 HT HyperFlash, Selb, Germany) at temperatures between 25 and 205 °C, with a 20 °C/step. The samples were cut into 10mm squares, seen in Figure 3.16 with thicknesses between 1-3mm using a waterjet machine and coated using a graphite spray.

Chemical. *In situ* Fourier-transform infrared (FTIR) (Thermal Fisher Scientific) spectroscopy, as seen in Figure 3.17, was used to compare the IR spectra during the curing process to determine how the BNNTs affected curing kinetics. The FTIR was equipped with a golden gate heated top-plate and controller that could control the temperature to 200°C. The diamond crystal of the FTIR was cleaned using ethanol followed by DI water before each sample and a background scan was completed. 100µL of resin was placed on top of the diamond crystal of the FTIR stage and covered using an alumina crucible to prevent air from further cooling the sample, as seen in Figure 3.18. Measurements began at room temperature and then followed the manufacturer-recommended curing parameters,

with measurements collected every 15 minutes between the wavenumber range 400cm^{-1} – 4000cm^{-1} with a spectral resolution of 0.482cm^{-1} collected over an average of 32 scans.

Figure 3.17. The FTIR setup for *in situ* chemical analysis during curing.

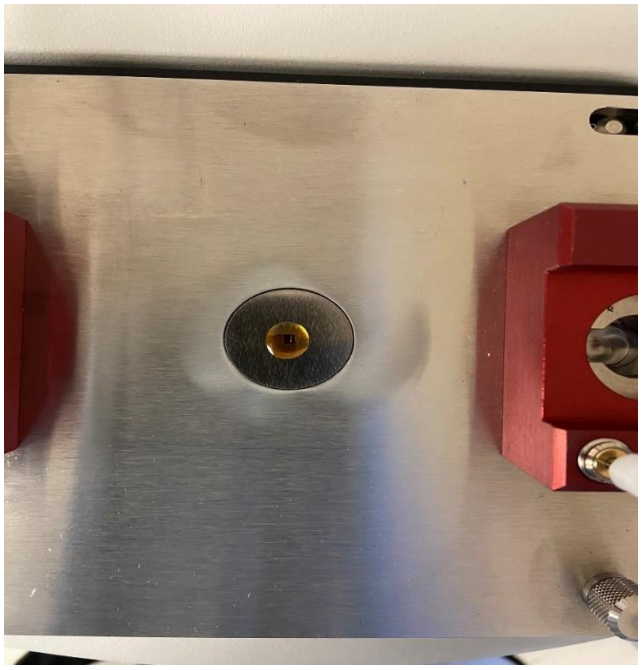

Figure 3.18. Cyanate ester resin on the FTIR sapphire crystal heating stage.

The first measurement was taken at room temperature and then the heating stage was turned on to 150°C. Before the next reading at 15 minutes, the sample was already uniformly heated to that temperature. After 4 readings at 150°C, the heating stage was set to 200°C. The measurements were conducted for 3 hours at this temperature. 200°C is the maximum temperature allowed by the heating stage on the FTIR, so the samples were not able to fully cure. FTIR was also used to compare the IR spectra between the cured composites. Cured samples were firmly pressed against the sapphire crystal on the FTIR using a torque-controlled knob. Measurements were conducted with a spectral resolution of 0.482cm^{-1} collected over an average of 32 scans.

Visual. A field emission scanning electron microscope (FE-SEM JEOL JSM-F100, JEOL Ltd. Tokyo, Japan) was used to observe the quality of dispersion of the BNNTs in the cyanate ester matrix and their morphology at a microscopic scale length. SEM specimens were prepared by fracturing the cured samples with a hammer. The fractured surfaces were placed facing upwards on a square copper plate (25 x 25 mm) and adhered using silver paste. The samples were gold coated twice for a total time of 100s. Each coating is estimated to deposit 50nm of gold. This gold coating helped prevent charging and drift during SEM imaging. An accelerating voltage of 3 kV was found to work well during imaging with standard and high-resolution modes of the SEM. An optical microscope (Zeiss Axioscope 5) was used to observe the quality of the dispersion at a macroscopic scale length. For optical microscopy, samples were polished to a 0.1µm surface roughness.

Mechanical. The elastic modulus and hardness of the samples were determined using quasi-static nanoindentation (Hysitron, Triboindenter TI-900). A diamond Berkovich tip with a radius of 10nm was used to indent the composites in load-controlled mode to a maximum load of 2mN. The loading function followed a 10s-5s-10s load, hold, and unload function respectively. The data was collected at a rate of 60 points/s. The Oliver-Pharr analytical model was used to analyze the load-displacement curve and calculate the hardness and elastic modulus.

Dynamic mechanical analysis (DMA) (insert name/ Netsch) was conducted to determine the effect of BNNTs on the stiffness of the polymer chains in the composites. Rectangular beams were cut using a waterjet to the dimensions of 4mm wide x 20mm long x 3mm thick seen in Figure 3.15. 3-point bend tests, with a gauge length of 10mm, were operated at a frequency of 1hz and displacement of 10μm from room temperature to 250°C with a ramp of 3°C/min.

NanoDMA (Triboindenter TI-900, Hysitron) allowed for localized DMA measurements to be assessed. Samples were cut to a thickness of 1mm which can be seen in Figure 3.19. The samples were placed on a glass slide and run using a frequency sweep between 10 - 300 Hz, a static force of 50μN, a dynamic force of 2.5μN (5% of the static force), and a conospherical probe geometry with a diameter of 1μm. The relationship between amplitude and damping was evaluated against frequency.

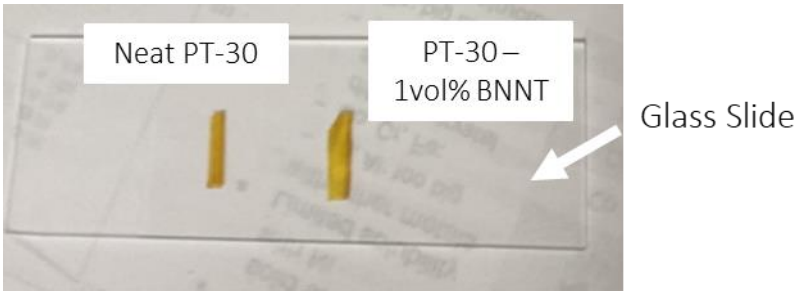

Figure 3.19. Neat PT-30 and PT-30 + 0.5vol% BNNT samples that were prepared for nanoDMA.

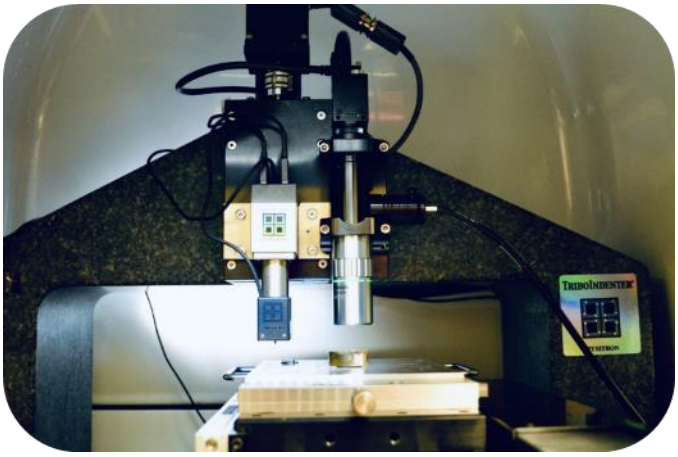

Figure 3.20. NanoDMA setup

Tensile testing was conducted using a linear, screw-driven micro-load frame (SEM tester 1000, MTI Instruments Inc.), seen in Figure 3.21. Dog bone-shaped samples were cut using a waterjet with a gauge length of 10mm, thickness of 3mm, radius of 3.5mm, and grip size of 5x5mm and 10x10mm, seen in Figure 3.13 and Figure 3.14. A displacement rate of 0.1 mm/min was used until complete fracture. A 4000N capacity load cell was used to measure the applied load on the sample. A stereoscope (Amscope, Irvine, CA) was used to capture real-time video of the tensile test. No additional lenses were installed and a magnification of 0.7x was used to visualize the entire gauge length of the samples. The true

displacement was measured from the corresponding real-time video using the image processing software ImageJ (National Institutes of Health, USA).

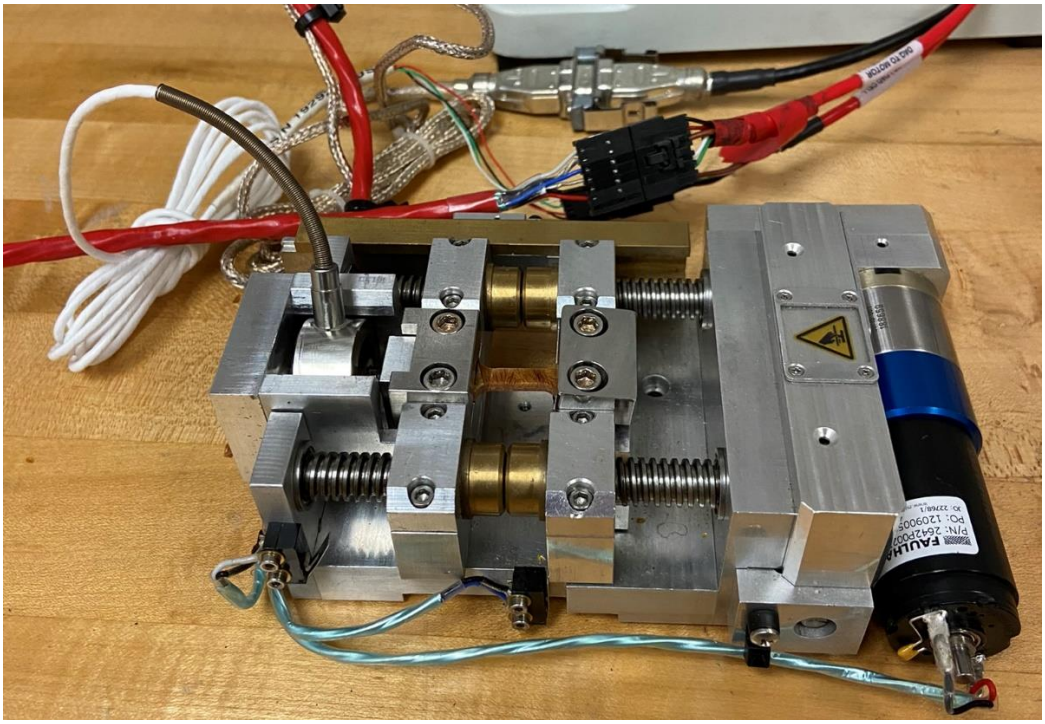

Figure 3.21. MTI Tensile tester apparatus.

In situ tensile testing was also conducted using a high-speed camera (i-Speed 727, iX Cameras, Woburn, MA). The goal was to visualize the crack propagation during fracturing from tension. The cyanate ester is very brittle and therefore fractures rapidly. Normal camera shutter speeds are not fast enough to capture these events. Therefore, a high-speed camera was utilized with frame rates ranging from 100,000 to 150,000 frames per second. At this frame speed, the resolution of the image is about 840x134 pixels. Specialized high-lumen outputting lights have to be used to properly illuminate the sample for these fast frame rates. The entire setup can be seen in Figure 3.22. The videos were edited and formatted using the video editing software Davinci Resolve.

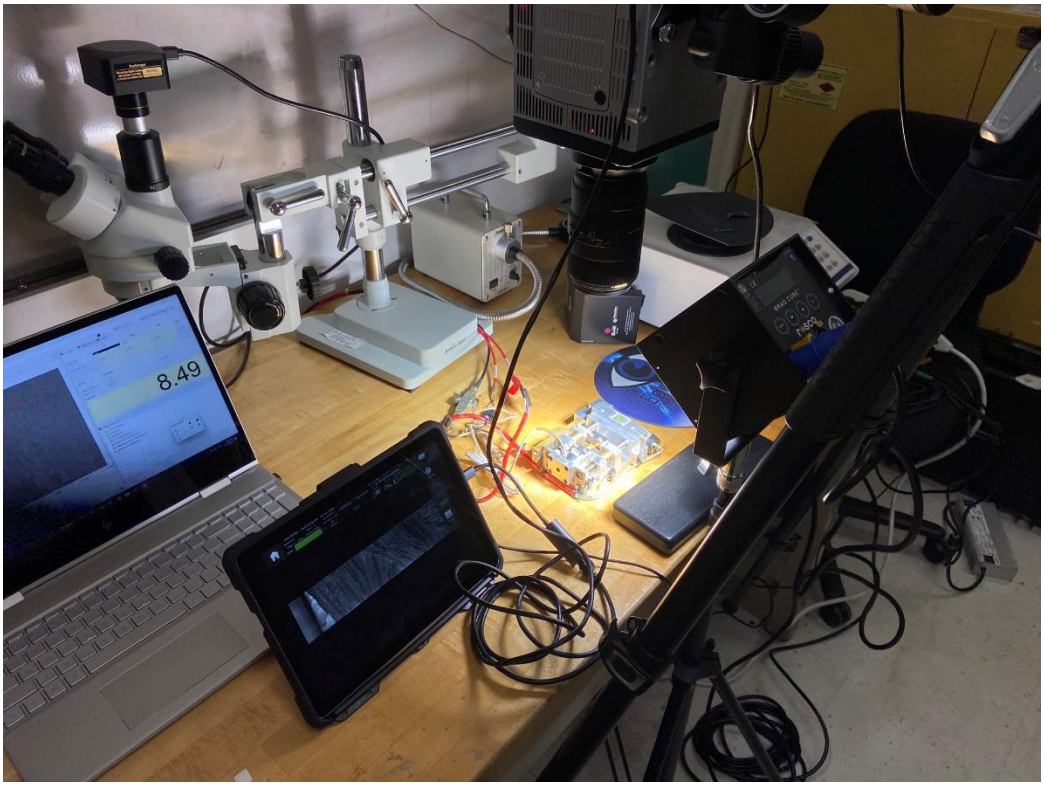

Figure 3.22. *In situ* high-speed tensile testing setup.

Quasi-Static Nanoindentation. *In-situ* nanoindentation characterizations were performed to visualize and evaluate localized mechanical phenomena and failure across the cyanate ester and foam composite architecture. Micro-pillars of dimensions 10µm in diameter by 10µm in height were fabricated using a fixed ion beam (FIB) (JEOL-JIB 4500 Multi-Beam Focused Ion Beam, Tokyo, Japan). The FIB uses accelerated gallium ions to locally erode material from the surface. Unfortunately, these ions are also implanted into the surface of the sample. Thus, it is important to mitigate the effects of this implantation so that the mechanical properties are not affected. One way to do this is to cover the top surface of the material with tungsten.

The foam-reinforced cyanate ester micro-pillars were mounted on the stage of an in situ Picoindenter (Hysitron PI 87, Minnesota, USA). The stage was installed inside a field emission scanning electron microscope (FE-SEM JEOL JSM-F100, JEOL Ltd. Tokyo, Japan). The SEM allowed for the capture of real-time videos showing the strain evolution and failure in the pillars as a function of applied indentation displacement. A diamond cylindrical flat punch tip of 10μm diameter was used to apply localized loads. The cylindrical probe geometry was utilized because it creates a homogeneous distribution of the load on the top of the pillar and therefore has a low-stress concentration factor. Quasi-static displacement-controlled nanoindentation tests were performed by programming the maximum indentation depth of 5μm with a loading–unloading rate of 0.1μm/s. An indentation depth of 5μm was selected to induce a large enough deformation to fracture the sample and witness the behavior of the interface between the hierarchical structure of interconnected walls and bridges and the cyanate ester.

Chapter 4 Results and Discussion

The objective of this research is to enhance the thermal and mechanical properties of cyanate esters (CE), expanding their potential applications. Previous literature has shown that the degradation mechanism of cyanate esters is related to the cutting of hydrocarbon chains, leading to a domino effect that compromises the stability of the triazine ring. However, covalently bonding a thermally stable and hydroxyl-functionalized additive and forming an imino-carbonate linkage has proven to be effective in reinforcing the chains. While materials like POSS, graphene oxide, and carboranes have been explored in previous studies, boron nitride nanotubes (BNNTs) offer superior thermal stability and mechanical strength. In this study, we leveraged the exceptional properties of hydroxyl-functionalized BNNTs to covalently bond with cyanate esters to form an imino-carbonate linkage (Figure 4.1) and further enhance the mechanical and thermal properties of cyanate ester composites.

4.1 Boron nitride nanotube (BNNT) reinforced cyanate ester composites

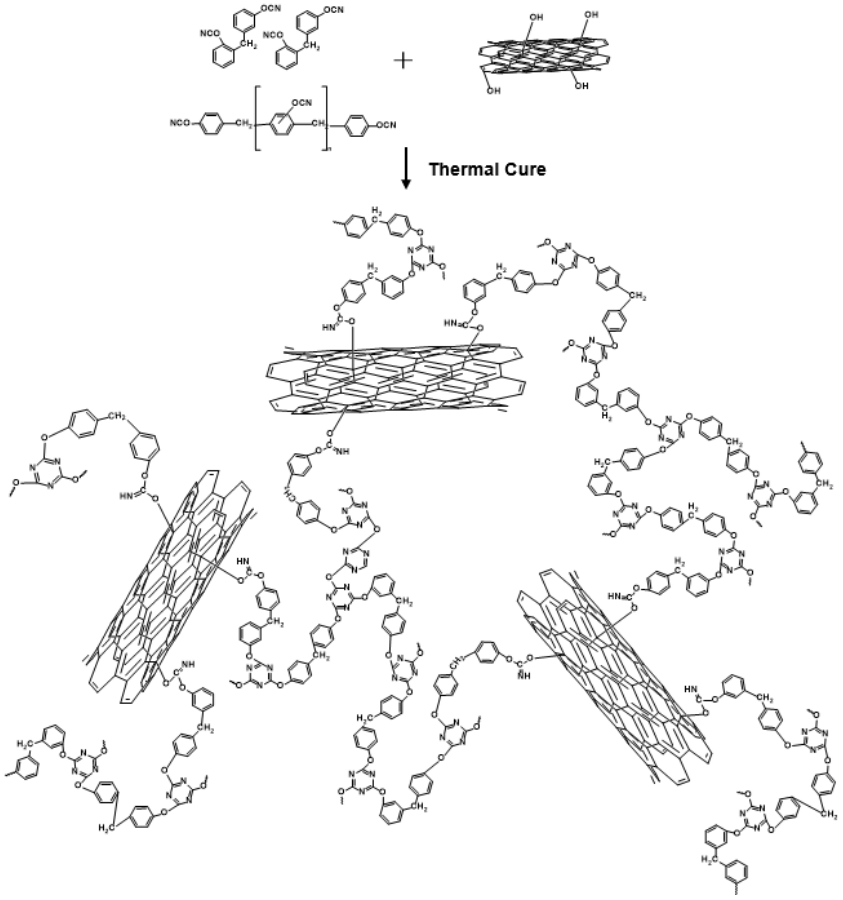

Figure 4.1. BNNTs forming imino-carbonate bonds with cyanate ester.

The morphology of boron nitride nanotubes (BNNTs) is a crucial factor in determining the effectiveness of the reinforcement they provide to composite materials. The length, number of walls, and texture of BNNTs can greatly influence the mechanical and thermal properties of the resulting composites. Therefore, it is essential to fully characterize the BNNTs morphology throughout the different manufacturing processes. Scanning electron microscopy (SEM) was used to investigate the morphology of BNNTs after various manufacturing steps. By analyzing SEM images of the BNNTs, the extent of

any morphological changes that have occurred during the manufacturing process was determined and how these changes may impact the performance of the resulting composite.

To begin with, a small section of as-received boron nitride nanotubes (BNNTs) was extracted from the larger cotton ball structure and attached to a copper plate using silver paste. Unlike some other imaging methods, gold or carbon coatings were not used to ensure the true morphology of the BNNTs was visualized. The sample was analyzed using scanning electron microscopy (SEM) with an accelerating voltage of less than 1kV, and the resulting micrographs are presented in Figure 4.2. The SEM images show that the BNNTs are highly agglomerated and entangled, making it difficult to determine their length accurately. However, the images reveal that the width of the BNNTs ranges from 10-50nm. Although the entanglement of the BNNTs complicates their characterization, these SEM images provided valuable insight into the morphology of the as-received BNNTs and will inform further investigations into their potential use as reinforcement materials in composite materials.

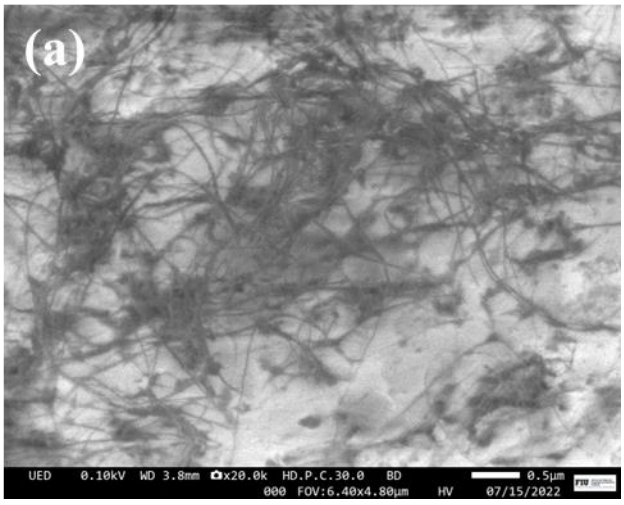

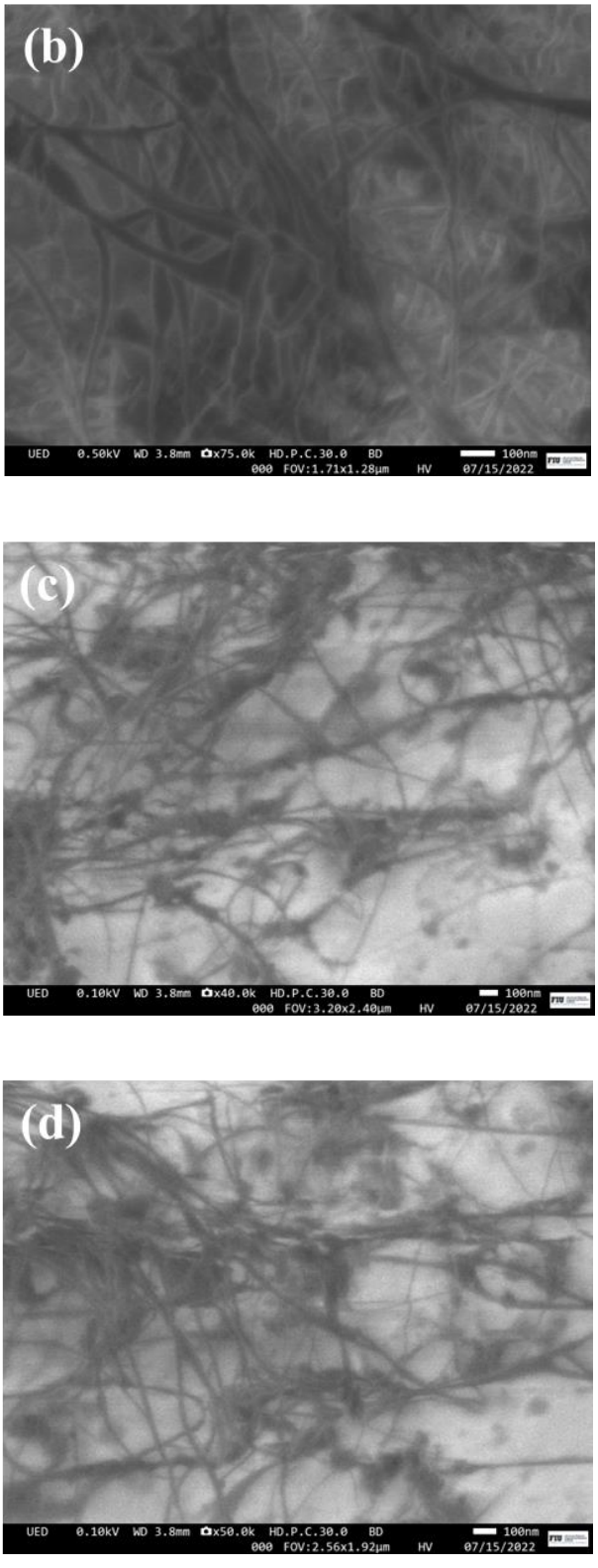

Figure 4.2. SEM images of as-received BNNTs

Dispersing and functionalizing boron nitride nanotubes (BNNTs) with hydroxyl groups are critical steps in this study. The BNNTs were tip ultrasonicated in DI water for 30 minutes at 40% amplitude the method outlined by Lu et al [10]. The B-N bonds near defect sites are prone to attack from by O atoms of H_2O molecule resulting in cutting open and unzipping of the BNNT during ultrasonication. These unzipped edges are then stabilized by the -OH groups, thus functionalizing the BNNTs. Since H_2O and –OH are both polar species, the electron clouds result in dipole-dipole interactions and a reduction in free energy, thus stabilizing the BNNTs in DI water and allowing for improved dispersion. This partial unzipping and dispersion of the BNNTs was examined using SEM. Specifically, BNNTs were tip ultrasonicated in DI water, and 10 µL of the resulting solution was deposited onto the back of a copper TEM grid with a mesh of 300. The grid was then adhered to a copper plate using a circular piece of carbon tape. SEM imaging was conducted with an accelerating voltage of 1kV, using the upper electron detector (UED) inside the SEM column with high-resolution mode selected. From the SEM images, seen in Figure 4.3, it can be observed that the BNNTs have been shortened to a length of 1-5µm, and many of them have become partially unzipped, especially in Figure 4.4d, suggesting that the hydroxyl functionalization has occurred. These observations suggest that our manufacturing process for functionalizing and dispersing the BNNTs is suitable for use in our composite materials and further analysis.

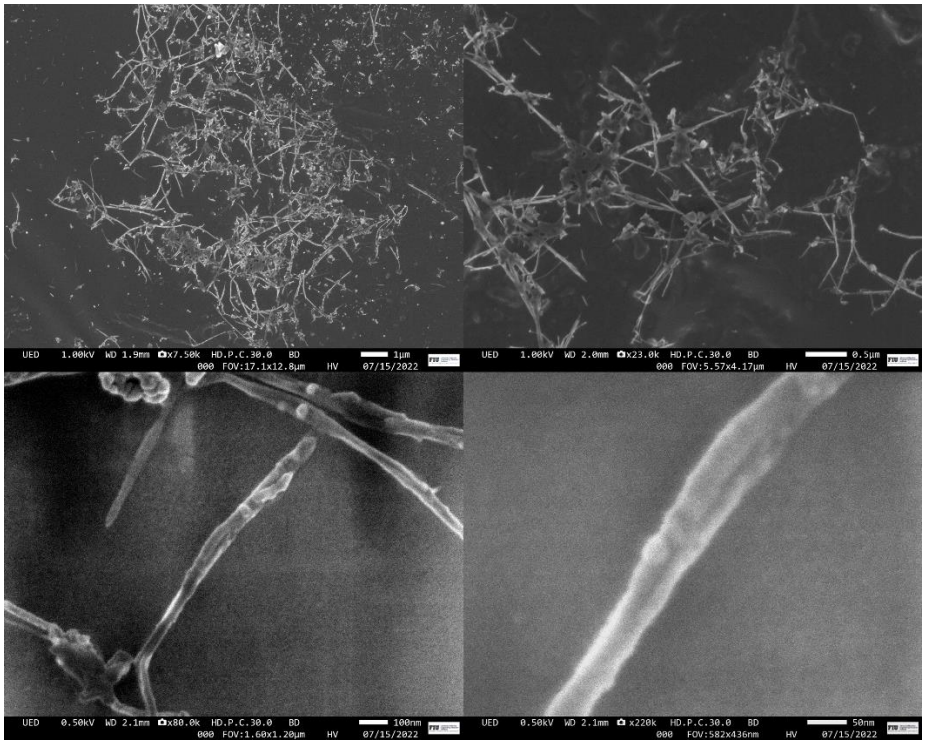

Figure 4.3. SEM images of BNNTS that were dispersed in DI water

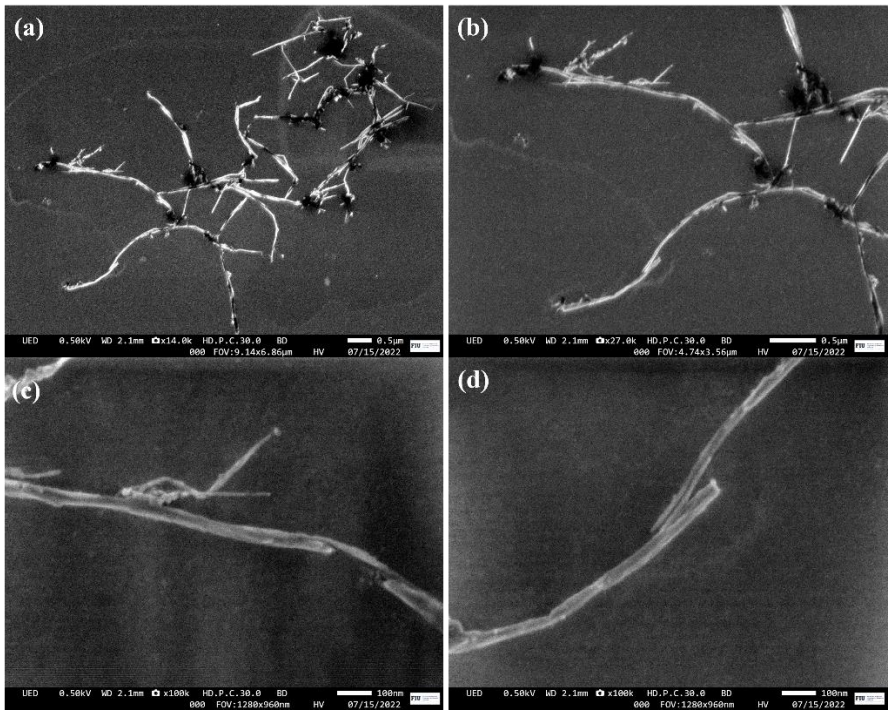

Figure 4.4. SEM images of BNNTs highlighting the unzipping due to functionalization

To further investigate the morphological changes of BNNTs due to tip sonication in DI water, such as the shortening and unzipping behavior, the SEM images of BNNTs dispersed in DI water were compared with those dispersed in IPA. BNNTs were tip ultrasonicated in IPA for 30 minutes with an amplitude of 40%. 10 µL of the resulting solution was deposited onto the back of a copper TEM grid with a mesh of 300 and then adhered to a copper plate using a circular piece of carbon tape. SEM imaging was performed using the upper electron detector (UED) and high-resolution mode with an accelerating voltage of 1kV. The SEM images of the BNNTs, seen in Figure 4.5, reveal that there is still shortening of the BNNTs, but they are longer than the BNNTs that were dispersed in the DI water. Although some damage to the BNNTs was observed, the unzipping behavior was not observed. These results further show that the BNNTs dispersed in DI were functionalized.

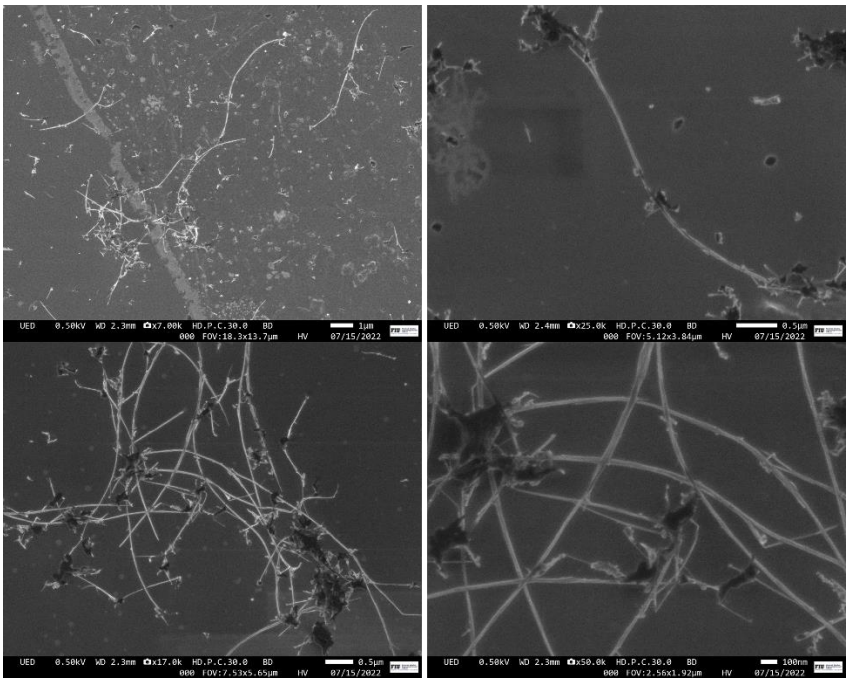

Figure 4.5. SEM images of BNNTs that were dispersed using IPA.

Fourier Transform Infrared Spectroscopy (FTIR) was employed to analyze the chemical composition of BNNTs and to identify any functional groups on their surfaces. Two separate solutions of BNNTs were prepared: one using isopropyl alcohol (IPA) to measure the chemical composition of pure BNNTs, and one using deionized (DI) water to detect the presence of hydroxyl functional groups. The solutions were prepared using the tip-sonication method described previously, and 100 µL of each solution was deposited onto a diamond crystal for FTIR analysis. After allowing the solvents to evaporate, a thin film of BNNTs remained on the diamond crystal. FTIR spectra were then collected between the wavenumbers 400cm^{-1} and 4000cm^{-1} and can be seen in Figure 4.6 and Figure 4.7. The resulting spectrums showed peaks corresponding to the characteristic stretching vibrations of the B–N bonds (811cm^{-1} and 1361cm^{-1}) and the O–H bonds from functional groups attached to the surface of the BNNTs at 3219 cm^{-1}. The pure BNNTs have a slight peak in the same area, but this is due to trapped moisture within the BNNTs. The two spectra were overlapped in Figure 4.8 to better visualize the changes in the peaks. Since this new broad hydroxyl peak was not observed in the spectrum of the pristine BNNTs, it confirms the presence of chemical functionalization. These results demonstrated that the hydroxyl functional groups were bonded to the BNNTs, which is required for forming the desired imino-carbonate linkage with the cyanate ester.

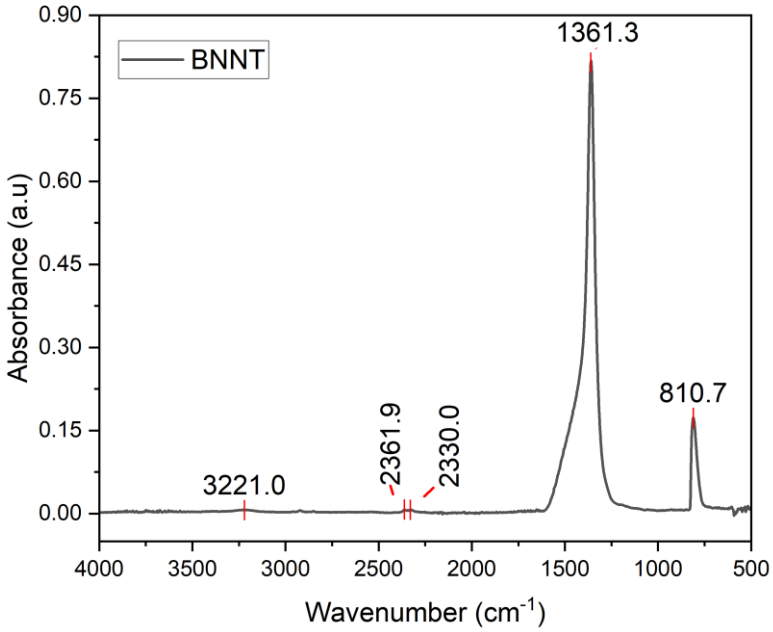

Figure 4.6. FTIR spectra between 500cm^{-1} and 4000cm^{-1} for BNNTs.

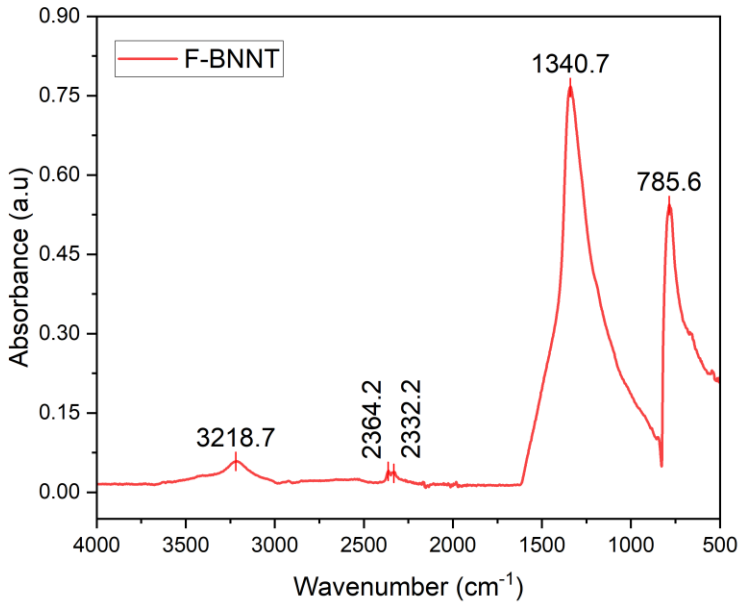

Figure 4.7. FTIR spectra between 500cm-1 and 4000cm-1 for functionalized BNNTs.

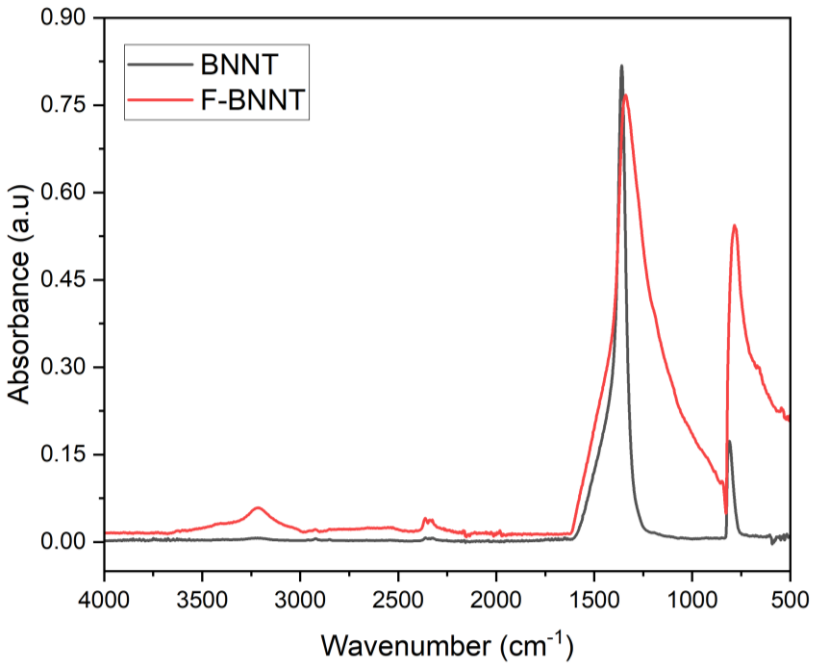

Figure 4.8. Overlapping FTIR spectra of BNNTs before and after functionalization

Thermogravimetric analysis (TGA) was used to evaluate the effect of adding boron nitride nanotubes on the thermal stability of cured cyanate ester (CE) samples. We tested pure CE, CE with 0.5 vol% of BNNTs, and CE with 0.5 vol% of functionalized BNNTs (F-BNNTs) in air, heating them from room temperature to 1000°C at a rate of 10°C/min. The results, seen in Figure 4.9, clearly show that while pure CE degraded completely at 1000°C, the addition of 0.5 vol% of BNNTs increased the char yield to 3.68%. The functionalized BNNTs further improved the char yield to 5.29%, as we had hypothesized.

The addition of functionalized BNNTs had an interesting effect of inhibiting the initial stages of degradation and delaying the onset of the second stage of degradation by about 4°C as seen in Figure 4.10. While previous studies have reported a decrease in the glass transition temperature (Tg) upon adding nanoparticles to cyanate ester (CE), our results show that the Tg remains unchanged after adding BNNTs, as illustrated in Figure

4.11. This finding suggests that BNNTs can improve the thermal stability of CE without negatively impacting its mechanical properties. The delay in the onset of degradation is particularly significant, as it indicates that the addition of BNNTs can prolong the useful lifespan of CE-based materials in high-temperature applications. Further research is needed to investigate the mechanism behind this effect and optimize the BNNT content for specific applications.

Previous studies have shown that increasing the loading of reinforcement additives can lead to further improvements in the thermal stability of CEs, including the final char yield[2], [35], [82]. Given the beneficial effects of functionalized BNNTs observed in our study, it is reasonable to expect that increasing the concentration of BNNTs would result in an even higher char yield. Moreover, BNNTs have been reported to be more efficient reinforcement agents than other nanoparticles due to their high aspect ratio and superior mechanical properties. Therefore, further optimization of the BNNT content and processing conditions could lead to significant improvements in the thermal stability and mechanical properties of cyanate ester composites.

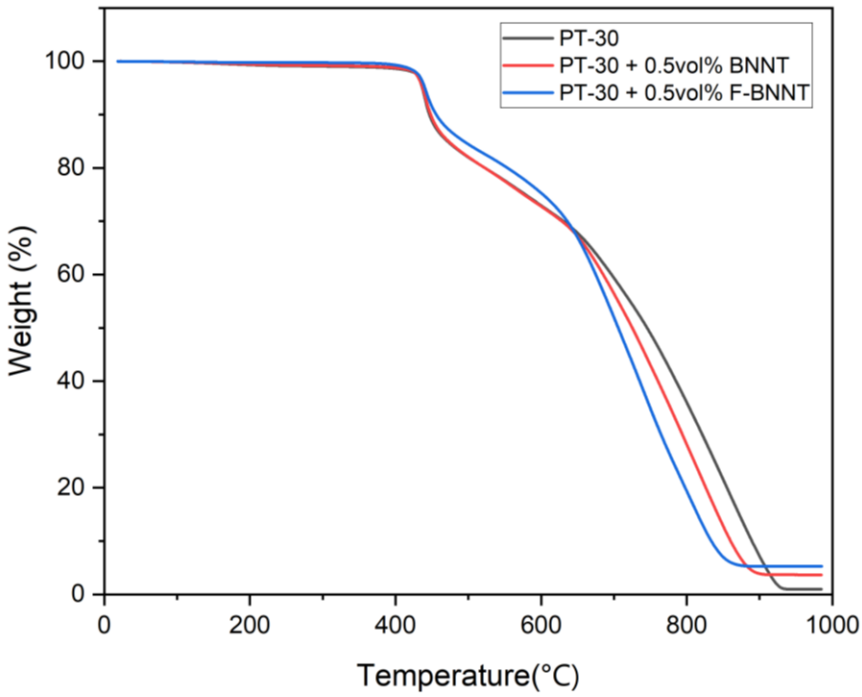

Figure 4.9. Thermal degradation in air to 1000°C for pure PT-30 and with the addition of BNNTs and functionalized BNNTs.

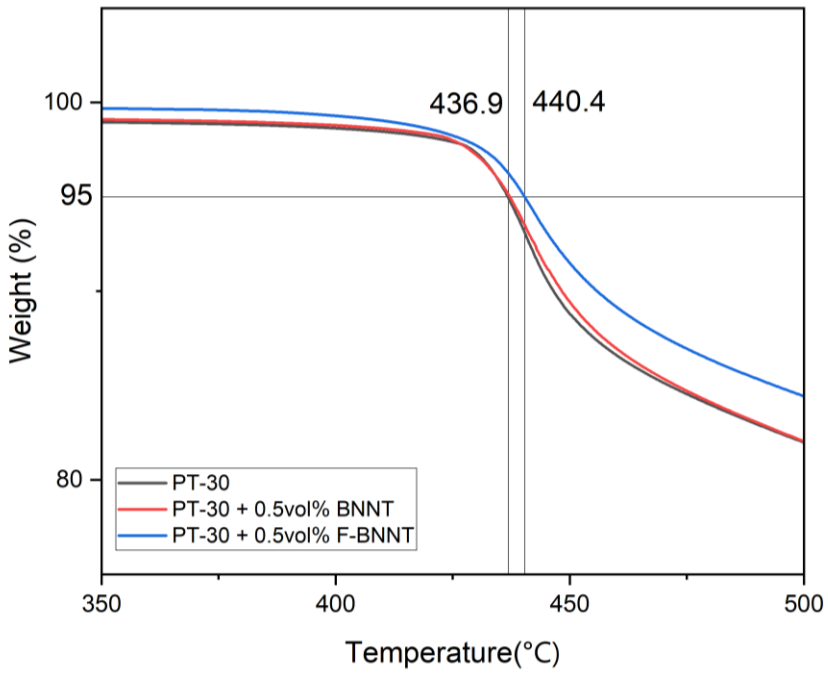

Figure 4.10. Zoomed in thermal degradation in air from 350 – 500°C for pure PT-30 and with the addition of BNNTs and functionalized BNNTs.

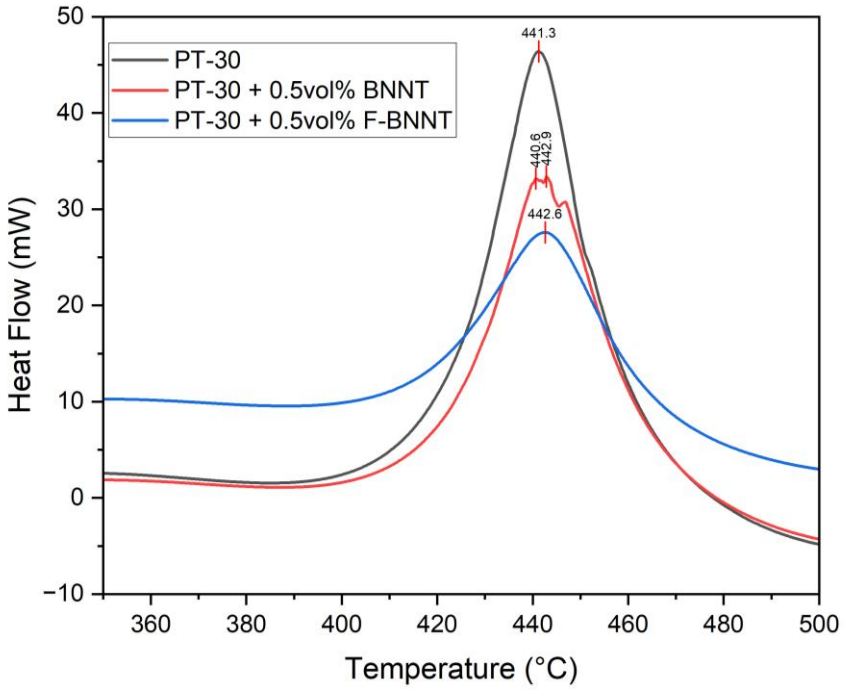

Figure 4.11. Zoomed in heat flow vs temperature from 350 – 500°C for pure PT-30 and with the addition of BNNTs and functionalized BNNTs.

Figure 4.12 compares the normalized FTIR spectra of functionalized BNNTs, pure PT-30, and PT-30 with 1vol% BNNTs. The PT-30/BNNT sample shows a very broad peak at 3367 cm^{-1} and a sharp peak at 1592 cm^{-1}, which can be attributed to the N-H group. This suggests that the -OH group on the BNNT reacted with the cyanate group -OCN to form -O-(C=NH)-O-. The new imine bond (C=N) found in this imino-carbonate link is indicated by the appearance of a new peak at 1710 cm^{-1}. The peak at 2260 cm^{-1} corresponds to the cyanate group -OCN, which can either form the triazine ring or react with -OH groups during the curing process.

Notably, the reduction in the 2260 cm^{-1} peak intensity observed in the PT-30/BNNT sample indicates a higher degree of curing compared to pure PT-30. This finding suggests that the introduction of BNNTs has further improved the curing efficiency of PT-30, which

could result in a more homogeneous and durable material. The formation of the imine bond (C=N) and the absence of any significant changes in the other peaks suggest that the functionalized BNNTs have reacted with the cyanate groups to form imino-carbonate linkages and contributed to the crosslinking network, which is crucial for improving the mechanical and thermal properties of polymer composites.

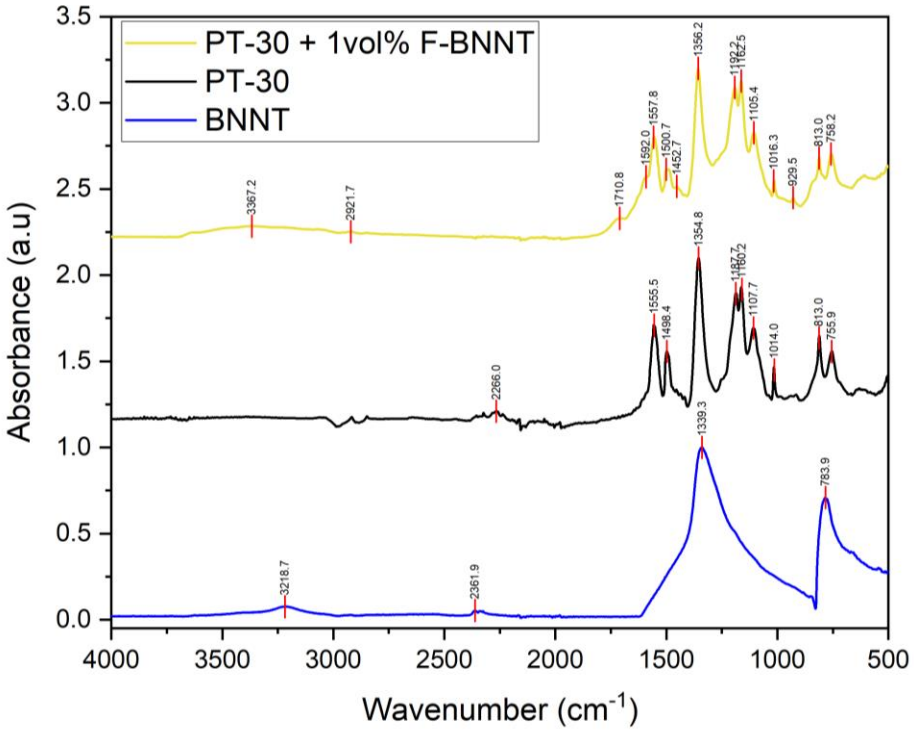

Figure 4.12. Comparison of FTIR spectra between functionalized BNNTs, cured PT-30, and cured PT-30 + 1vol% BNNT.

To investigate the impact of BNNTs on the curing kinetics of cyanate ester, we employed in situ FTIR spectroscopy to compare the spectra of neat PT-30 with a composite containing 1vol% F-BNNT at various stages of the manufacturer-recommended curing process. The first measurement was taken before heating, indicated as time zero, to represent the resin's initial state. Subsequently, the heating stage was activated, and the

curing process began, reaching the first stage (150°C) within 15 minutes, at which point another measurement was taken. The FTIR spectra were collected at different stages to enable a thorough analysis of the curing process's effect on the composite. These spectra were normalized and stacked with respect to time to appropriately quantify and compare the changes in peaks and absorbance intensity, as seen in Figure 4.13.

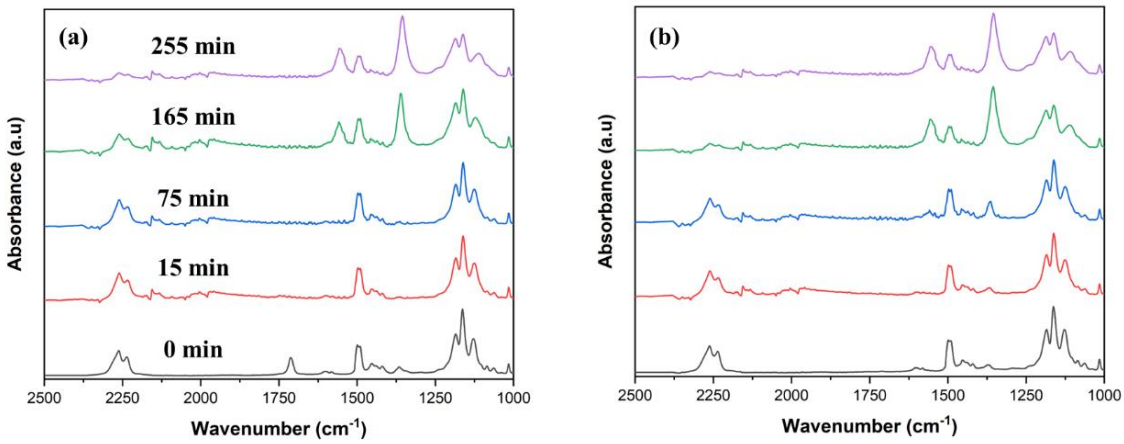

Figure 4.13. FTIR spectra of (a) PT-30 and (b) PT-30 + 1vol% F-BNNT at different curing stages

After reaching the 15-minute mark, the manufacturer-recommended curing cycle was initiated, which consisted of maintaining the temperature at 150°C for 60 minutes, followed by a three-hour period at 200°C. Due to the limitations of the FTIR heating stage, we were unable to reach the final curing step of 260°C. The FTIR spectra collected during the curing process in Figure 4.13 revealed the disappearance of the -OCN peaks at 2236 cm^{-1} and 2262 cm^{-1}, while the emergence of triazine ring peaks at 1355 cm^{-1} and 1554 cm^{-1} was observed, consistent with previous literature.

The addition of functionalized BNNTs to the resin resulted in a faster emergence of the triazine ring absorbance peaks and a reduction of the cyanate ester peaks, as clearly

indicated by the spectra at the 75-minute mark. To further investigate this phenomenon, the intensity ratio of the -OCN absorbance peak at 2262 cm^{-1} was normalized with reference to the phenyl absorbance peak (1500 cm^{-1}) (I_{OCN}/I_{Phenyl}), which remains unaffected by the curing process. Similarly, the ratio of the intensity of the triazine ring peak (1355 cm^{-1}) was normalized to the phenyl absorbance peak ($I_{Triazine\ Ring}/I_{Phenyl}$). The resulting ratios are presented in Figure 4.14 and Figure 4.15, respectively. It is observed that the absorbance intensity for the -OCN peak decreased more rapidly in the presence of functionalized BNNTs than in neat resin. These cyanate ester bands can either react with free hydroxyl groups on BNNTs or cyclotrimerize to form triazine rings. Therefore, the decrease in I_{OCN}/I_{Phenyl} is likely due to the -OH group on the BNNTs reacting with the -OCN group to form the imino-carbonate linkage -O-(C=NH)-O-.

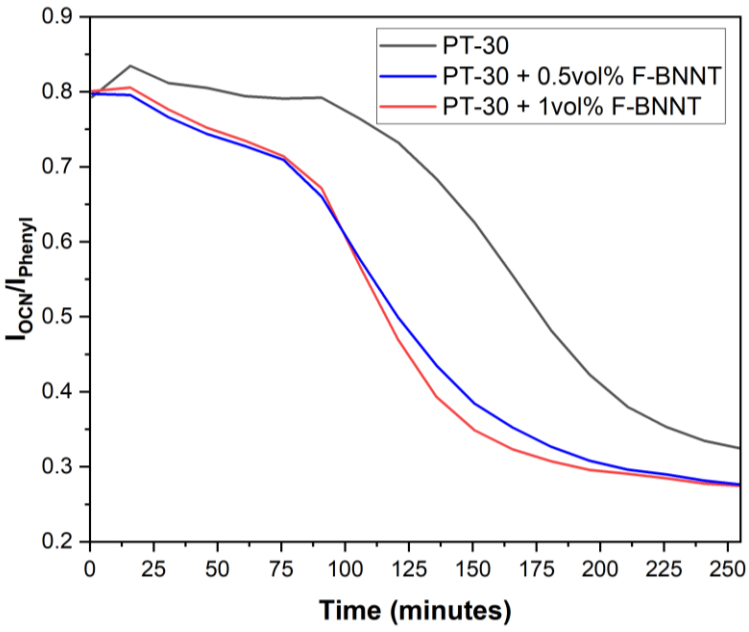

Figure 4.14, The normalized intensity of the cyanate ester peak with reference to the phenyl reference peak for different volumetric loadings of BNNTs.

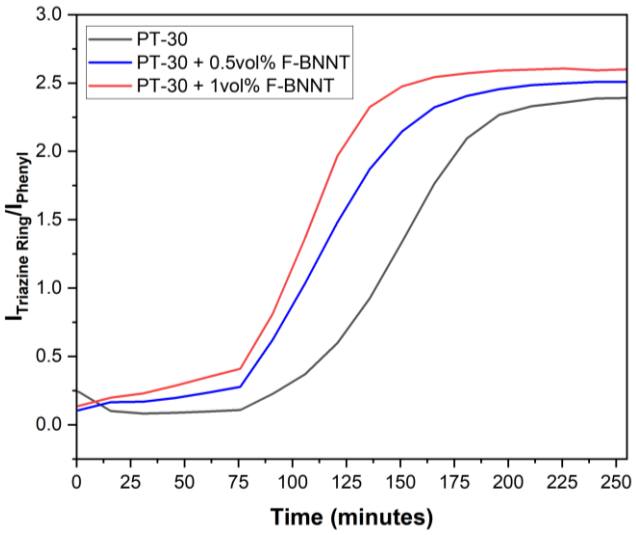

Figure 4.15. The normalized intensity of the triazine ring peak with reference to the phenyl reference peak for different volumetric loadings of BNNTs.

To quantify the change in the overall intensity of each bond over time, the area under the normalized curves was integrated and the results are presented in Figure 4.16. For the -OCN peak, it is observed that there is a 18.95% decrease in overall area with the addition of 0.5vol% BNNTs and a 20.26% decrease with the addition of 1vol%.

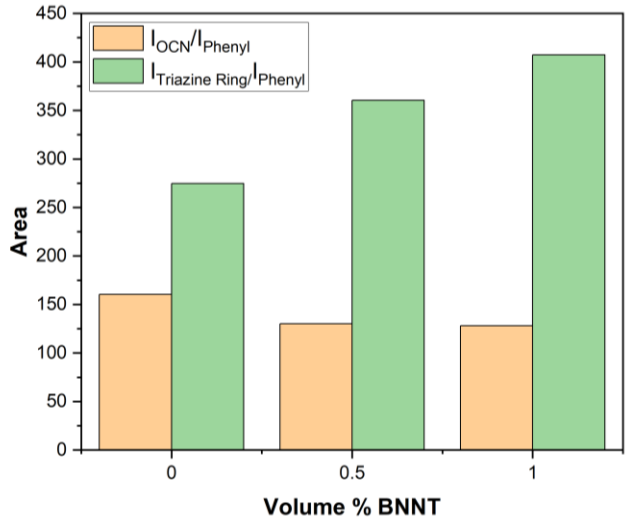

Figure 4.16. The area under the curves for the cyanate ester and triazine peak normalized by the phenyl peak from time 0 to 255 minutes of curing.

The disappearance of the -OCN peak can be correlated to the degree of cure (α), which was calculated at each time interval using Equation 4.1 and is presented in Figure 4.17.

Equation 4.1. Degree of cure

$$\alpha(t) = 1 - \frac{I_{OCN}(t)/I_{Phenyl}(t)}{I_{OCN}(0)/I_{Phenyl}(0)}$$

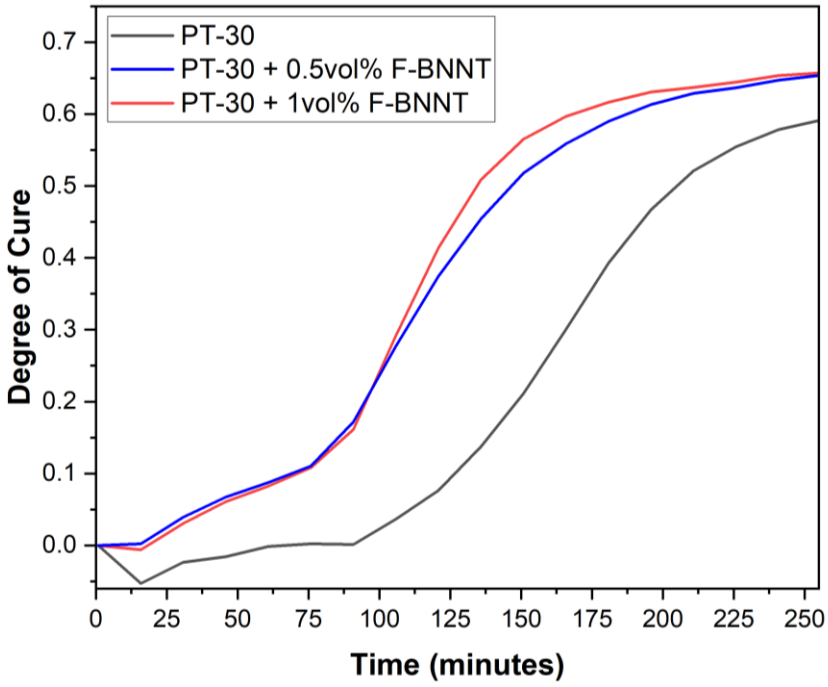

Figure 4.17. Calculated degree of cure

The addition of BNNTs was found to enhance the rate and final degree of cure. Specifically, the degree of cure increased by 10.52% and 11.08% with the addition of 0.5 and 1.0 vol% BNNT, respectively. However, the final degree of cure did not reach 100% as the FTIR spectra could only be obtained up to 200°C, whereas the manufacturer-recommended final curing step is completed at 260°C. The minimal increase in degree of cure from 0.5 to 1.0 vol% BNNT could be attributed to the hindrance of cross-linking of the polymer chain at higher volumetric loadings, as reported in the literature for other 2D

materials[82]. Additionally, the increase by ~48% at 1.0 vol% in the $I_{Triazine\ Ring}/I_{Phenyl}$ ratio suggests that the BNNTs act as a catalyst for the cyclotrimerization reaction at an early stage during the curing process.

To gain further insight into how BNNTs affect the curing kinetics, the curing activation energies (E_{ac}) were calculated using dynamic differential scanning calorimetry (DSC) experiments. The Kissinger method, shown in Equation 3.2, was used to calculate the curing activation energy, as cyanate esters typically exhibit first-order kinetics during curing. The left plots in Figure 4.18 - Figure 4.20 show the DSC heat flow vs temperature curves for neat PT-30 resin, with the addition of 0.5vol% BNNT, and with the addition of 1vol% BNNT, respectively. The curing activation energy was estimated by plotting $\ln(\beta/Tp2)$ vs $1/T_p$, and the slope of the linear fit was taken to be the curing activation energy (E_{ac}) value. The pre-exponential factor A was estimated by finding the y-intercept of this line. A comparison between the curing activation energies and pre-exponential factors are presented in Figure 4.21.

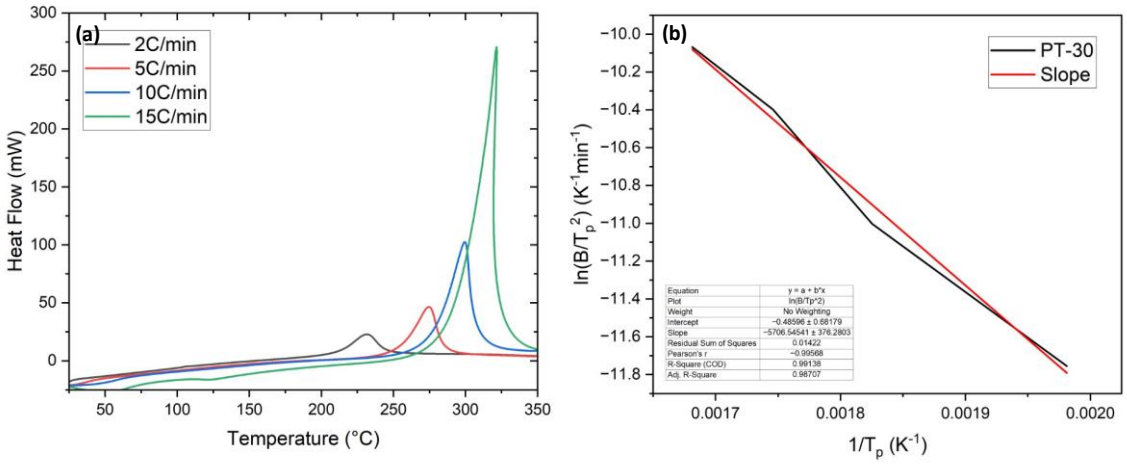

Figure 4.18. (a) DSC heat flow scans for PT-30 and (b) Kissinger plot used for calculating activation energy and pre-exponential factor

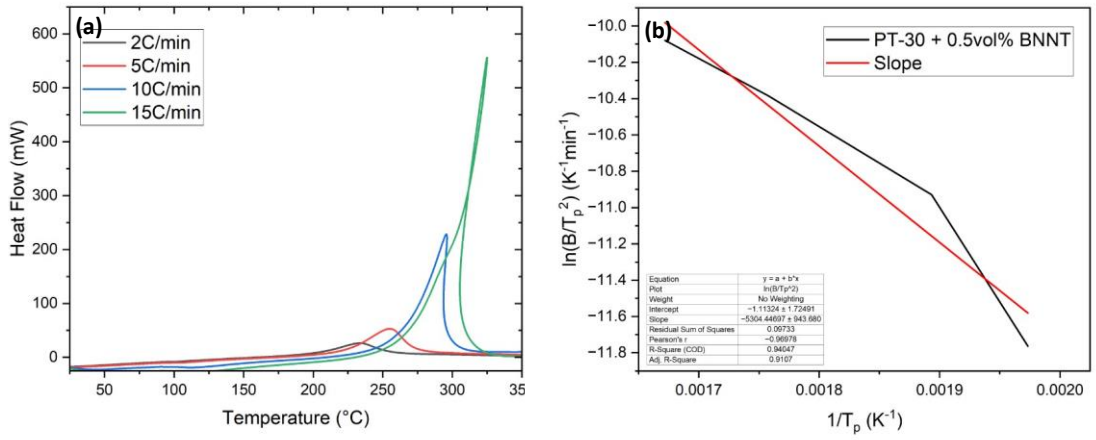

Figure 4.19. (a) DSC heat flow scans for PT-30 + 0.5vol% BBNT and (b) Kissinger plot used for calculating activation energy and pre-exponential factor

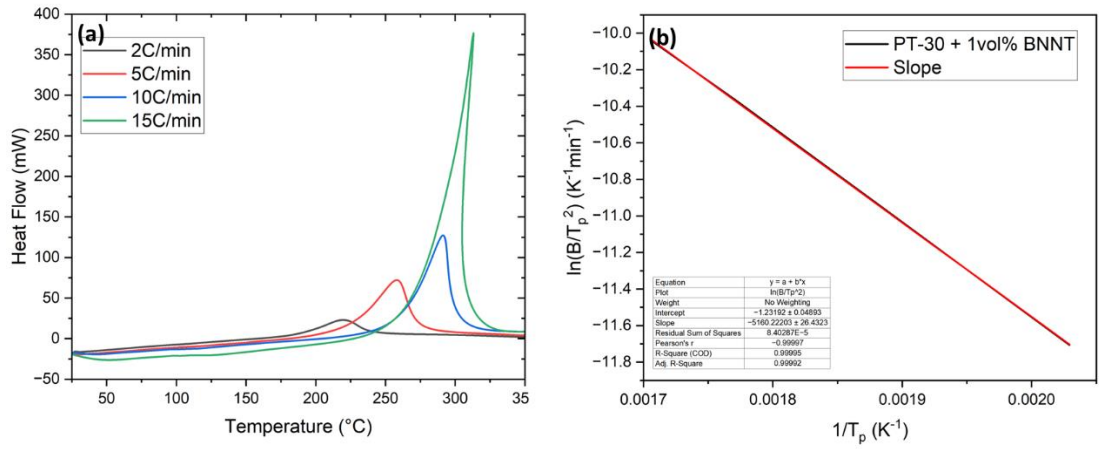

Figure 4.20. (a) DSC heat flow scans for PT-30 + 1.0 vol% BBNT and (b) Kissinger plot used for calculating activation energy and pre-exponential factor

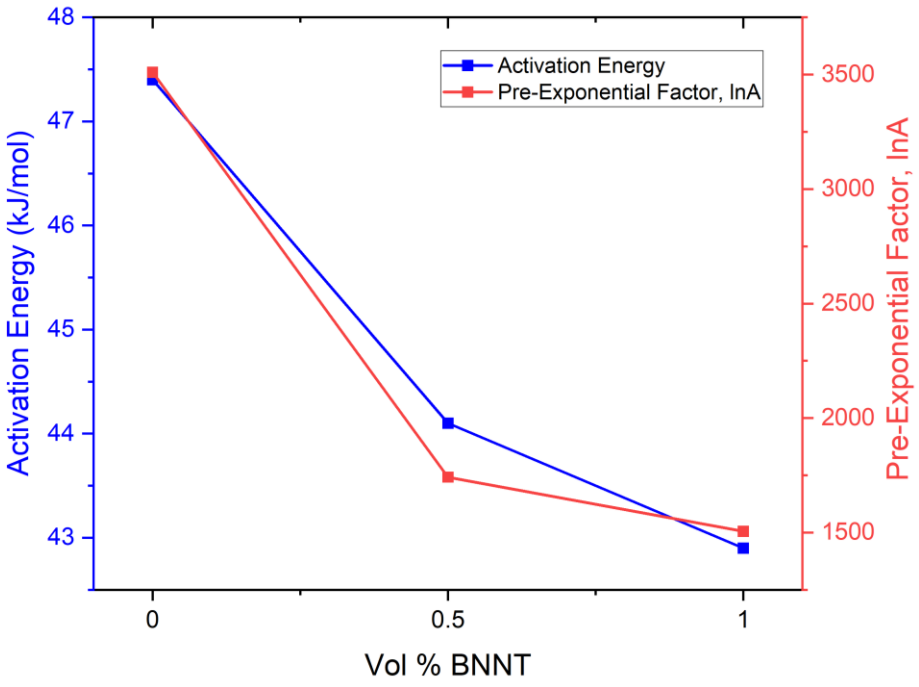

Figure 4.21. Curing activation energies and pre-exponential factors for different BNNT loadings

The addition of 0.5 and 1.0 vol% functionalized BNNTs led to a significant reduction in activation energy, with decreases of 7.05% and 9.57%, respectively. However, it is worth noting that our measurements showed a significant deviation from the literature value of the curing activation energy for CE, which is around 100 kJ/mol[83]. The deviation of about 50% could be due to the exponential nature of the Kissinger method, where a small deviation in peak temperature can result in a large change. Therefore, further measurements at other heating rates should be investigated to obtain a more accurate plot. Nevertheless, the curing activation energy for resin with 1 vol% of BNNT addition was found to be lower than the activation energy observed for 20wt% of carborane addition, indicating that BNNTs are more effective at reducing the activation energy than other additives[84]. This decrease in activation energy indicates that the reaction between the

hydroxyl group on the BNNTs and the -OCN cyanate group is kinetically favorable. Furthermore, previous literature has shown that the formation of the imino-carbonate linkage has a heat of formation of 1364 kJ/mol, while the heat of formation for the triazine ring is 2724 kJ/mol, providing further evidence that the reaction is thermodynamically favorable[2]. The cure kinetics also demonstrate that the addition of BNNTs has altered the chemistry of the system and confirmed the presence of a covalent bond between the BNNTs and the CE matrix. Thus, it is important to evaluate the mechanical and thermal properties at various length scales to fully comprehend the impact of using chemically bonded BNNTs to reinforce CE.

The mechanical and thermal properties of a nano-reinforced matrix are known to be strongly influenced by both the interfacial interaction between the particle and the matrix and the quality of dispersion. Therefore, in this study, the dispersion of BNNTs in the CE matrix was evaluated at both the micro- and nanoscale. Optical microscopy images presented in Figure 4.22 indicate that the addition of BNNTs only slightly affects the surface texture, and the texture appears to be uniform throughout the sample.

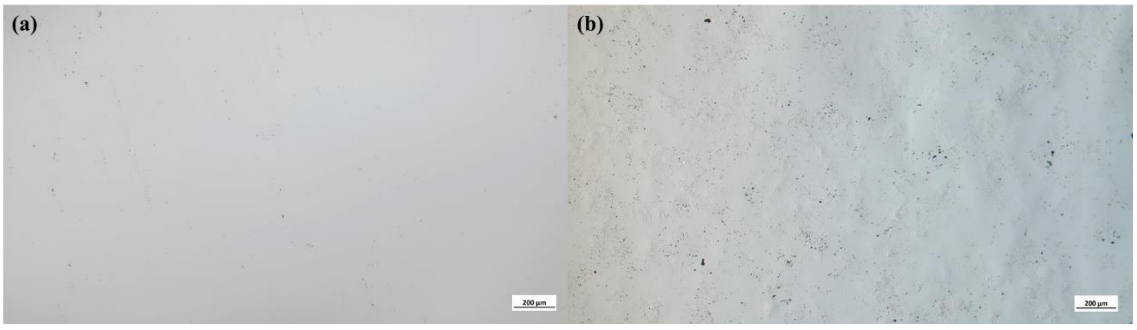

Figure 4.22. (a) Optical image of PT-30 (b) optical image of PT-30 + 0.5vol% BNNT.

Furthermore, SEM images of the fracture surface of the neat resin (Figure 4.23) and with 1 vol% BNNT addition (Figure 4.24) demonstrate that the BNNTs are well dispersed even at the nanoscale, with only a few small agglomerations, which are challenging to eliminate entirely due to the high surface energy of BNNTs. Notably, Figure 4.24d shows the partial pullout of BNNTs from the matrix, indicating a strong interface between the BNNT and the polymer matrix. This is crucial for enhancing the mechanical strength of the nanocomposites, as the energy required to pull these nanotubes out of the matrix contributes to this strength. Additionally, the bridging of cracks by BNNTs enhances fracture toughness and crack deflection, particularly in brittle polymers such as CEs. Thus, the assessment of BNNT dispersion in the CE matrix at multiple length scales provides insight into the potential for improved mechanical and thermal properties of these nanocomposites.

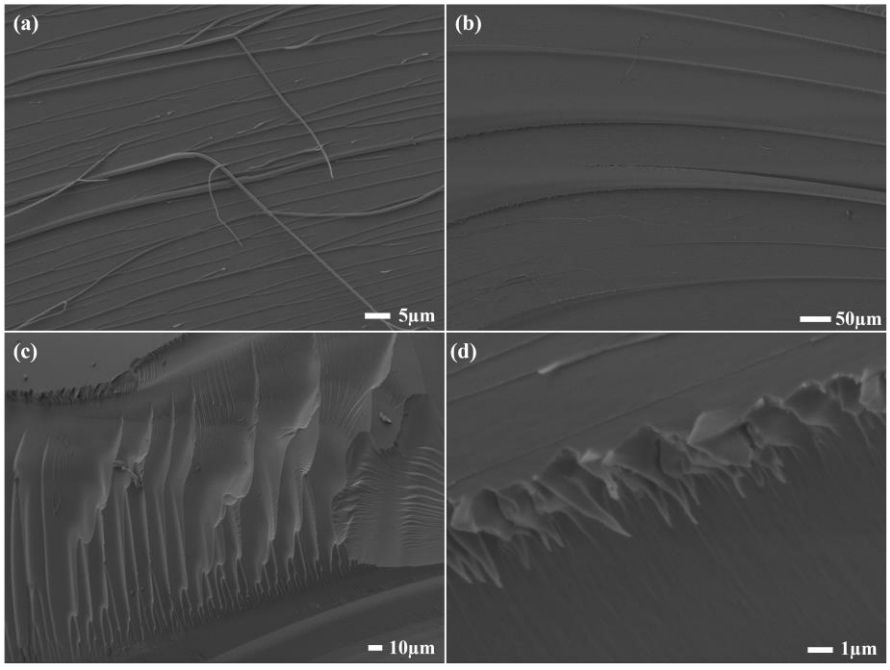

Figure 4.23. SEM images of the fracture surface of neat PT-30

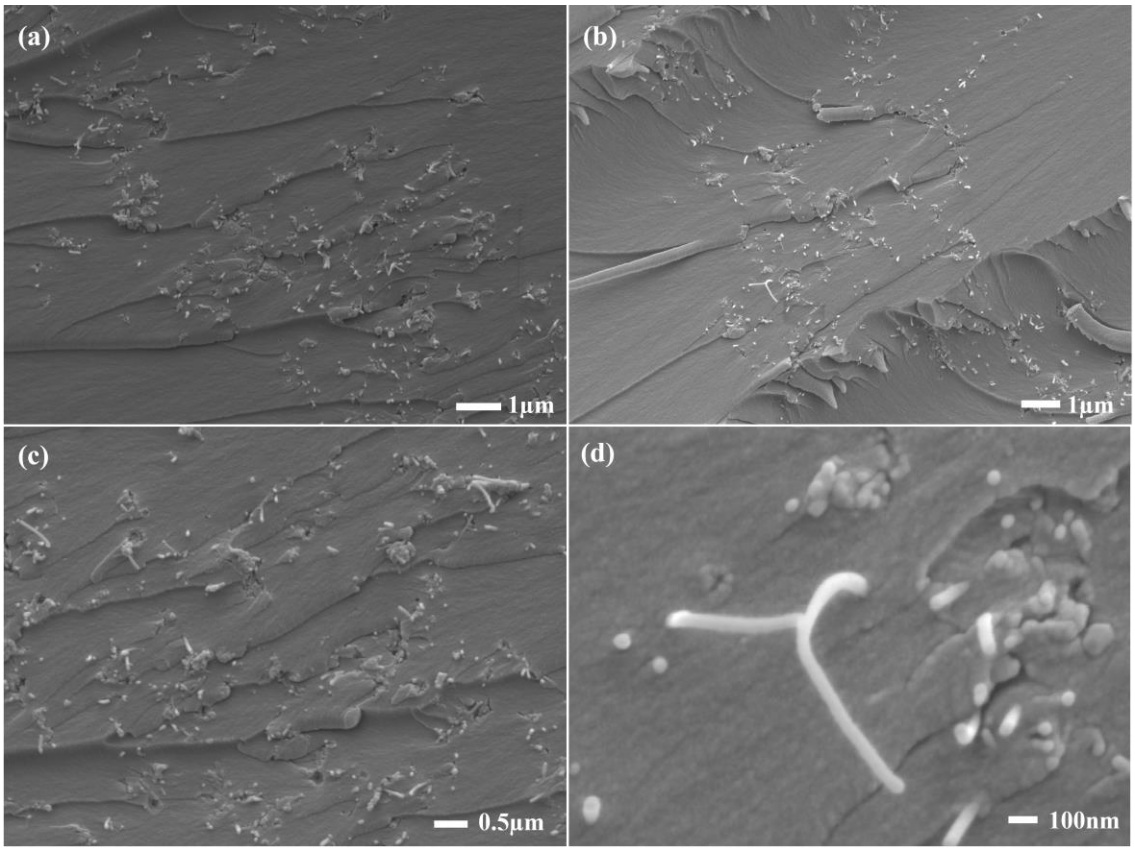

Figure 4.24. SEM images of the fracture surface of PT-30 + 1vol% F-BNNT

The effect of BNNTs on the thermal conductivity of cyanate ester composites was investigated using a laser flash diffusivity method to measure thermal conductivity. As shown in Figure 4.25, the thermal conductivity measurements were taken from room temperature to 205°C. The addition of 0.5 and 1.0 vol% of BNNTs resulted in a 3.85% and 5.69% increase, respectively, in thermal conductivity at room temperature. This improvement is attributed to the homogeneous dispersion of BNNTs in the CE matrix, which has an excellent thermal conductivity of ~350 W/m*K. The imino-carbonate linkage between BNNTs and CE also plays a significant role in reducing thermal resistance, leading to further improvement in thermal conductivity[10].

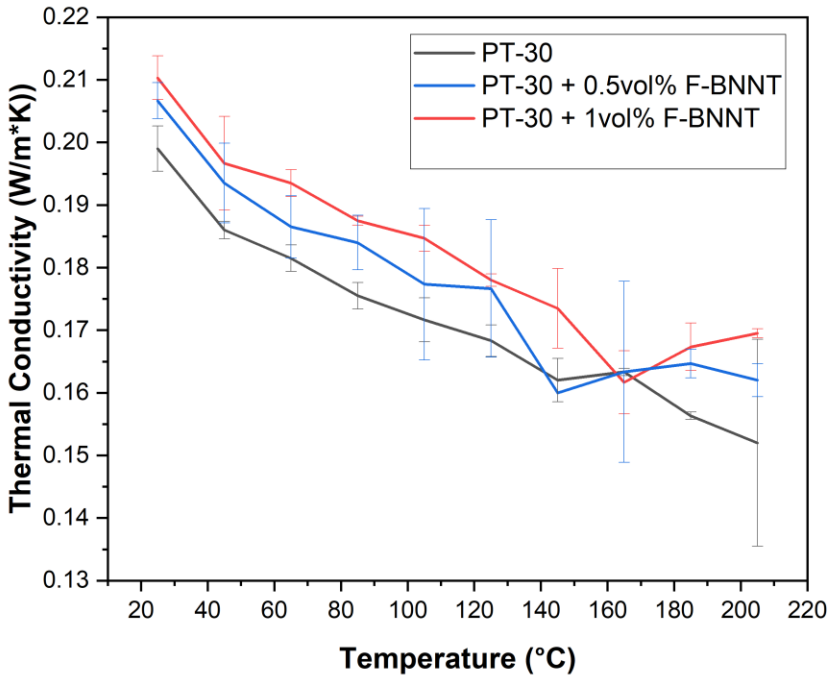

Figure 4.25. Thermal conductivity of CE composites at different temperatures for varying volumetric loadings of BNNTs

To analytically determine the thermal conductivity of BNNT reinforced cyanate esters, a method described in the literature was used that is suitable for low loadings of randomly oriented nanotubes. This method takes into account the anisotropy, aspect ratio, non-straightness, and interfacial resistance of the nanotubes [85]. By using this method, we were able to accurately fit the thermal conductivity data and gain insights into the mechanisms that influence the heat transfer in these materials.

For a low reinforcement of randomly oriented, straight BNNTs with an average length L and diameter d, it can be estimated that the overall thermal conductivity of the composite (k_c) is:

Equation 4.2. Modeling of thermal conductivity for randomly oriented, straight BNNTs

$$\frac{k_c}{k_m} = 1 + \frac{v_f}{3}\left[\frac{1}{(\frac{k_{33}^f}{k_m} - 1)^{-1} + H} + \frac{2}{(\frac{k_{11}^f}{k_m} - 1)^{-1} + (1-H)/2}\right]$$

Where k_m is the thermal conductivity of the matrix (0.199 W/m*K), v_f is the volume fraction of the BNNT reinforcement, k_{33} is the axial thermal conductivity of the fiber (350W/m*K), k_{11} is the transverse thermal conductivity of the fiber (20W/m*K), and H is a function of the aspect ratio, p = L/d, in the form:

Equation 4.3. Variable H as a function of aspect ratio

$$H(p) = \frac{1}{p^2 - 1}\left[\frac{p}{\sqrt{p^2 - 1}} \ln\left(p + \sqrt{p^2 - 1}\right) - 1\right]$$

These equations already account for the aspect ratio and the anisotropy of the fibers, but to account for the non-straightness of the BNNTs and interfacial resistance between the BNNTs and the CE matrix, the model becomes:

Equation 4.4. Modeling of thermal conductivity for randomly oriented, anisotropic, non-straight BNNTs

$$\frac{k_c}{k_m} = 1 + \frac{\delta v_f/3}{k_m \Big/ \left[\delta k_{33}^f \Big/ 1 + \frac{2R_k k_{33}^f}{L}\right] + H(\delta p)}$$

Where the straightness ratio $\delta = L_e/L$, L_e is the equivalent conductive length of the BNNTs, and R_k is the Kaptiza resistance. In a study of PT-30 reinforced with multi-walled carbon nanotubes (MWCNTs), a set of parameters, $\delta = 0.2$ and $R_k = 8 \times 10^{-8}$ m^2K/W, was found to accurately fit the data[86]. Since CNTs have a similar structure and size to BNNTs, it is

reasonable to use these parameters to investigate the effects of BNNTs on the thermal conductivity of cyanate ester composites. Based on SEM images of the dispersed BNNTs seen previously in Figure 4.3, we estimated the average length and diameter to be 1 μm and 50 nm, respectively, resulting in an aspect ratio of 20. By applying the fitted parameters, we developed an analytical model that is presented alongside the experimental data in Figure 4.26. The analytical model developed using the fitted parameters accurately represents the experimental data. Equation 4.4 indicates that increasing the aspect ratio, volume fraction, and alignment of the BNNTs can significantly enhance the overall thermal conductivity of the composite. To enhance the thermal conductivity of the composite, it is necessary to optimize the dispersion process of BNNTs without causing severe damage. This would improve the aspect ratio and purity of the BNNTs, resulting in a better thermal conductivity as indicated by the model. Although increasing the volume fraction of BNNTs is another viable option, loading them excessively may cause agglomeration, leading to a reduction in the efficiency of mechanical and thermal transport. Moreover, improving the alignment of BNNTs can further enhance thermal conductivity by facilitating the transfer of heat in the material. However, achieving this requires reinforcing with prefabricated mats or scaffolds of BNNTs, which will be discussed later in this study.

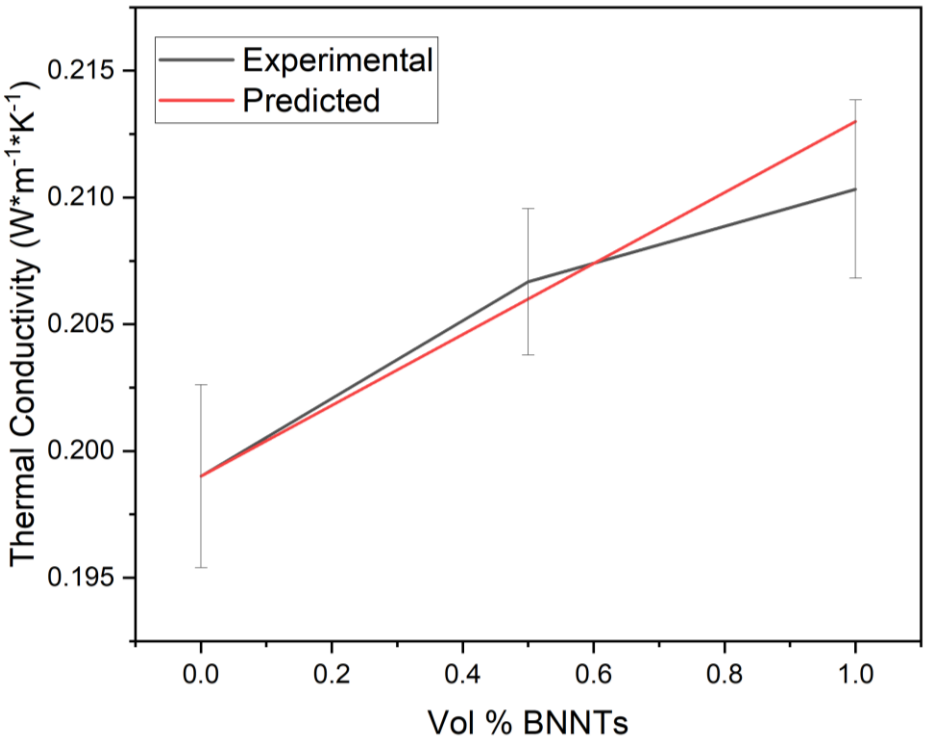

Figure 4.26. Analytical vs experimental thermal conductivity data for BNNT reinforced cyanate ester composites.

The mechanical strength of the composites was evaluated through nanoindentation to assess the impact of BNNT reinforcement. Using the Oliver-Pharr method[87], the elastic modulus and hardness of the samples were calculated and plotted in Figure 4.27. As nanoindentation is a highly localized testing method, 10 indents were performed across the sample to obtain an average load-displacement curve that ensured reliability in the distribution of data. The results confirmed consistency in the data which further highlights the quality in the dispersion of BNNTs. As shown in Figure 4.27, an increase in the volumetric loading of BNNTs resulted in a corresponding increase in hardness and elastic modulus. Even a small percentage of BNNT addition, such as 0.5 and 1.0 vol%, led to significant improvements of 3.26% and 18.48% in hardness, and 8.01% and 12.42% in

elastic modulus, respectively. These enhancements can be attributed to both the inherent strength of the BNNT and the covalently formed imino-carbonate bond resulting in good interfacial bonding between the CE matrix and the BNNT. This bond allows for more efficient transfer of stress from the matrix to the BNNT which results in better mechanical properties. While the addition of BNNTs enhances the mechanical properties of the composite, further loading beyond a critical point can cause agglomerations, which may negatively impact the performance. To optimize the mechanical properties, it is also necessary to improve the aspect ratio and alignment of BNNTs, similar to the enhancement of thermal conductivity. Such improvements would lead to a more efficient transfer of stress, resulting in an overall improvement in the mechanical properties of the composite.

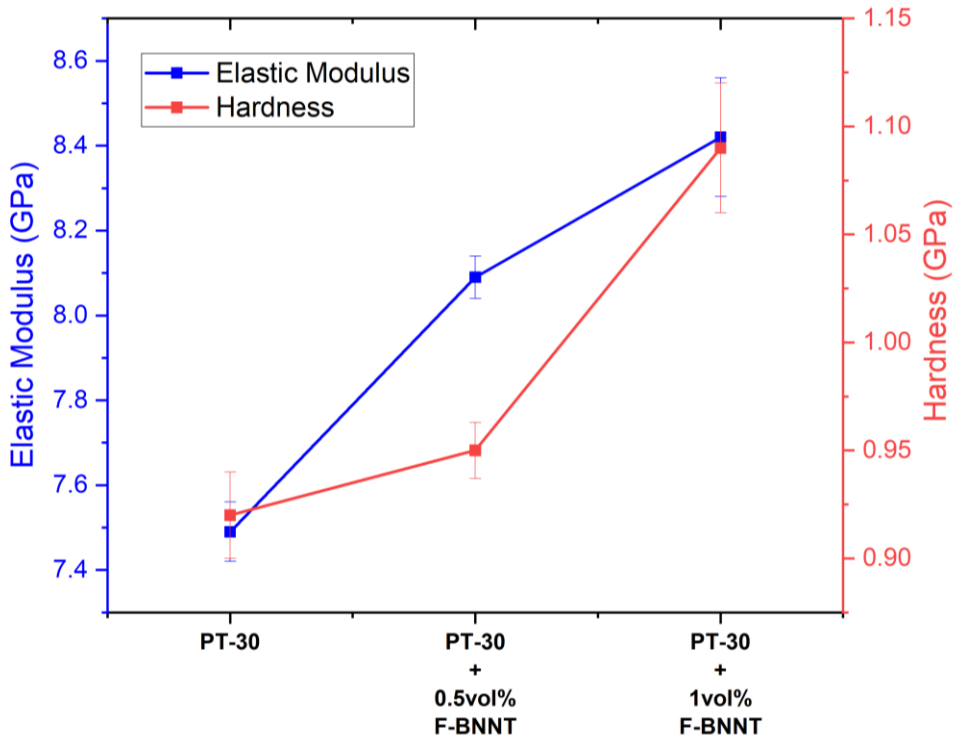

Figure 4.27. Experimental elastic modulus and hardness of CE composites reinforced with varying volumetric loadings of BNNTs determined through nanoindentation.

Hierarchically structured high-volume fraction boron nitride reinforced cyanate ester composites

As demonstrated in the previous section, the covalent bonding between the cyanate ester matrix and hydroxyl-functionalized BNNTs significantly influenced the resulting polymer chemistry, curing kinetics, and mechanical and thermal properties of the cyanate ester composites. Despite the enhancement of mechanical and thermal properties with low volumetric loading of BNNTs, the study also revealed the limiting factors of further reinforcement, including the alignment and volume fraction of BNNTs in the composite. Therefore, in this section of the study, we aim to address these limitations by incorporating hierarchically structured high-volume fraction boron nitride structures such as free-standing boron nitride nanoplatelet (BNNP) and BNNP/BNNT foams. This new approach for reinforcing cyanate esters has not been previously reported in literature and aims to improve the mechanical and thermal properties of the composite through optimization of the alignment and volume fraction of the boron nitride (BN) structures in the matrix.

In this study, the fabrication of highly aligned BNNP and BNNP/BNNT foams with a lamellar morphology was achieved using the Freeze-Drying approach, as detailed in the methodologies section. The microstructure of the foams was designed to feature parallel nanoplatelet walls that were highly aligned and interconnected with bridges composed of both nanoplatelets and nanotubes. The strategic alignment of BNNPs and BNNTs along the lamellar foam walls was intended to enhance their anisotropic properties. These hierarchically structured architectures were then infiltrated with cyanate ester resin to create advanced composites. The incorporation of these hierarchically structured architectures resulted in significant improvements to the mechanical and thermal properties

of the resulting composites due to the increased alignment and volume fraction, which could not be achieved through the dispersion of nanotubes alone.

Orikasa et al. conducted a comprehensive investigation on the fabrication and characterization of boron nitride nanoplatelet (BNNP) foams, revealing novel structures with exceptional properties. These foams exhibit an incredibly low density of 0.05 g/cm3, a remarkable porosity of 97%, and highly interconnected walls. The walls are composed of stacked nanoplatelets and bridges, forming a lamellar morphology with micro-scale pores of size 86.48 ± 10.7 μm. The thickness of these walls was measured to be 1.79 ± 0.35 μm.

As the BNNPs are 2D materials, they have anisotropic properties. They have thermal conductivity of 600 W/(m*K) in the basal-plane and a through-plane thermal conductivity of 30 W/(m*K)[68]. The thermal conductivity of the BNNP foam was measured in parallel ($K_{\parallel}$) and perpendicular ($K_{\perp}$) pore orientations with respect to the heat transfer direction. The experimental thermal conductivities of BNNP foam yielded $\kappa_{\parallel,exp} = 0.31 \pm 0.01 \frac{W}{m \cdot K}$ and $\kappa_{\perp,exp} = 0.08 \pm 0.01 \frac{W}{m \cdot K}$. BNNPs also exhibit a remarkable mechanical anisotropy due to their high basal-plane stiffness and strength, which can reach up to 950 GPa[69], whereas their through-plane strength is typically around 30 GPa[70]. In the case of BNNP foams, the mechanical properties are also affected by the orientation of the pores with respect to the loading direction. Experimental results have shown that BNNP foams with parallel pore orientations have a higher modulus, measuring at 120.0 ± 39 kPa, compared to those with perpendicular pore orientations which measure at 11.4 ±

1.1 kPa. These findings highlight the importance of alignment of the foams depending on the properties desirable.

The mechanical strength and failure mechanisms of BNNP foams were studied using in situ nanoindentation inside an SEM with a 500um titanium flat punch and displacement of 150μm. Both parallel and perpendicular alignments of the foams were investigated, and the results are shown in Figure 4.28. The alignment of the pores had a significant impact on the mechanical behavior of the foams. The parallel-oriented foams exhibited inelastic buckling of the walls, resulting in sharp peaks of energy absorbance before energy was dissipated through buckling failure, but overall, the alignment of the walls along the basal plane of the BNNPs increased the resistance to failure.

In contrast to the parallel-oriented foams, the perpendicular-oriented foams exhibited elastic buckling of the walls with up to 70% recovery. This recovery is due to the bridges between the walls buckling under loading, absorbing energy, and acting like springs, which help the foam to retain its original shape. Figure 4.29 demonstrates the cyclic behavior of the perpendicularly oriented foams and further illustrates their elastic nature. The anisotropy observed in these foams must be considered in the overall composite design, but it also provides opportunities for tailoring their mechanical and thermal properties.

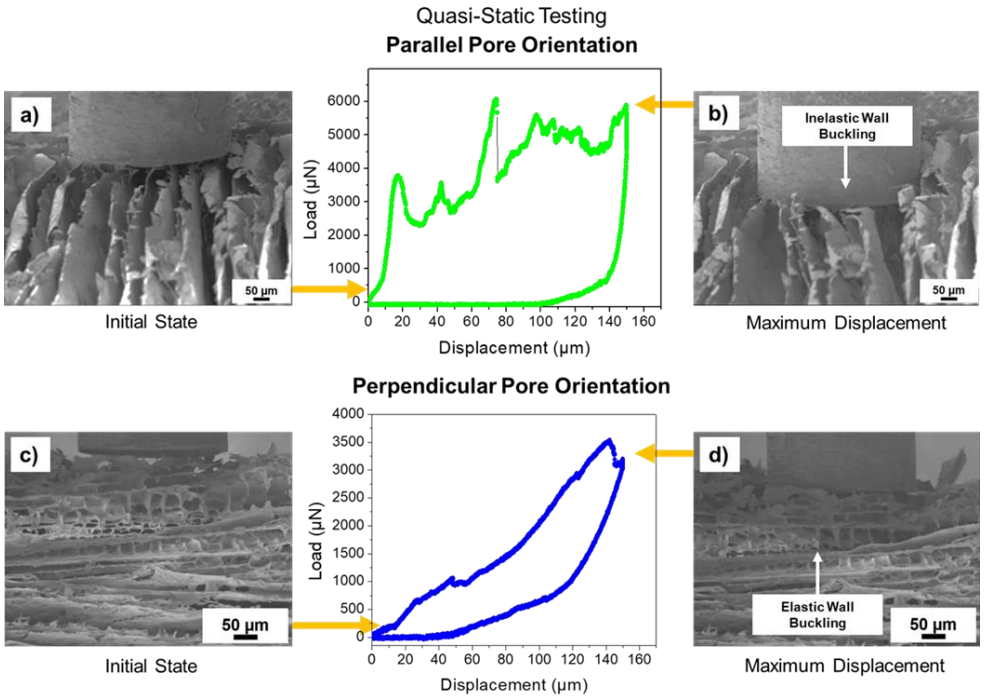

Figure 4.28. Quasi-static stress transfer mechanisms in the parallel and perpendicular configuration for BNNP foams.

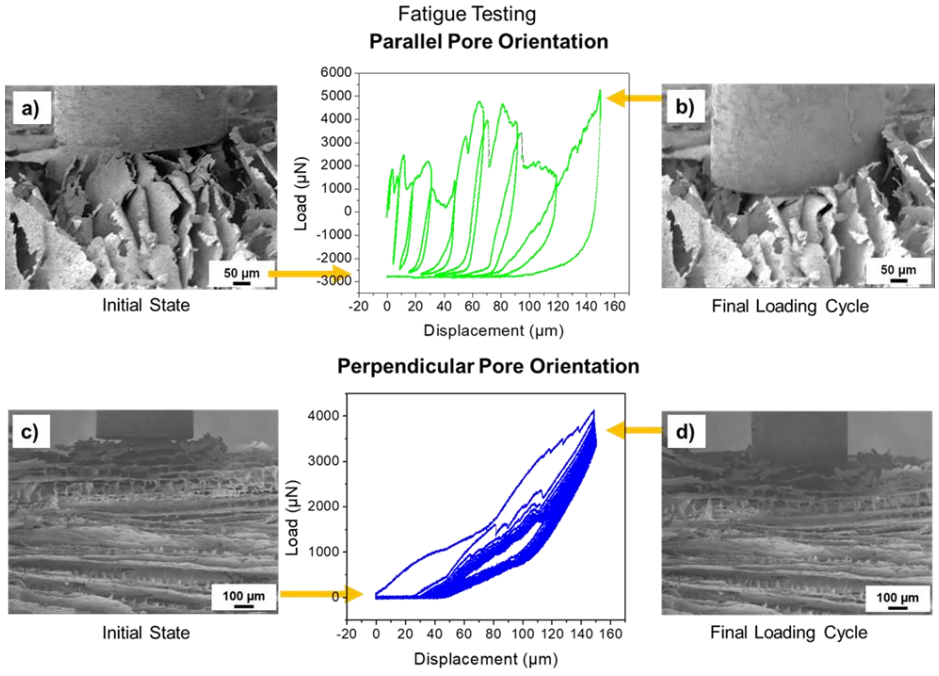

Figure 4.29. Dynamic stress transfer mechanisms in the parallel and perpendicular configuration for BNNP Foams.

4.2 Hierarchical Boron Nitride Architectures

Until now, there has been no literature on the combination of BNNPs and BNNTs in a free-standing foam. Therefore, to effectively infiltrate these novel architectures with cyanate ester resin, it is crucial to first understand their morphology and characteristics. To achieve this, BNNP/BNNT foams were fabricated, and their morphology was analyzed through SEM imaging. This pioneering work on the synthesis and characterization of BNNP/BNNT foams provides insights into the potential applications of these materials in various industries.

Figure 4.30 displays low magnification images of BNNP/BNNT foams, revealing that their overall morphology and structure looks similar to that of BNNP foams. This is not unexpected, given the low weight loading of the BNNTs compared to the BNNPs. However, closer inspection at higher magnification, as shown in Figure 4.31, reveals differences in their microstructures. While the walls of both foams mostly consist of stacked BNNPs, the BNNTs are observed adhering to the surface of the BNNPs, connecting individual BNNPs together, and bridging the micro-pores within the foam's walls. High-resolution SEM images in Figure 4.32 demonstrate the advantages of adding BNNTs to these foams, as they create an enhanced woven architecture that promotes improved thermal and mechanical transport across the foams. BNNTs act as pathways for transferring energy from nanoplatelet to nanoplatelet, thereby strengthening the overall foam structure.

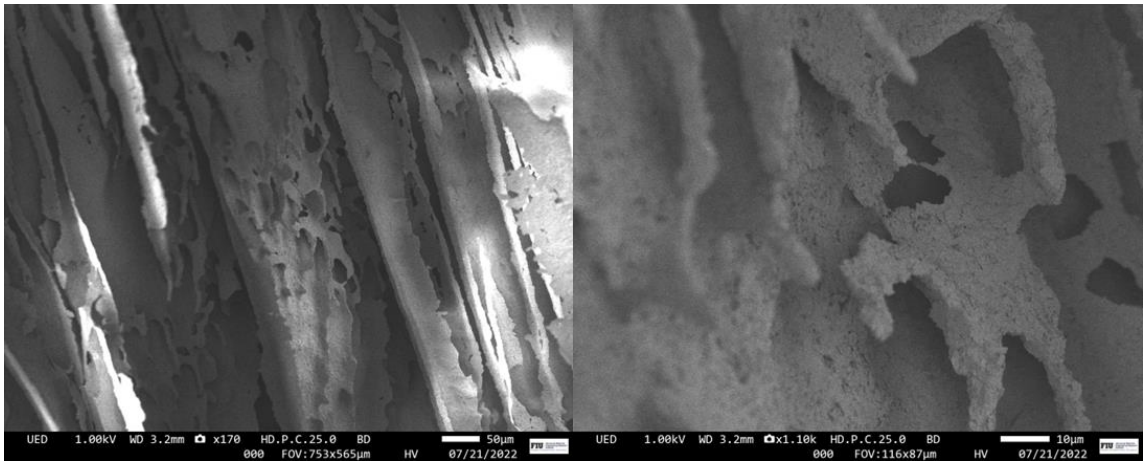

Figure 4.30. Low magnification SEM images of BNNP/BNNT foam

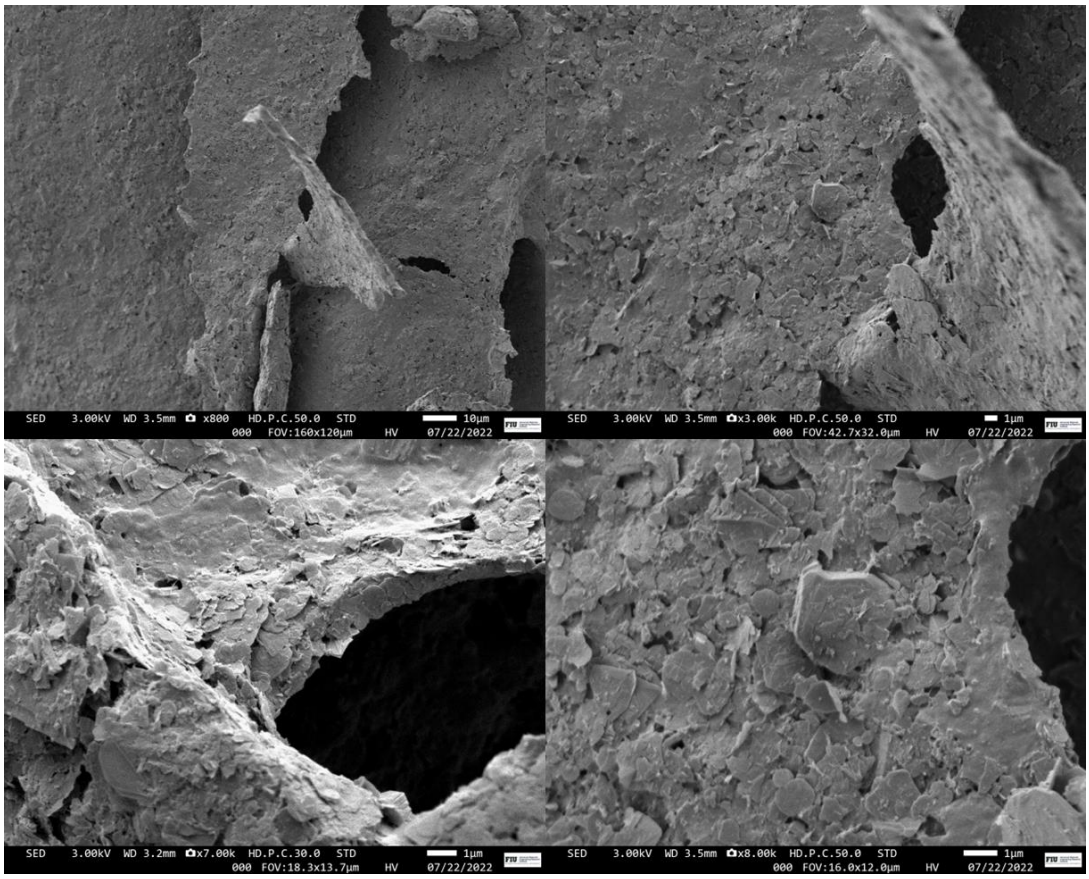

Figure 4.31. SEM images of BNNP/BNNT foams showing the interconnected walls of stacked BNNPs and covered by BNNTs.

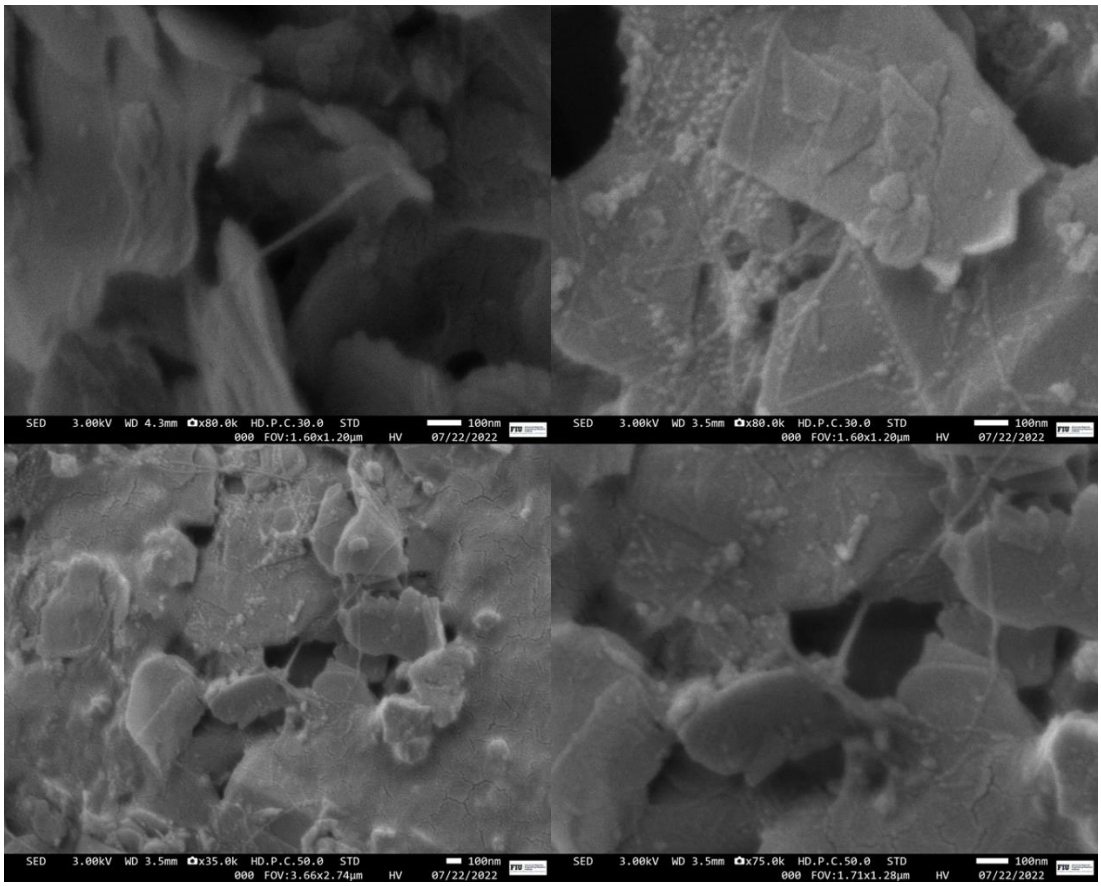

Figure 4.32. High-resolution SEM images of BNNTs on top of BNNPs bridging the micro-pores between BNNPs.

As explained in the methodology section, the presence of the binding agent SBR creates difficulties when infiltrating the BNNP and BNNP/BNNT foams with cyanate ester, as it reacts to form a volatile char. To overcome this issue, the binding agent was removed by placing the foam in a furnace at 600°C for four hours. However, the removal of the binding agent causes the free-standing foam to become fragile. To understand the effects of the binder's removal, an investigation was conducted into the morphology of the foam after the removal process. This analysis allowed for better understanding the role of the binder and how its removal influences the properties of the BNNP and BNNP/BNNT foams.

Low magnification SEM images in Figure 4.33 reveal that the stacked BNNP walls are still present, even after the polymer binder is removed. It is likely that Van der Waals forces between individual BNNPs and the BNNTs are responsible for holding the walls together, as the BNNTs bridge the gaps between the nanoplatelet surfaces.

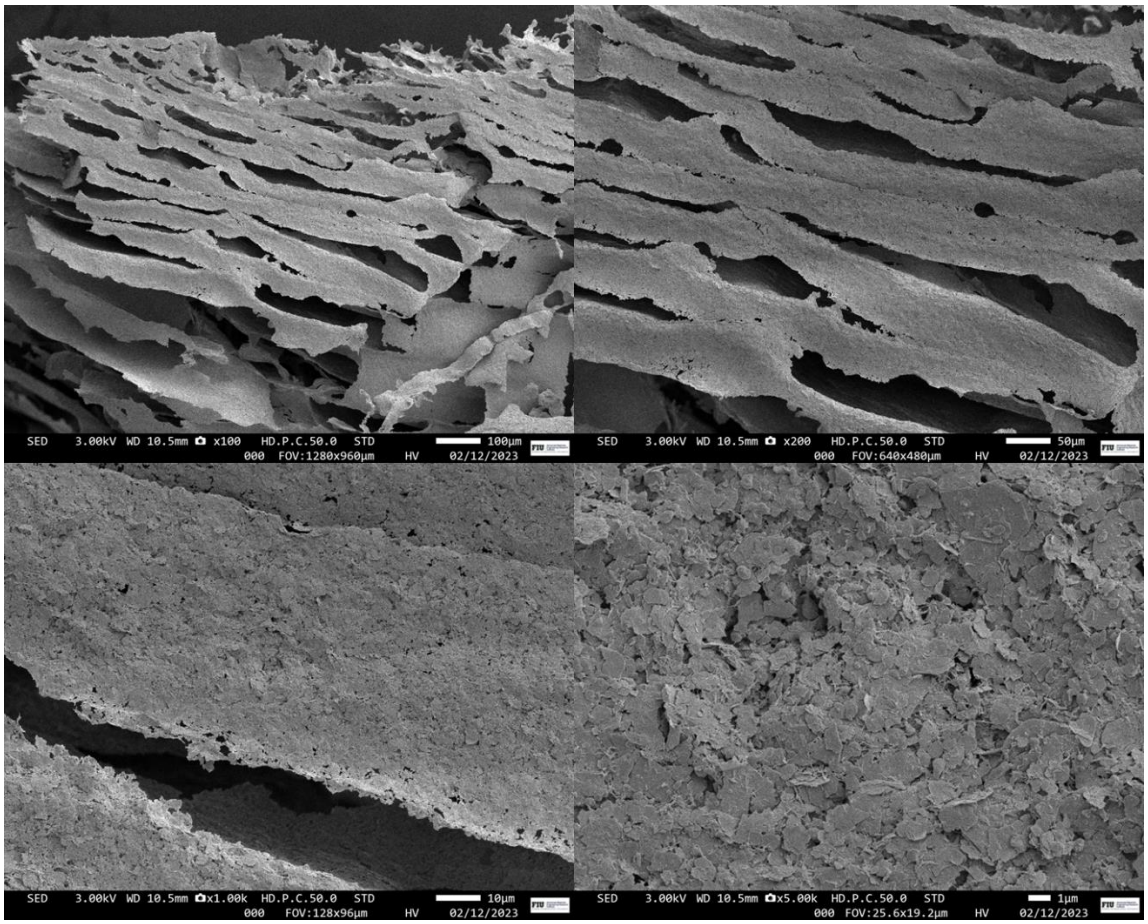

Figure 4.33. SEM images of purified BNNP/BNNT foams at lower magnification.

Higher magnification SEM images in Figure 4.34 confirmed this hypothesis, showing stacked BNNP walls that consist of a greater percentage of micro-pores, which are likely formed due to the burnout of the polymer binder. The high level of intertwining seen in these areas indicates that the BNNTs were properly dispersed within the polymer

binder and were not visible before the burnout process. When the binder is removed, the BNNTs remain and continue to act as bridges between the nanoplatelets, contributing to the overall stability of the foam structure. This observation emphasizes the potential for significant mechanical and thermal reinforcement by adding BNNTs to the foams. This woven architecture created through the interconnectivity of the BNNTs enhances the overall strength and stability of the foam structure by providing a means of efficient energy transfer, while also promoting improved thermal conductivity.

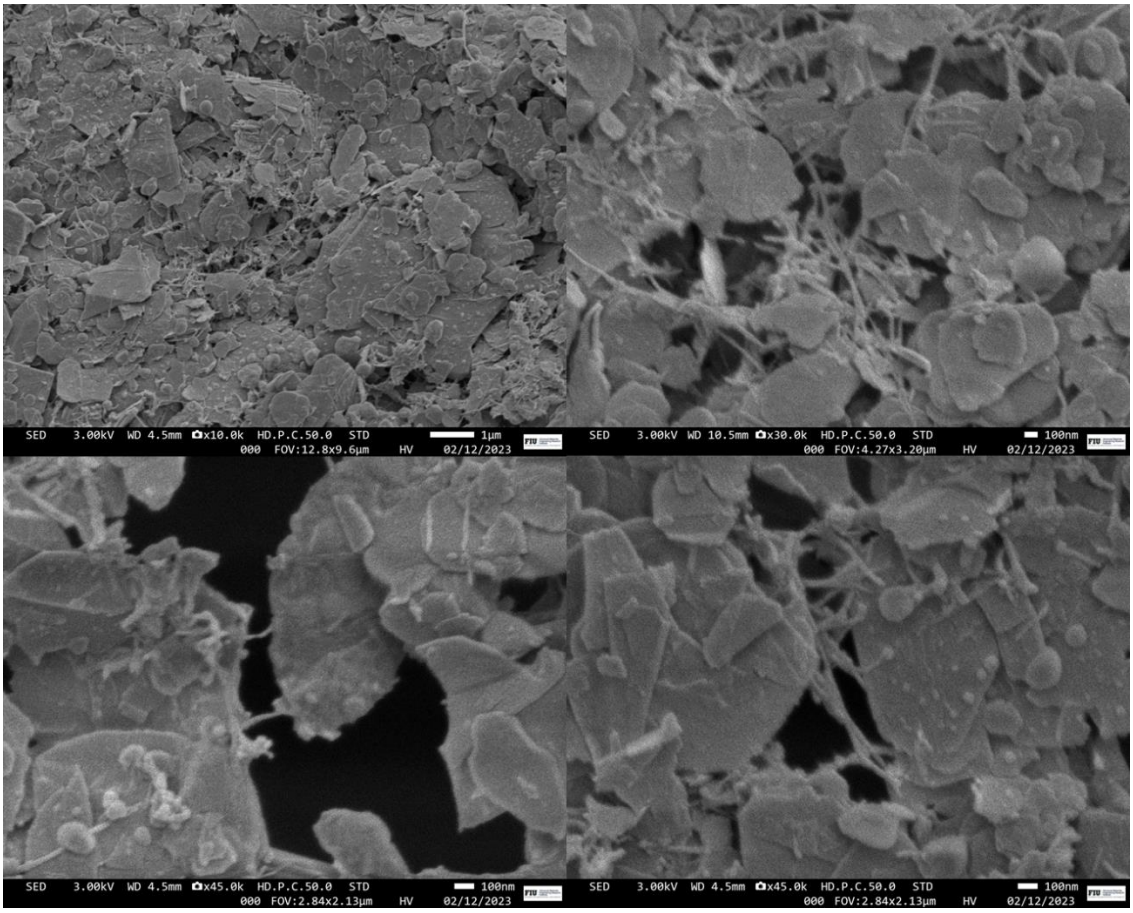

Figure 4.34. High-resolution SEM images of purified BNNP/BNNT foams showing the highly interconnected architecture.

After understanding the foam microstructure, hierarchically structured composites were formed by infiltrating the foams with cyanate ester. Optical images of the BNNP-reinforced cyanate ester composites are presented in Figure 4.35 - Figure 4.37. In these figures, the dark field imaging allows for the lamellar morphology of the BNNP foams to be clearly visible, as indicated by the light areas of the image. In Figure 4.35(d) and Figure 4.36 (c) – (d), brightfield imaging reveals that the interface between the BNNP foam and the cyanate ester matrix is excellent. This interfacial interaction allows for efficient transfer of mechanical and thermal stress, leading to improved properties and functionality of the composites.

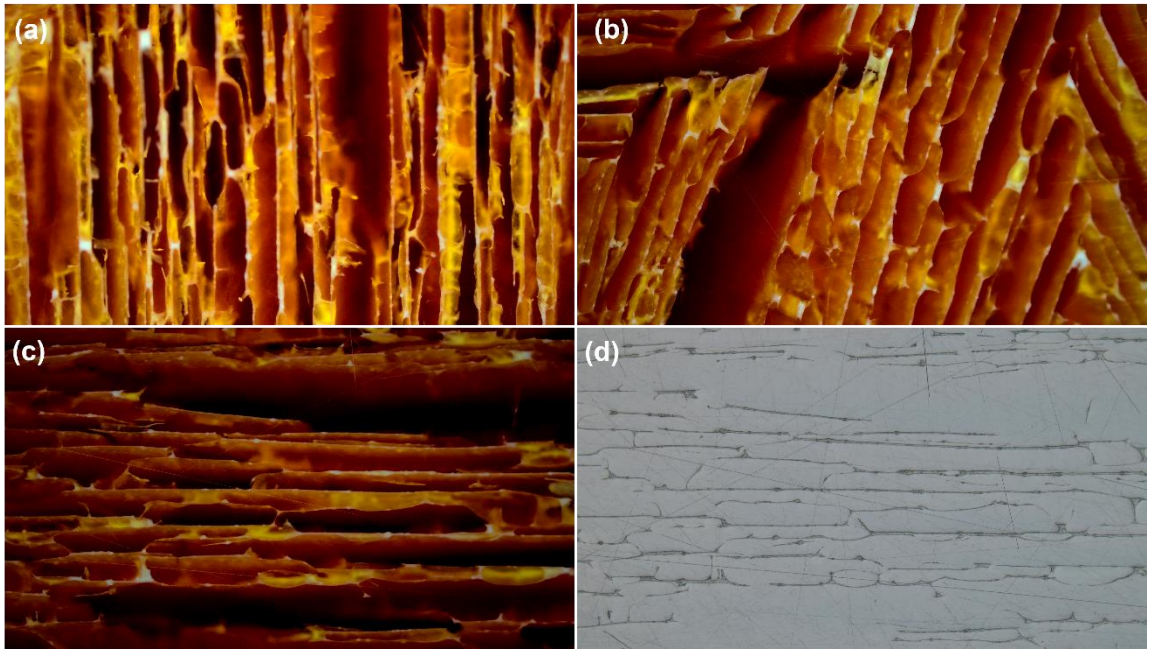

Figure 4.35. (a) - (c) dark field optical images and (d) brightfield image of the top surface of the BNNP - CE composite.

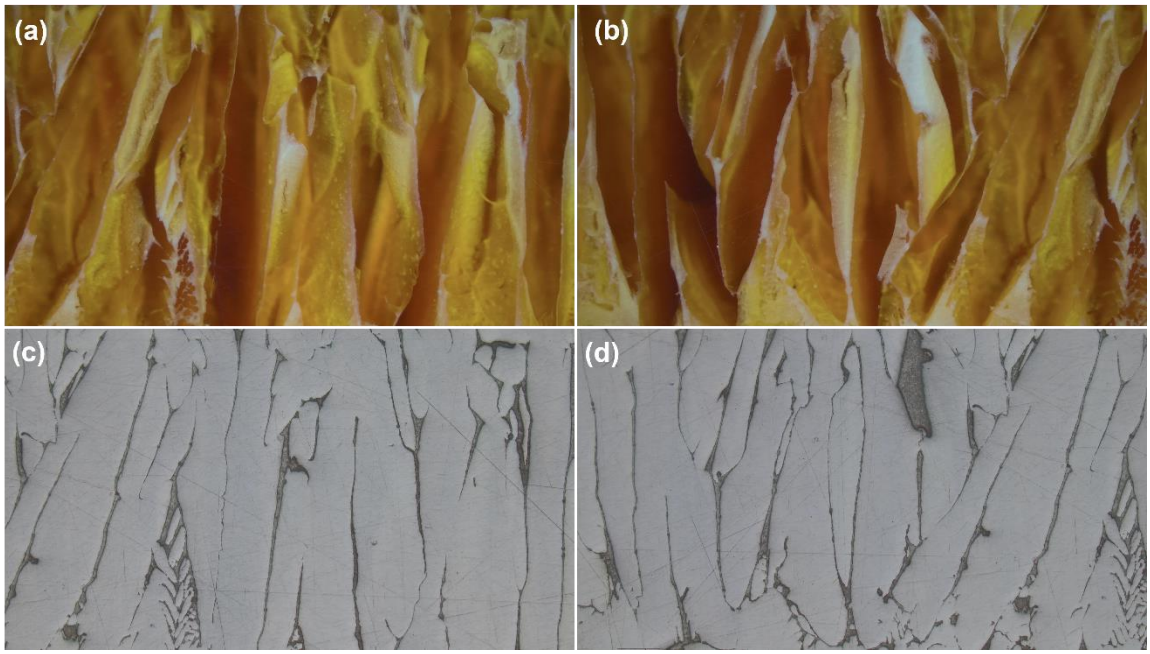

Figure 4.36. (a) - (b) dark field optical images and (c) - (d) brightfield images of the side surface of the BNNP - CE composite.

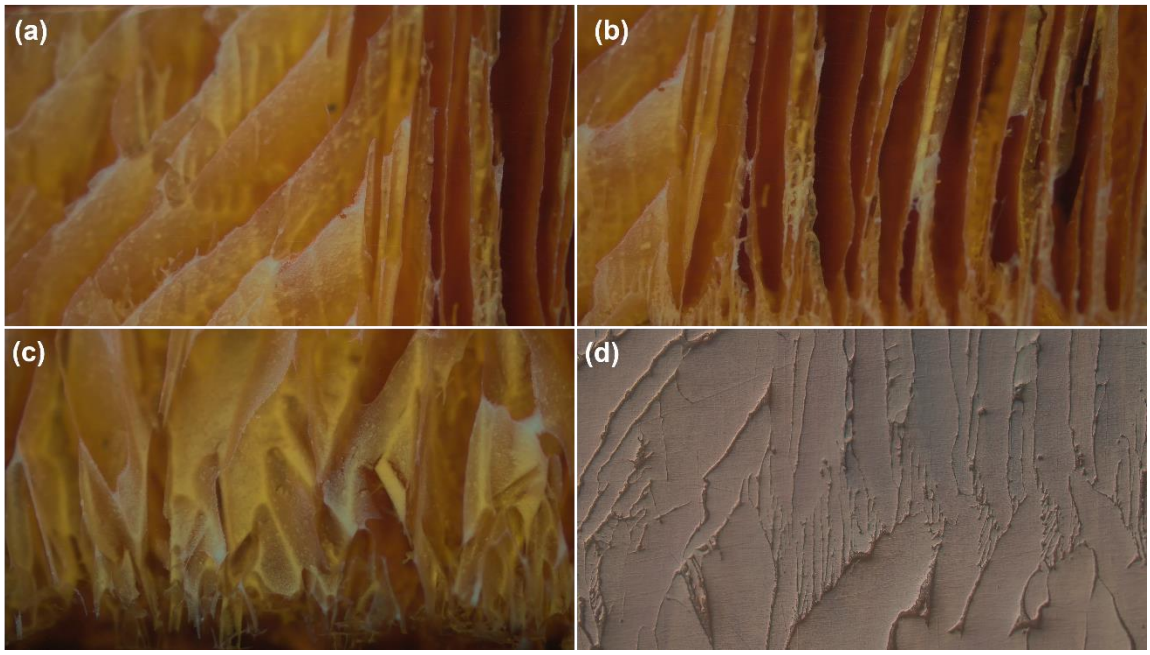

Figure 4.37. (a) - (c) dark field optical images and (d) DIC images of the side surface of the BNNP - CE composite.

Given the critical role of the interface between the foam and the matrix in facilitating efficient mechanical and thermal stress transfer, a detailed examination of this interface was undertaken. Figure 4.38 presents a stitched SEM image of the top surface of the BNNP-reinforced cyanate ester composite, where the darker grey regions correspond to the cyanate matrix and the lighter grey regions represent the BNNP walls. A closer view of the interface between the matrix and BNNP walls, depicted in Figure 4.39, reveals no porosities or delamination. This is attributable to the $\pi - \pi$ interactions between the BNNP and cyanate ester, which promote strong interfacial bonding.

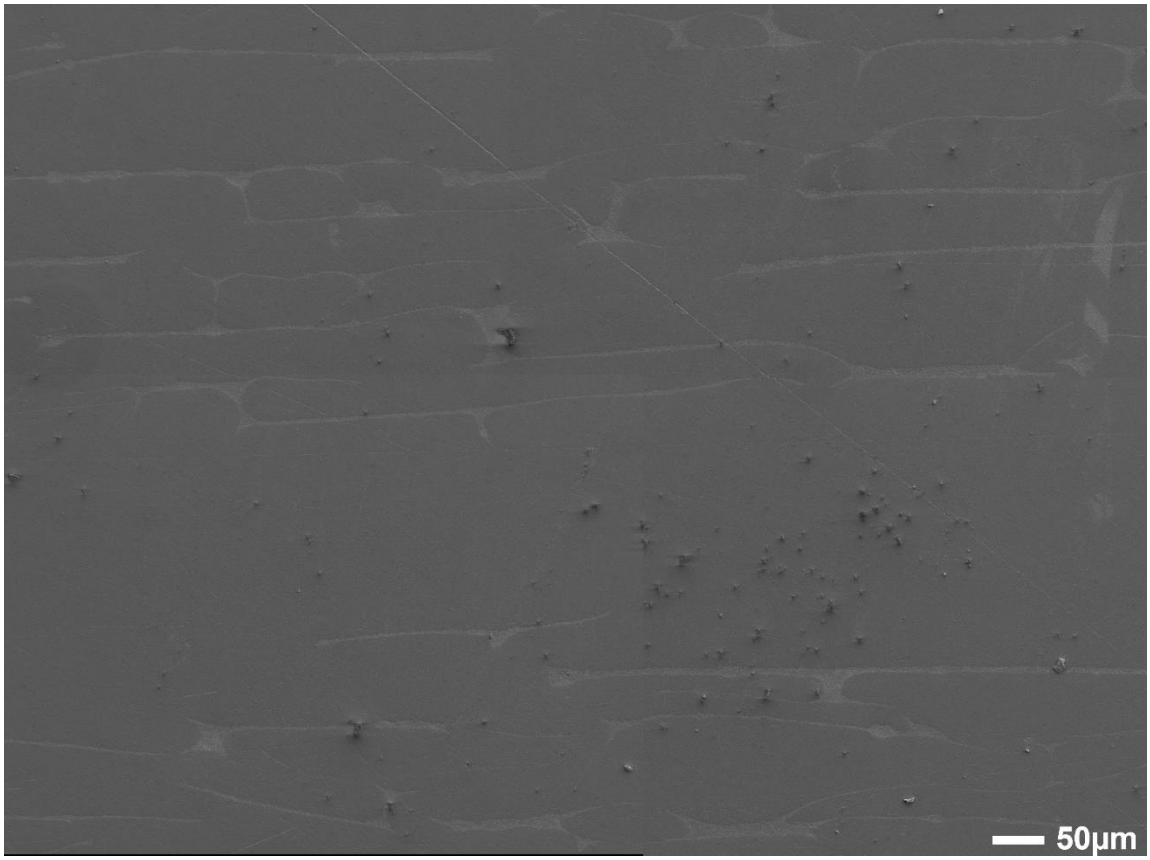

Figure 4.38. SEM image of the surface of an infiltrated BNNP foam - CE composite. The foam structure is parallel to the viewing direction.

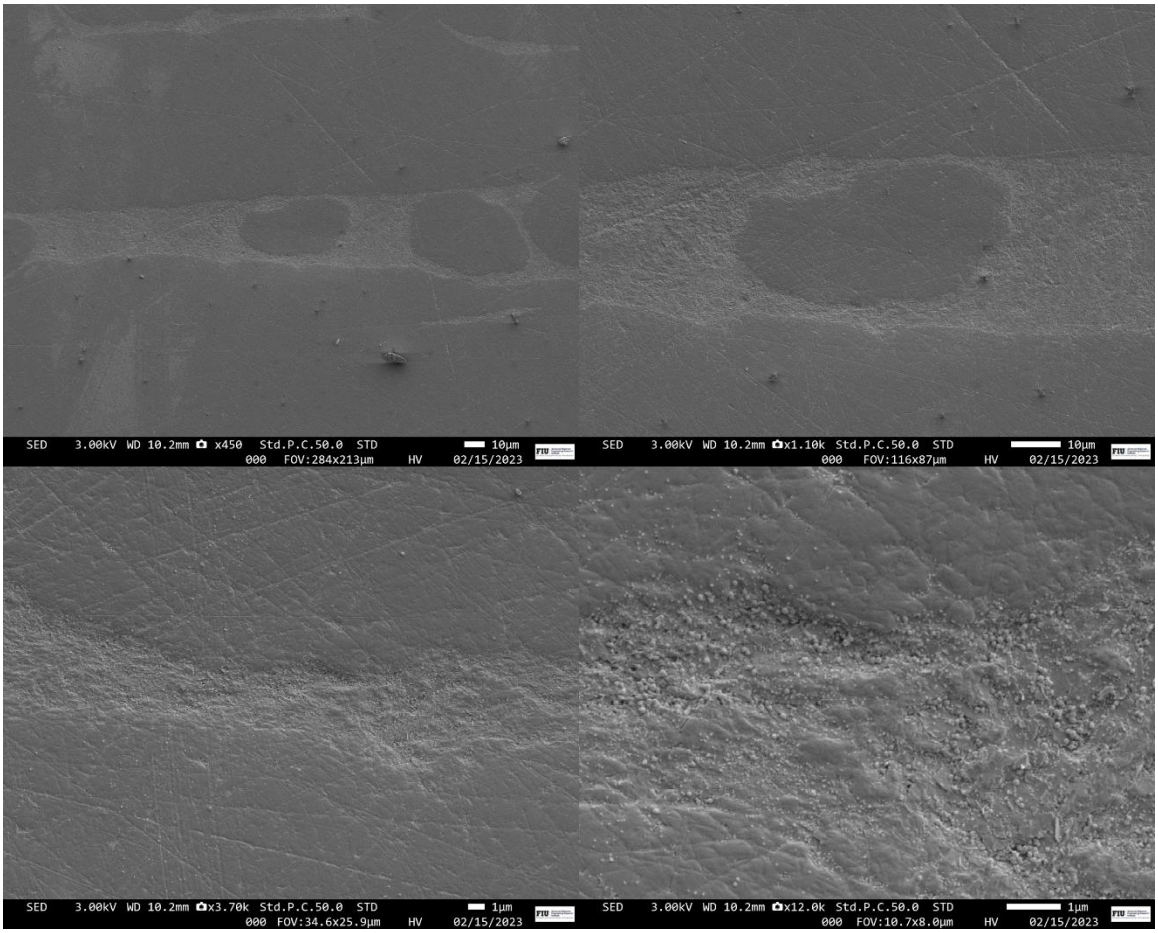

Figure 4.39. SEM images highlighting the excellent interface between the BNNP foam and the cyanate ester.

In order to evaluate the impact of BNNP foam reinforcement on the mechanical strength of cyanate ester composites, a combination of tensile testing and in situ monitoring using both an optical and high-speed camera was employed. The top surface microstructure of the tensile sample was imaged before and after fracture to gain insight into how the crack propagated through the sample and to shed light on the underlying failure mechanisms.

The load-displacement data for the pure cyanate ester sample and BNNP-reinforced composite are presented in Figure 4.40.

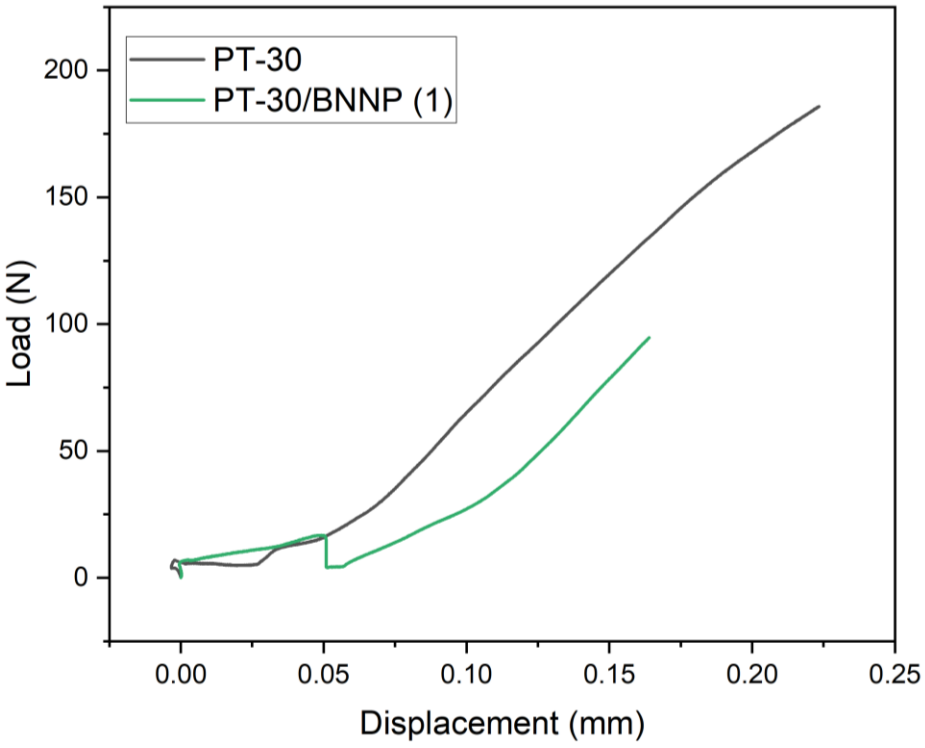

Figure 4.40. Maximum tensile load for CE and BNNP/CE samples.

As shown in Figure 4.41, crack propagation in the BNNP-reinforced composite follows the laminar wall of the foam. Since the orientation of the foam is perpendicular to the loading direction, this explains why the maximum stress is considerably lower than that of the pristine cyanate ester. This anisotropic behavior of the BNNP foams was previously highlighted by Orikasa et al.

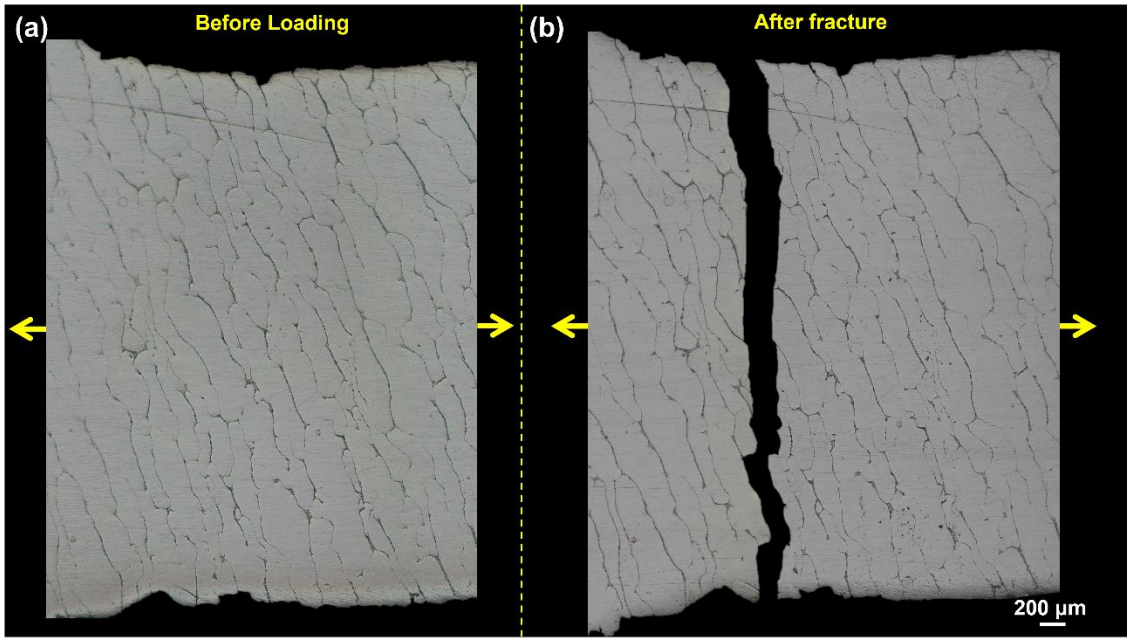

Figure 4.41. Optical image of the PT-30/BNNP (1) tensile sample (a) before and (b) after fracture.

Furthermore, SEM imaging of the tensile sample fracture surface, presented in Figure 4.42, clearly shows that the crack propagated through the stacked BNNPS within the laminar wall of the foam rather than at the interface between the BNNP foam and cyanate ester matrix. This is attributed to the alignment of the BNNPs, which possess a lower through-plane strength compared to their basal plane, as well as to the removal of the binder within the foam, which results in reduced stability.

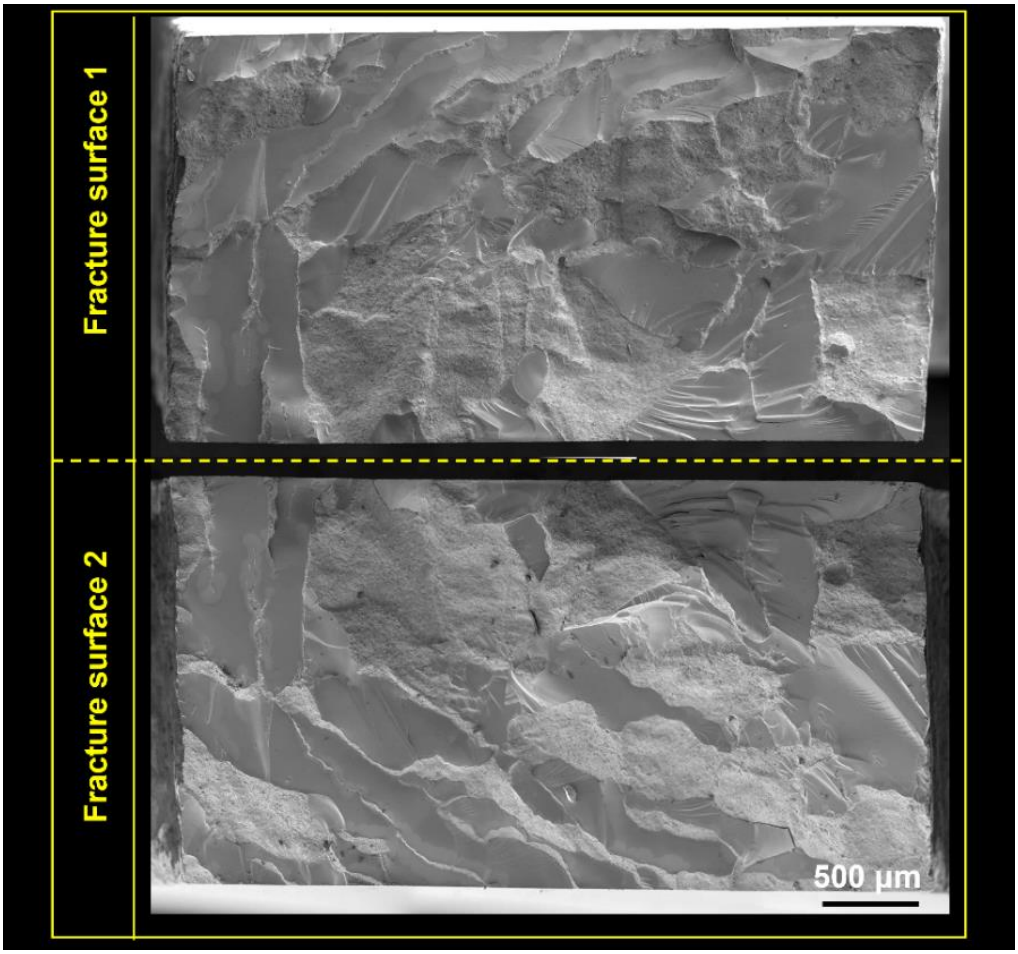

Figure 4.42. SEM imaging of the fracture surface of the BNNP-CE tensile sample after fracture.

A series of tensile tests were carried out to explore how the orientation of BNNP foam affects the mechanical strength of the composite. Although complete alignment of the BNNP foams with the loading direction was unattainable, Figure 4.43 reveals that the samples had different angles of alignment. Among them, the highest level of alignment was observed in Figure 4.43c, which corresponds to the maximum tensile load measured in all PT-30/BNNP samples shown in Figure 4.44. The angle of misalignment was measured using ImageJ and was found to be 32 degrees. The lowest load corresponded with the highest misalignment angle and was found to be 81 degrees. This indicates that

the degree of alignment of the BNNP foam has a significant influence on the mechanical properties of the composite. These results indicate that increasing the degree of alignment of BNNP foam and enhancing the stability within the foam walls could potentially increase the mechanical strength of cyanate ester composites reinforced with BNNP. Therefore, it is important to optimize these factors to improve the overall performance of the composite.

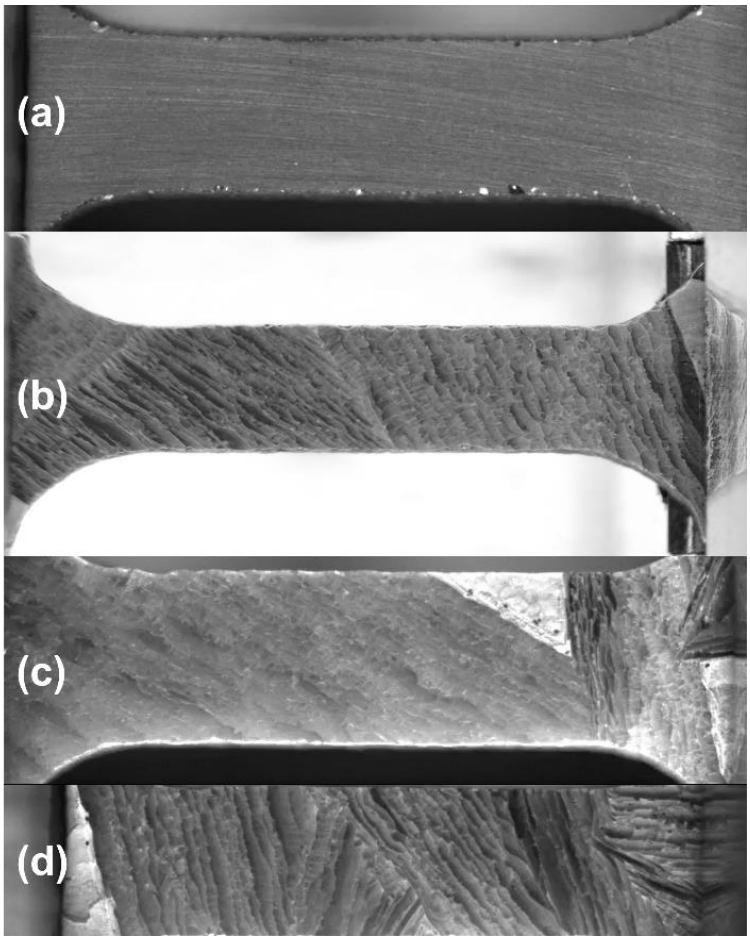

Figure 4.43. Tensile samples highlighting the orientation of the BNNP Foam structure for (a) PT-30 (b) PT-30/BNNP (1) (c) PT-30/BNNP (2) and (d) PT-30/BNNP (3)

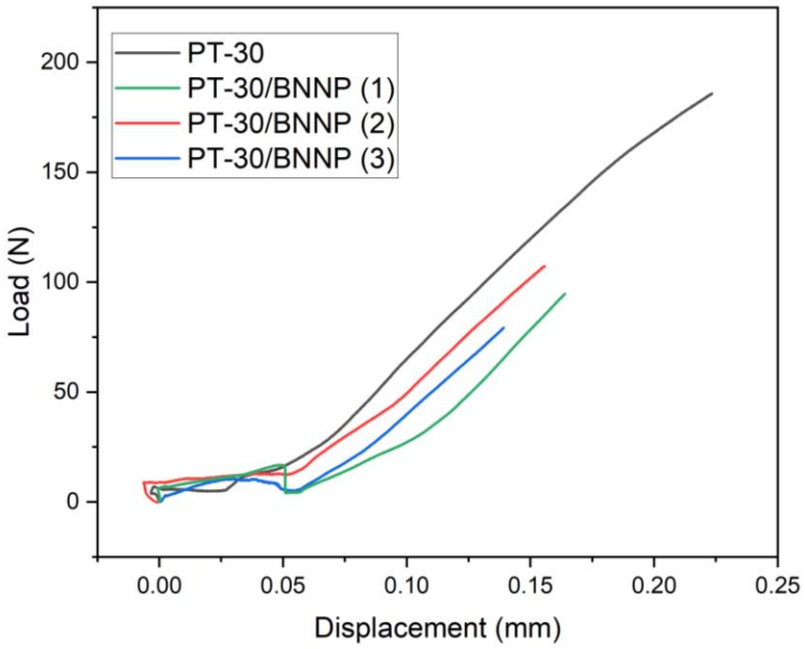

Figure 4.44. Tensile strength data for PT-30/BNNP samples.

To understand the energy transfer mechanisms during deformation in BNNP/BNNT reinforced cyanate ester composites, in situ micropillar compression was performed. The load vs depth of compression can be seen below in Figure 4.45. In situ micropillar compression allowed for real time visualization of the deformation mechanisms within the pillar. The pure cyanate ester pillar exhibited barreling as it was compressed, resulting in a load increase as the depth of compression increased. The pillar made of BNNP/BNNT foam reinforced cyanate ester exhibited unique deformation mechanisms such as buckling, compression, and sliding of the BNNP/BNNT walls. This can be seen in the load vs depth curve as the load reaches a critical point and then it stays constant even as the depth of compression continues. This deformation mechanism is similar to how a car absorbs the energy during an accident. Due to these unique deformation mechanisms,

these composites could be used for aerospace applications such as micro-meteorite shielding.

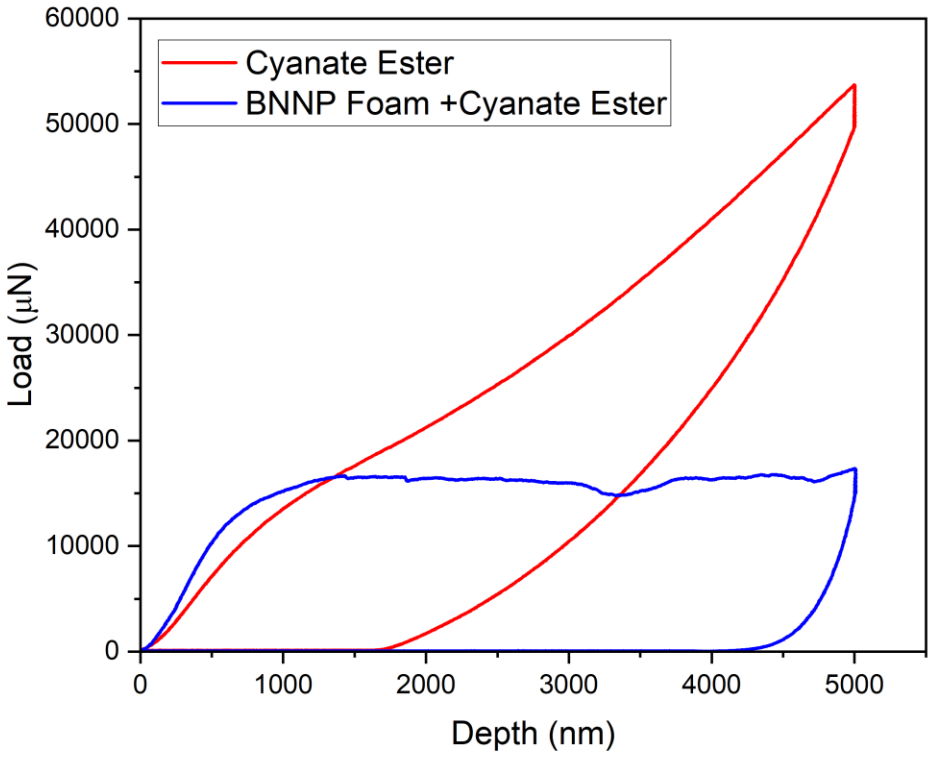

Figure 4.45. Load vs depth curve for micro-pillar compression

To evaluate the impact of BNNP and BNNP/BNNT foams on the thermal transport in cyanate ester composites, thermal conductivity was measured using a laser flash diffusivity method. In all measurements, the foam orientation was kept parallel to the direction of heat transfer, thereby leveraging the high thermal conductivity along the basal plane of BNNPs and the axial direction of BNNTs for optimization of the thermal conductivity results.

Figure 4. illustrates the thermal conductivity data for BNNP foam samples plotted against the data for pure cyanate ester. On average, the addition of BNNP foams led to a

41.21% increase in thermal conductivity at room temperature, with a value of 0.281 (W/m*K), compared to pure cyanate ester. This increase in thermal conductivity is significant, especially considering that the thermal conductivity of the BNNP foam before purification in the furnace was 0.31 (W/m*K). The high improvement of the BNNP reinforced cyanate ester composite could be attributed to the foam's purity and the strong interfacial interaction between the foam and the cyanate ester.

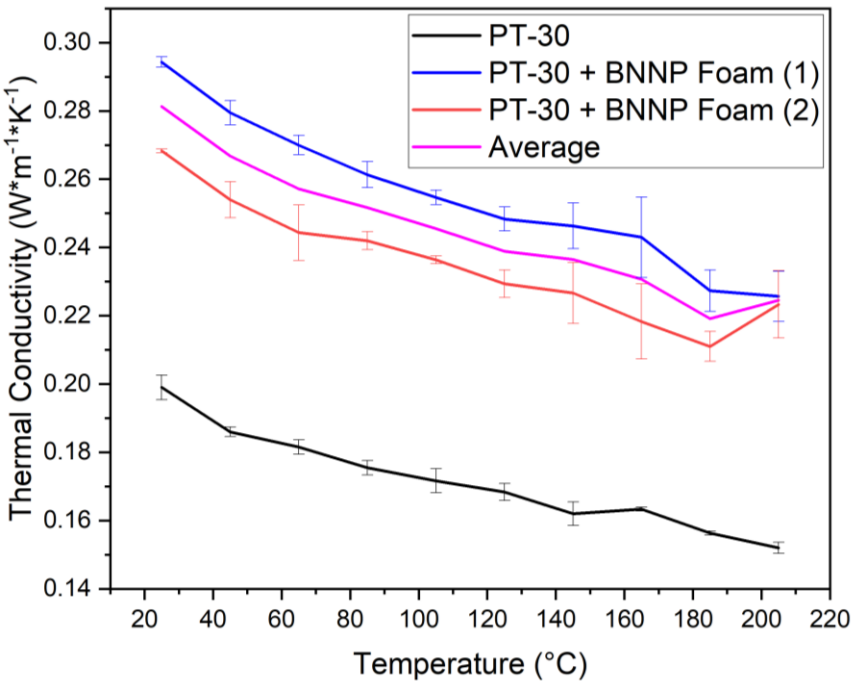

Figure 4.46. Thermal conductivity data comparing BNNP foam reinforced cyanate ester composites with pure cyanate ester.

Figure 4.47 compares the thermal conductivity data for the BNNP/BNNT foam samples with pure cyanate ester. The addition of BNNP/BNNT foams resulted in a remarkable 104.5% increase in thermal conductivity at room temperature, with a value of 0.405 (W/m*K), compared to pure cyanate ester. Figure 4.48 presents a comparison of the foam reinforced samples to the pure cyanate ester and resin reinforced with BNNTs. The

thermal conductivity of BNNP/BNNT reinforced composites was further enhanced than the BNNP reinforced composites due to the highly intertwined network of BNNTs bridging the gaps between individual BNNPs and micro-pores, which allowed for highly efficient thermal transport. Due to the alignment of the entire foam morphology, with the BNNPs aligned in their basal plane direction, and BNNTs bridging nanoplatelets and pores, these novel composites represent a pathway to optimize the thermal conductivity of polymers for advanced applications.

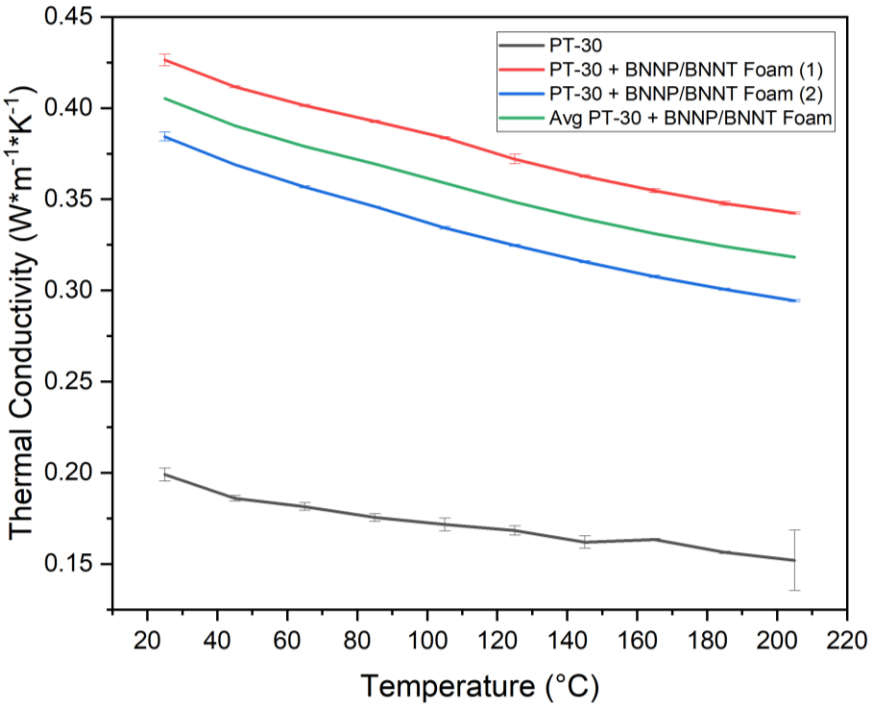

Figure 4.47. Thermal conductivity data comparing BNNP/BNNT foam reinforced cyanate ester composites with pure cyanate ester.

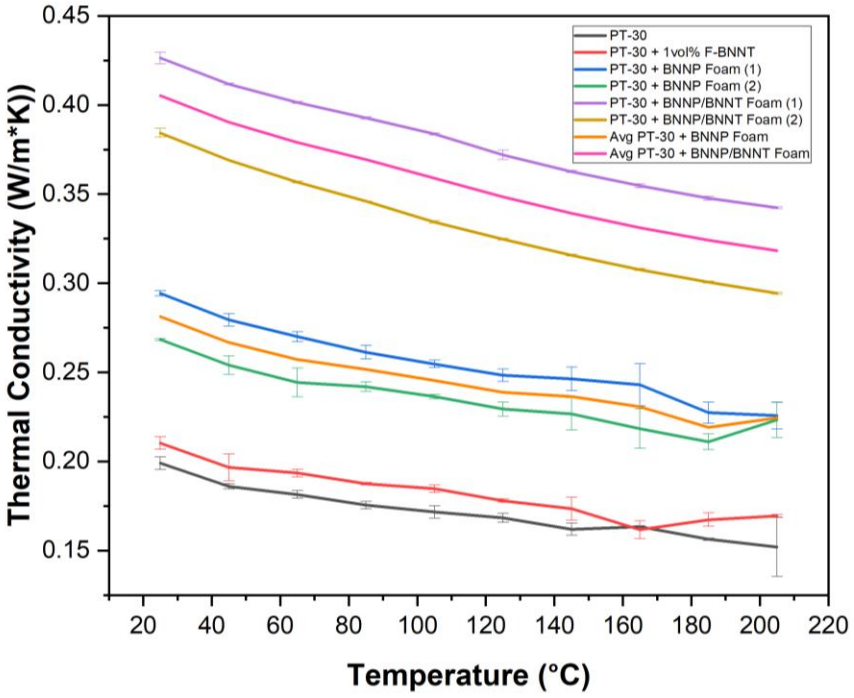

Figure 4.48. Thermal conductivity data comparing BNNP and BNNP/BNNT foam composites with BNNT reinforced CE composites.

The thermal conductivity of these composites can be significantly improved through several methods, including enhancing the alignment, aspect ratio, and loading of BNNTs within the composite's lamellar walls. By aligning the BNNTs parallel with the direction of heat transfer, the efficiency of thermal transport along the axial direction of BNNTs can be enhanced. Longer BNNTs can bridge pores with reduced thermal resistance. The aspect ratio could be increased through optimizing the dispersion process or using less energy-intensive methods, albeit at the cost of longer processing time. Furthermore, increasing the loading percentage of BNNTs can lead to more bonding with the cyanate ester matrix, reducing the interfacial thermal resistance between the two materials. By employing these methods, the thermal conductivity of composites can be considerably enhanced.

Chapter 5 Conclusion

In today's demanding technological sectors, lightweight, strong, and thermally stable materials that can withstand high temperatures and thermal cycling are highly sought after. This research fabricated novel hierarchical boron nitride-based composites which exhibit enhanced thermal and mechanical properties ideal for these demanding environments. This was accomplished through covalently bonding hydroxyl-functionalized boron nitride nanotubes with cyanate ester monomers to form imino-carbonate linkages. This covalent bond resulted in superior interfacial interactions between the cyanate ester and the BNNT, resulting not only in improved dispersion, but also in more efficient thermal and mechanical energy transfer. The addition of just one volume percent of functionalized BNNTs to cyanate ester reduced the curing activation energy to lower than any previously reported literature value, increased the hardness and elastic modulus by 18.48% and 12.42% respectively, and improved the thermal conductivity by 5.69%. The reduction in curing activation energy has substantial implications for the manufacturing of cyanate ester composites, as it opens the possibility of modifying the required temperature and curing parameters for lower temperature curing. This, in turn, could potentially lead to lower production costs while still achieving enhanced thermal and mechanical properties in the resulting cyanate ester polymers. This advancement could significantly benefit the manufacturing industry by allowing for greater flexibility and cost savings without sacrificing the quality of the final product. By lowering the curing temperature, manufacturers can also reduce the energy input required, resulting in more sustainable production practices.

Further optimization of the manufacturing methods on increasing the aspect ratio and volume fraction of the BNNTs in the cyanate ester matrix could lead to further enhancement of mechanical and thermal properties. Increasing the volume fraction of BNNTs is specifically problematic because the high surface of the BNNTs require tedious, high energy dispersion methods which would be difficult to allow for large scale processing and manufacturing. Therefore, it is important to investigate other methods for dispersing the BNNTs without negatively affecting the aspect ratio.

Novel composites consisting of boron nitride nanoplatelets (BNNPs) and BNNTs free-standing foams were fabricated, and their hierarchically structured morphologies were investigated. Through reinforcing cyanate ester with these highly aligned and high-volume percent architectures, the thermal conductivity was increased by an incredible 104.5%. The enhanced thermal conductivity of the foam structure was primarily attributed to the tailored orientation of its constituent materials, the BNNPs and BNNTs. The BNNPs were aligned with their basal planes oriented parallel to the laminar walls of the foam, which facilitated efficient heat transfer along the plane of the walls. Meanwhile, the BNNTs formed an interconnecting network between individual nanoplatelets and micro-pores, creating a highly conductive pathway for heat transfer not seen in other foam composites. The synergistic effect of these factors resulted in a significant improvement in the overall thermal conductivity of the foam reinforced composites. There are several possibilities for further enhancing the mechanical and thermal properties of these composites. Optimizing the alignment within the foams and reducing the interaction energy between the foams and cyanate ester matrix are two key areas that could be explored. One potential approach to optimizing alignment is the use of thermally insulating molds, which could prevent heat

transfer in all directions except for one specific direction, leading to nucleation of the ice crystals and propagation in only that direction. This, in turn, would lead to a more uniform foam structure. To reduce interaction energy, further modification of the BNNP surface to facilitate covalent bonding with the cyanate ester could be pursued. These areas represent promising avenues for future research, as further improvements in alignment could lead to enhanced strength and stiffness, while minimizing the interaction energy could result in better thermal stability. Addressing these factors could also help to overcome any limitations in the current design, leading to more robust and durable composites. Therefore, exploring these possibilities further is crucial to unlocking the full potential of these composites and advancing the field of materials science and engineering. Furthermore, the research conducted on these hierarchical structures paves the way for reinforcement of other polymer systems and can lead to incredibly strong and thermally stable polymers for high temperature applications and demanding environments.

This research has made significant contributions to the field of materials science and engineering. First, it filled a current gap in literature by providing a manufacturing processing map for reinforcing high temperature polymers with novel hierarchical boron nitride structures. These structures are highly efficient in enhancing the thermal and mechanical properties of polymers, even at lower loadings. This makes them a promising option for producing high-performance polymer composites. Second, this research has helped to better understand the impact of micro-scale reinforcement functionalization on the resulting chemical structure, curing kinetics, and mechanical and thermal properties of cyanate ester resins. Third, the study successfully fabricated novel hierarchically structured foam composites using boron nitride nanoplatelets (BNNPs) and boron nitride nanotubes

(BNNTs) that exhibit remarkable thermal properties. Their synergistic abilities allowed for the improvement of thermal properties that could not be achieved by each additive alone. Further, these composites offer tunable mechanical and thermal properties, making them a promising choice for applications in electronic packaging and aerospace components. Finally, the research established the mechanisms governing the interfacial interactions and efficiency of energy transfer between high-volume fraction boron nitride structures and the surrounding matrix. These outcomes have significant implications for the development of improved high-temperature polymers and composites that can be used in demanding industries such as aerospace and energy. Overall, this research presents valuable insights and advances in the field of materials science and engineering, paving the way for the development of new and improved materials with enhanced properties.

The development of these high-strength, lightweight, and thermally stable composites hold immense potential for use in various commercial sectors, including aerospace, robotics, and electronics. Although the extent of thermal stability achievable through reinforcement with BNNTs and hierarchical BNNT structures has not been fully established, they appear to be a highly efficient reinforcer compared to any previously reported additive. This suggests that BNNTs could be a promising option for developing polymer composites that can withstand high temperatures of up to 1000°C in air. Such composites would revolutionize the aerospace industry by enabling the creation of lightweight and intricate components for spaceships, airplanes, missiles, and satellites. This would significantly reduce fuel consumption and costs, which are currently substantial at between $9,000 and $43,000 per pound for NASA to send supplies to the International Space Station. Therefore, the potential implications of BNNTs for advancing aerospace

technology are significant and should be explored further to unlock the full potential of these materials.

While this research has yielded promising results for the mechanical and thermal properties of hierarchical boron nitride composites, their multifunctional abilities have yet to be explored. The inherent radiation shielding and piezoelectric properties of BNNTs and BNNPs suggest that these composites may possess similar abilities on a bulk scale. This opens up a wealth of possibilities for their use in a variety of fields, including actuation, robotics, human health monitoring, energy conversion and production systems, and structural integrity monitoring. Given the potential for commercialization in areas such as biomedical, mechanical, materials, and civil engineering industries, exploring and optimizing these multifunctional properties is of utmost importance. By doing so, these composites may be able to find a wide range of practical applications, thus driving further innovation and growth in materials science and engineering.

REFERENCES

[1] X. Ning, J. Danj, X. Yue, and J. Yuan, “Properties Analysis of Novel Composites for Space Robots,” *Polym. Compos.*, no. 35, pp. 564–569, 2014, doi: 10.1002/pc.22696.

[2] S. Goyal, M. J. Forrester, D. Coverdell, S. Torres, M. W. Lee, and E. W. Cochran, “High-Temperature-Performance Cyanate Ester Composites with Carboranes,” *Macromolecules*, vol. 54, no. 19, pp. 9155–9164, 2021, doi: 10.1021/acs.macromol.1c01410.

[3] R. N. Walters and R. E. Lyon, “Flammability of polymer composites,” *Int. SAMPE Symp. Exhib.*, vol. 52, no. January 2007, 2007, doi: 10.1002/9781118097298.weoc091.

[4] M. L. Ramirez, R. N. Walters, E. P. Savitski, and R. E. Lyon, “THERMAL DECOMPOSITION OF CYANATE ESTER RESINS,” *US DOT*, pp. 1–20, 2001, doi: 10.1016/b978-1-4557-3149-7.00010-3.

[5] H. Wu *et al.*, “Recent developments in polymers/polymer nanocomposites for additive manufacturing,” *Prog. Mater. Sci.*, vol. 111, no. January, 2020, doi: 10.1016/j.pmatsci.2020.100638.

[6] M. Dogan, S. D. Dogan, L. A. Savas, G. Ozcelik, and U. Tayfun, “Flame retardant effect of boron compounds in polymeric materials,” *Compos. Part B Eng.*, vol. 222, no. June, p. 109088, 2021, doi: 10.1016/j.compositesb.2021.109088.

[7] S. Ganguli, D. Dean, K. Jordan, G. Price, and R. Vaia, “Chemorheology of cyanate ester - Organically layered silicate nanocomposites,” *Polymer (Guildf).*, vol. 44, no. 22, pp. 6901–6911, 2003, doi: 10.1016/j.polymer.2003.08.031.

[8] S. Goyal and E. W. Cochran, “Cyanate ester composites to improve thermal performance: a review,” *Polym. Int.*, vol. 71, no. 5, pp. 583–589, 2022, doi: 10.1002/pi.6373.

[9] M. Venkatesh, S. Gouthaman, S. O. Kanemoto, M. S. Lakshmi, and I. Hamerton, “Development of epoxy-cyanate ester-clay nanocomposites offering enhanced thermally stability,” *J. Appl. Polym. Sci.*, vol. 136, no. 28, p. 47754, Jul. 2019, doi: 10.1002/APP.47754.

[10] X. Lu *et al.*, “Hydroxylated boron nitride nanotube-reinforced polyvinyl alcohol nanocomposite films with simultaneous improvement of mechanical and thermal properties,” *Polym. Compos.*, vol. 41, no. 12, pp. 5182–5194, 2020, doi: 10.1002/pc.25785.

[11] P. Nautiyal, N. Denis, T. Dolmetsch, C. Zhang, B. Boesl, and A. Agarwal, “Interface Engineering and Direct Observation of Strengthening Behavior in Field-Sintered Boron Nitride Nanotube–Magnesium Alloy Composite,” *Adv. Eng. Mater.*, vol. 22, no. 7, pp. 1–5, 2020, doi: 10.1002/adem.202000170.

[12] P. Nautiyal, C. Rudolf, A. Loganathan, C. Zhang, B. Boesl, and A. Agarwal, “Directionally Aligned Ultra-Long Boron Nitride Nanotube Induced Strengthening of Aluminum-Based Sandwich Composite,” *Adv. Eng. Mater.*, vol. 18, no. 10, pp. 1747–1754, 2016, doi: 10.1002/adem.201600212.

[13] X. Lu, T. Dolmetsch, C. Zhang, Y. Chen, B. Boesl, and A. Agarwal, “In-situ synthesis of Boron Nitride Nanotube reinforced aluminum oxide composites by molecular mixing,” *Ceram. Int.*, vol. 47, no. 10, pp. 13970–13979, 2021, doi: 10.1016/j.ceramint.2021.01.266.

[14] D. Kim, M. You, J. H. Seol, S. Ha, and Y. A. Kim, “Enhanced Thermal Conductivity of Individual Polymeric Nanofiber Incorporated with Boron Nitride Nanotubes,” *J. Phys. Chem. C*, vol. 121, no. 12, pp. 7025–7029, 2017, doi: 10.1021/acs.jpcc.7b00047.

[15] M. B. Jakubinek *et al.*, “Thermal conductivity of bulk boron nitride nanotube sheets and their epoxy-impregnated composites,” *Phys. Status Solidi Appl. Mater. Sci.*, vol. 213, no. 8, pp. 2237–2242, 2016, doi: 10.1002/pssa.201533010.

[16] J. Ho Kang *et al.*, “Multifunctional Electroactive Nanocomposites Based on Piezoelectric Boron Nitride Nanotubes,” *ACS Nano*, vol. 9, no. 12, pp. 11942–11950, Nov. 2015, doi: 10.1021/acsnano.5b04526.

[17] S. A. Thibeault, J. H. Kang, G. Sauti, C. Park, C. C. Fay, and G. C. King, “Nanomaterials for radiation shielding,” *MRS Bull.*, vol. 40, no. 10, pp. 836–841, 2015, doi: 10.1557/mrs.2015.225.

[18] N. Saba and M. Jawaid, “A review on thermomechanical properties of polymers and fibers reinforced polymer composites,” *J. Ind. Eng. Chem.*, vol. 67, pp. 1–11, Nov. 2018, doi: 10.1016/J.JIEC.2018.06.018.

[19] E. Grossman and I. Gouzman, “Space environment effects on polymers in low earth orbit,” *Nucl. Instruments Methods Phys. Res. Sect. B Beam Interact. with Mater. Atoms*, vol. 208, no. 1–4, pp. 48–57, Aug. 2003, doi: 10.1016/S0168-583X(03)00640-2.

[20] I. Gouzman, E. Grossman, R. Verker, N. Atar, A. Bolker, and N. Eliaz, “Advances in Polyimide-Based Materials for Space Applications,” *Adv. Mater.*, vol. 31, no. 18, pp. 1–15, 2019, doi: 10.1002/adma.201807738.

[21] A. Kandelbauer, “Cyanate ester resins,” *Handb. Thermoset Plast.*, pp. 587–617, 2021, doi: 10.1016/B978-0-12-821632-3.00004-X.

[22] A. Leroy *et al.*, “MATERIALS SCIENCE High-performance subambient radiative cooling enabled by optically selective and thermally insulating polyethylene aerogel,” *Sci. Adv.*, vol. 5, no. 10, pp. 1–9, 2019, doi: 10.1126/sciadv.aat9480.

[23] L. Di Fino, M. Larosa, V. Zaconte, M. Casolino, P. Picozza, and L. Narici, “Measurements on radiation shielding efficacy of Polyethylene and Kevlar in the ISS (Columbus),” *J. Radiat. Res.*, vol. 55, no. suppl 1, pp. i64–i65, 2014, doi: 10.1093/jrr/rrt198.

[24] F. Xie, L. Huang, J. Leng, and Y. Liu, “Thermoset shape memory polymers and their composites,” *J. Intell. Mater. Syst. Struct.*, vol. 27, no. 18, pp. 2433–2455, 2016, doi: 10.1177/1045389X16634211.

[25] S. E. Hall *et al.*, “Mechanical Properties of High-Temperature Fiber-Reinforced Thermoset Composites with Plain Weave and Unidirectional Carbon Fiber Fillers,” *J. Compos. Sci.*, vol. 6, no. 7, pp. 1–12, 2022, doi: 10.3390/jcs6070213.

[26] A. Kandelbauer, “Cyanate ester resins,” *Handb. Thermoset Plast.*, no. September, pp. 587–617, 2021, doi: 10.1016/B978-0-12-821632-3.00004-X.

[27] J. Dubon *et al.*, “Multifunctional MEN-Doped Adhesives: Strengthening, Bond Quality Evaluation, and Variations in Magnetic Signal with Environmental Exposure,” *Appl. Sci.*, vol. 12, no. 16, 2022, doi: 10.3390/app12168238.

[28] E. Frollini and A. Castellan, “Phenolic Resins and Composites,” *Wiley Encycl. Compos.*, pp. 2059–2068, 2012, doi: 10.1002/9781118097298.weoc167.

[29] G. La Delfa, W. Voigt, and M. Abgottspon, “High Temperature and Flame Retardant Cyanate Ester Resins for Aerospace Applications,” *SAMPE Eur. Tech. Conf. Table-Top Exhib.*, no. October, 2010, [Online]. Available: http://www.lonza.com/~/media/Files/Presentations Lonza Employees/CYANATE ESTER RESINS_2010-07-15 GLD.ashx.

[30] A. Osei-Owusu, G. . Martin, and J. . Gotro, “Analysis of the Curing Behvior of Cyanate Ester Resin Systems,” *Polmyer Eng. Sci*, vol. 31, no. 22, pp. 1604–1609, 1991.

[31] S. Gouthaman, V. Madhu, S. O. Kanemoto, S. L. Madurai, and I. Hamerton, “Examining the thermal degradation behaviour of a series of cyanate ester homopolymers,” *Polym. Int.*, vol. 68, no. 10, pp. 1666–1672, 2019, doi: 10.1002/pi.5886.

[32] C. Agents, T. Properties, and S. Life, “Primaset ® PT-30S A Multifunctional Cyanate Ester Delivering High Tg and Inherent Flame Retardancy Curing Agents Highlights Handling / Safety Precautions.”

[33] S.-Y. Lu and I. Hamerton, “Recent developments in the chemistry of halogen-free flame retardant polymers,” *Synthesis (Stuttg).*, vol. 27, no. 12, pp. 1661–1712, 2002, doi: 10.1055/s-2002-33635.

[34] T. J. Wooster, S. Abrol, J. M. Hey, and D. R. MacFarlane, “Thermal, mechanical, and conductivity properties of cyanate ester composites,” *Compos. Part A Appl. Sci. Manuf.*, vol. 35, no. 1, pp. 75–82, 2004, doi: 10.1016/j.compositesa.2003.09.002.

[35] N. Synthesis, K. Liang, G. Li, H. Toghiani, J. H. Koo, and C. U. Pittman, “Cyanate Ester / Polyhedral Oligomeric Silsesquioxane (POSS),” *Society*, pp. 301–312, 2006.

[36] X. Wang, J. Jin, and M. Song, “Cyanate ester resin/graphene nanocomposite: Curing dynamics and network formation,” *Eur. Polym. J.*, vol. 48, no. 6, pp. 1034–1041, 2012, doi: 10.1016/j.eurpolymj.2012.03.012.

[37] Z. Fang, J. Wang, and A. Gu, “Structure and Properties of Multiwalled Carbon Nanotubes/Cyanate Ester Composites,” *Soc. Plast. Eng.*, vol. 46, pp. 670–679, 2006, doi: 10.1002/pen.20487.

[38] H. Wu and M. R. Kessler, “Multifunctional Cyanate Ester Nanocomposites Reinforced by Hexagonal Boron Nitride after Noncovalent Biomimetic Functionalization,” *ACS Appl. Mater. Interfaces*, vol. 7, no. 10, pp. 5915–5926, 2015, doi: 10.1021/acsami.5b00147.

[39] G. Sachdeva *et al.*, “Mechanical response of polymer/BN composites investigated by molecular dynamics method,” *J. Mater. Res.*, vol. 37, no. 24, pp. 4533–4543, 2022, doi: 10.1557/s43578-022-00725-9.

[40] X. Wei, M. S. Wang, Y. Bando, and D. Golberg, “Tensile tests on individual multi-walled boron nitride nanotubes,” *Adv. Mater.*, vol. 22, no. 43, pp. 4895–4899, 2010, doi: 10.1002/adma.201001829.

[41] M. B. Jakubinek *et al.*, “Boron nitride nanotube composites and applications,” *Nanotub. Superfiber Mater. Sci. Manuf. Commer.*, pp. 91–111, 2019, doi: 10.1016/B978-0-12-812667-7.00005-7.

[42] D. Golberg *et al.*, “Boron nitride nanotubes and nanosheets,” *ACS Nano*, vol. 4, no. 6, pp. 2979–2993, 2010, doi: 10.1021/nn1006495.

[43] C. Y. Zhi, Y. Bando, T. Terao, C. C. Tang, H. Kuwahara, and D. Golberg, “Chemically activated boron nitride nanotubes,” *Chem. - An Asian J.*, vol. 4, no. 10, pp. 1536–1540, 2009, doi: 10.1002/asia.200900158.

[44] N. G. Chopra, R. J. Luyken, K. Cherrey, V. H. Crespi, and A. Cohen, Marvin L., Louie Steven G., Zettl, "Boron nitride nanotubes," *Am. Assoc. Adv. Sci.*, vol. 269, pp. 966–967, 1995, doi: 10.1016/j.mser.2010.06.004.

[45] Y. Huang *et al.*, "Bulk synthesis, growth mechanism and properties of highly pure ultrafine boron nitride nanotubes with diameters of sub-10 nm," *Nanotechnology*, vol. 22, no. 14, p. 145602, Apr. 2011, doi: 10.1088/0957-4484/22/14/145602.

[46] X. Yang *et al.*, "Significant improvement of thermal conductivities for BNNS/PVA composite films via electrospinning followed by hot-pressing technology," *Compos. Part B Eng.*, vol. 175, no. June, p. 107070, 2019, doi: 10.1016/j.compositesb.2019.107070.

[47] N. News *et al.*, "(12) United States Patent," vol. 2, no. 12, 2015.

[48] J. H. Kim, T. V. Pham, J. H. Hwang, C. S. Kim, and M. J. Kim, "Boron nitride nanotubes: synthesis and applications," *Nano Converg.*, vol. 5, no. 1, 2018, doi: 10.1186/s40580-018-0149-y.

[49] A. Taghavi Nasrabadi and M. Foroutan, "Interactions between Polymers and Single-Walled Boron Nitride Nanotubes: A Molecular Dynamics Simulation Approach," *J. Phys. Chem. B*, vol. 114, no. 47, pp. 15429–15436, Nov. 2010, doi: 10.1021/jp106330c.

[50] X. Chen, L. Zhang, C. Park, C. C. Fay, X. Wang, and C. Ke, "Mechanical strength of boron nitride nanotube-polymer interfaces," *Appl. Phys. Lett.*, vol. 107, no. 25, 2015, doi: 10.1063/1.4936755.

[51] A. Niguès, A. Siria, P. Vincent, P. Poncharal, and L. Bocquet, "Ultrahigh interlayer friction in multiwalled boron nitride nanotubes," *Nat. Mater.*, vol. 13, no. 7, pp. 688–693, 2014, doi: 10.1038/nmat3985.

[52] K. S. Kim *et al.*, "Polymer nanocomposites from free-standing, macroscopic boron nitride nanotube assemblies," *RSC Adv.*, vol. 5, no. 51, pp. 41186–41192, 2015, doi: 10.1039/c5ra02988k.

[53] D. M. Tang *et al.*, "Mechanical properties of bamboo-like boron nitride nanotubes by in situ TEM and MD simulations: Strengthening effect of interlocked joint interfaces," *ACS Nano*, vol. 5, no. 9, pp. 7362–7368, 2011, doi: 10.1021/nn202283a.

[54] M. F. Yu, O. Lourie, M. J. Dyer, K. Moloni, T. F. Kelly, and R. S. Ruoff, "Strength and breaking mechanism of multiwalled carbon nanotubes under tensile load," *Science (80-.).*, vol. 287, no. 5453, pp. 637–640, 2000, doi: 10.1126/science.287.5453.637.

[55] M. F. Yu, B. I. Yakobson, and R. S. Ruoff, “Controlled sliding and pullout of nested shells in individual multiwalled carbon nanotubes,” *J. Phys. Chem. B*, vol. 104, no. 37, pp. 8764–8767, 2000, doi: 10.1021/jp002828d.

[56] M. B. Jakubinek *et al.*, “Nanoreinforced epoxy and adhesive joints incorporating boron nitride nanotubes,” *Int. J. Adhes. Adhes.*, vol. 84, no. March, pp. 194–201, 2018, doi: 10.1016/j.ijadhadh.2018.03.008.

[57] P. Snapp, C. Cho, D. Lee, M. F. Haque, S. W. Nam, and C. Park, “Tunable Piezoelectricity of Multifunctional Boron Nitride Nanotube/Poly(dimethylsiloxane) Stretchable Composites,” *Adv. Mater.*, vol. 32, no. 43, pp. 1–8, 2020, doi: 10.1002/adma.202004607.

[58] D. Golberg, Y. Bando, C. Tang, and C. Zni, “Boron nitride nanotubes,” *Adv. Mater.*, vol. 19, no. 18, pp. 2413–2432, 2007, doi: 10.1002/adma.200700179.

[59] D. Golberg, Y. Bando, K. Kurashima, and T. Sato, “Synthesis and characterization of ropes made of BN multiwalled nanotubes,” *Scr. Mater.*, vol. 44, no. 8–9, pp. 1561–1565, 2001, doi: 10.1016/S1359-6462(01)00724-2.

[60] Y. Chen, J. Zou, S. J. Campbell, and G. Le Caer, “Boron nitride nanotubes: Pronounced resistance to oxidation,” *Appl. Phys. Lett.*, vol. 84, no. 13, pp. 2430–2432, 2004, doi: 10.1063/1.1667278.

[61] J. Zhang *et al.*, “3D printed piezoelectric BNNTs nanocomposites with tunable interface and microarchitectures for self-powered conformal sensors,” *Nano Energy*, vol. 77, no. April, p. 105300, 2020, doi: 10.1016/j.nanoen.2020.105300.

[62] J. Yu, Y. Chen, R. G. Elliman, and M. Petravic, “Isotopically enriched 10BN nanotubes,” *Adv. Mater.*, vol. 18, no. 16, pp. 2157–2160, 2006, doi: 10.1002/adma.200600231.

[63] O. Matarredona, H. Rhoads, Z. Li, J. H. Harwell, L. Balzano, and D. E. Resasco, “Dispersion of single-walled carbon nanotubes in aqueous solutions of the anionic surfactant NaDDBS,” *J. Phys. Chem. B*, vol. 107, no. 48, pp. 13357–13367, 2003, doi: 10.1021/jp0365099.

[64] A. Tessema *et al.*, “Effect of filler loading, geometry, dispersion and temperature on thermal conductivity of polymer nanocomposites,” *Polym. Test.*, vol. 57, pp. 101–106, 2017, doi: 10.1016/j.polymertesting.2016.11.015.

[65] S. R. Bakshi, D. Lahiri, and A. Agarwal, “Carbon nanotube reinforced metal matrix composites - A review,” *Int. Mater. Rev.*, vol. 55, no. 1, pp. 41–64, 2010, doi: 10.1179/095066009X12572530170543.

[66] D. Lahiri *et al.*, “Insight into reactions and interface between boron nitride nanotube and aluminum,” *J. Mater. Res.*, vol. 27, no. 21, pp. 2760–2770, 2012, doi: 10.1557/jmr.2012.294.

[67] D. Lahiri *et al.*, “Boron nitride nanotubes reinforced aluminum composites prepared by spark plasma sintering: Microstructure, mechanical properties and deformation behavior,” *Mater. Sci. Eng. A*, vol. 574, pp. 149–156, 2013, doi: 10.1016/j.msea.2013.03.022.

[68] V. Guerra, C. Wan, and T. McNally, “Thermal conductivity of 2D nano-structured boron nitride (BN) and its composites with polymers,” *Prog. Mater. Sci.*, vol. 100, no. October 2018, pp. 170–186, 2019, doi: 10.1016/j.pmatsci.2018.10.002.

[69] W. J. Hyun *et al.*, “High-Modulus Hexagonal Boron Nitride Nanoplatelet Gel Electrolytes for Solid-State Rechargeable Lithium-Ion Batteries,” *ACS Nano*, vol. 13, no. 8, pp. 9664–9672, 2019, doi: 10.1021/acsnano.9b04989.

[70] R. J. Jiménez-Riobóo, L. Artús, R. Cuscó, T. Taniguchi, G. Cassabois, and B. Gil, “In- and out-of-plane longitudinal acoustic-wave velocities and elastic moduli in h -BN from Brillouin scattering measurements,” *Appl. Phys. Lett.*, vol. 112, no. 5, 2018, doi: 10.1063/1.5019629.

[71] J. Wu, B. Wang, Y. Wei, R. Yang, and M. Dresselhaus, “Mechanics and mechanically tunable band gap in single-layer hexagonal boron-nitride,” *Mater. Res. Lett.*, vol. 1, no. 4, pp. 200–206, 2013, doi: 10.1080/21663831.2013.824516.

[72] O. T. Picot *et al.*, “Using graphene networks to build bioinspired self-monitoring ceramics,” *Nat. Commun.*, vol. 8, 2017, doi: 10.1038/ncomms14425.

[73] T. Thomas, C. Zhang, P. Nautiyal, B. Boesl, and A. Agarwal, “3D Graphene Foam Reinforced Low-Temperature Ceramic with Multifunctional Mechanical, Electrical, and Thermal Properties,” *Adv. Eng. Mater.*, vol. 21, no. 7, pp. 1–9, 2019, doi: 10.1002/adem.201900085.

[74] G. Nuytten *et al.*, “Development and application of a mechanistic cooling and freezing model of the spin freezing step within the framework of continuous freeze-drying,” *Pharmaceutics*, vol. 13, no. 12, 2021, doi: 10.3390/pharmaceutics13122076.

[75] G. Chen and W. Wang, “Role of freeze drying in nanotechnology,” *Dry. Technol.*, vol. 25, no. 1, pp. 29–35, 2007, doi: 10.1080/07373930601161179.

[76] P. Niksiar *et al.*, “External Field Assisted Freeze Casting,” *Ceramics*, vol. 2, no. 1, pp. 208–234, 2019, doi: 10.3390/ceramics2010018.

[77] H. Zhang, I. Hussain, M. Brust, M. F. Butler, S. P. Rannard, and A. I. Cooper, "Aligned two- and three-dimensional structures by directional freezing of polymers and nanoparticles," *Nat. Mater.*, vol. 4, no. 10, pp. 787–793, 2005, doi: 10.1038/nmat1487.

[78] N. Zhao, J. Li, W. Wang, W. Gao, and H. Bai, "Isotropically Ultrahigh Thermal Conductive Polymer Composites by Assembling Anisotropic Boron Nitride Nanosheets into a Biaxially Oriented Network," *ACS Nano*, vol. 16, no. 11, pp. 18959–18967, 2022, doi: 10.1021/acsnano.2c07862.

[79] W. Lei, V. N. Mochalin, D. Liu, S. Qin, Y. Gogotsi, and Y. Chen, "Boron nitride colloidal solutions, ultralight aerogels and freestanding membranes through one-step exfoliation and functionalization," *Nat. Commun.*, vol. 6, pp. 1–8, 2015, doi: 10.1038/ncomms9849.

[80] P. S. Owuor *et al.*, "Lightweight Hexagonal Boron Nitride Foam for CO2 Absorption," *ACS Nano*, vol. 11, no. 9, pp. 8944–8952, 2017, doi: 10.1021/acsnano.7b03291.

[81] J. Han, G. Du, W. Gao, and H. Bai, "An Anisotropically High Thermal Conductive Boron Nitride/Epoxy Composite Based on Nacre-Mimetic 3D Network," *Adv. Funct. Mater.*, vol. 29, no. 13, 2019, doi: 10.1002/adfm.201900412.

[82] M. Zhang, H. Yan, X. Yang, and C. Liu, "Effect of functionalized graphene oxide with a hyperbranched cyclotriphosphazene polymer on mechanical and thermal properties of cyanate ester composites," *RSC Adv.*, vol. 4, no. 86, pp. 45930–45938, 2014, doi: 10.1039/c4ra06411a.

[83] X. Wang, J. Jin, and M. Song, "Cyanate ester resin/graphene nanocomposite: Curing dynamics and network formation," *Eur. Polym. J.*, vol. 48, no. 6, pp. 1034–1041, 2012, doi: 10.1016/j.eurpolymj.2012.03.012.

[84] C. Zhang, B. Boesl, and A. Agarwal, "Oxidation resistance of tantalum carbide-hafnium carbide solid solutions under the extreme conditions of a plasma jet," *Ceram. Int.*, vol. 43, no. 17, pp. 14798–14806, 2017, doi: 10.1016/j.ceramint.2017.07.227.

[85] F. Deng, Q. S. Zheng, L. F. Wang, and C. W. Nan, "Effects of anisotropy, aspect ratio, and nonstraightness of carbon nanotubes on thermal conductivity of carbon nanotube composites," *Appl. Phys. Lett.*, vol. 90, no. 2, 2007, doi: 10.1063/1.2430914.

[86] X. Wang, Y. Zhao, J. Jin, and M. Song, "A comparative study on the effect of carbon fillers on electrical and thermal conductivity of a cyanate ester resin," *Polym. Test.*, vol. 60, pp. 293–298, 2017, doi: 10.1016/j.polymertesting.2017.04.013.

[87] W. C. Oliver and G. M. Pharr, “Nanoindentation in materials research: Past, present, and future,” *MRS Bull.*, vol. 35, no. 11, pp. 897–907, 2010, doi: 10.1557/mrs2010.717.

VITA

TYLER DOLMETSCH

Born, York, Pennsylvania

August 2014 – July 2018	B.S., Mechanical Engineering Florida International University Miami, Florida
January 2019 – July 2020	M.S., Mechanical Engineering Florida International University Miami, Florida
August 2020-Present	FIU Presidential Fellow Florida International University Miami, Florida
August 2022-December 2022	Teaching Instructor Florida International University Miami, Florida
August 2022 - Present	PhD Candidate in Materials Sci. and Engineering Florida International University Miami, Florida

1. Sarvesha, R., Garcia, D., Dolmetsch, T., Eberheim, R., Wang, T., Aguiar, B., Paul, T., Ross, K. A., Champagne, V. K., Agarwal, A., In-Situ and Correlative Microscopy Study on Fracture Behavior of Thick Section Friction Stir Welded Al 5083 Alloy. Available at SSRN: https://ssrn.com/abstract=4245026 or http://dx.doi.org/10.2139/ssrn.4245026
2. Lou, L., Paul, T., Aguiar, B., Dolmetsch, T., Zhang, C., Arvind A. Direct Observation of Adhesion and Mechanical Behavior of a Single Poly(lactic-co-glycolic acid) (PLGA) Fiber Using an In Situ Technique for Tissue Engineering. ACS Applied Materials & Interfaces 2022 14 (38), 42876-42886. DOI: 10.1021/acsami.2c09665
3. Paul, T, Lou, L, Nautiyal, P, Dolmetsch, T, Zhang, C, Boesl, B, Agarwal, A. Micro-Deformation in Cold Sprayed Aluminum Single Splat Revealed by *In-Situ* Indentation and Image Analysis of Interface Strains. Submitted to *Scripta Materialia* May 2022. Available at SSRN: https://ssrn.com/abstract=4153557 or http://dx.doi.org/10.2139/ssrn.4153557

4. Nisar, A, Dolmetsch, T, Paul, T, Sakthivel, TS, Zhang, C, Boesl, B, et al. Unveiling enhanced oxidation resistance and mechanical integrity of multicomponent ultra-high temperature carbides. *J Am Ceram Soc*. 2022; 105: 2500– 2516. https://doi.org/10.1111/jace.18281
5. Nisar, A., Dolmetsch, T., Paul, T., Zhang, C., Boesl, B. and Agarwal, A. (2021), Electric field assisted solid-state interfacial joining of TaC-HfC ceramics without filler. *J Am Ceram Soc*, 104: 2483-2494. https://doi.org/10.1111/jace.17692
6. Lu, X., Dolmetsch, T., Zhang, C., Chen, Y., Boesl, B., Agarwal, A., In-situ Synthesis of Boron Nitride Nanotube Reinforced Aluminum Oxide Composites by Molecular Mixing. *Ceram Int.* 2021; 47:13970-13979. https://doi.org/10.1016/j.ceramint.2021.01.266
7. Nautiyal, P., Denis, N., Dolmetsch, T., Zhang, C., Boesl, B. and Agarwal, A. (2020), Interface Engineering and Direct Observation of Strengthening Behavior in Field-Sintered Boron Nitride Nanotube–Magnesium Alloy Composite. *Adv. Eng. Mater*., 22: 2000170. https://doi.org/10.1002/adem.202000170
8. Oral: "Deformation mechanisms of hierarchically structured 2D single-crystal materials revealed by real-time high-resolution in-situ nanomechanical testing", ECI Nanomechanical Testing in Materials Research and Development VIII 2022, Split, Croatia.
9. Oral: "Real-Time Deformation Mechanisms of Hierarchically Structured Nanocomposites using High-Resolution In Situ Testing", TMS 2022, Los Angeles, California, USA
10. Poster: "Interlayer Delamination Response of 2D Single Crystal WSe2Revealed by In-situ Nano-scratch", MRS PREM 2021, Virtual.
11. Poster: "Influence of Processing Parameters and Field Effects on the Microstructure and Mechanical Properties of Advanced Materials", Materials Science & Technology (MS&T 2019), Portland, Oregon, USA